QUANTIFYING LONG-TERM GLACIAL DENUDATION WITH LOW-TEMPERATURE THERMOCHRONOLOGY

by

Mathew Scott Densmore

A dissertation submitted in partial fulfillment
of the requirements for the degree of
Doctor of Philosophy
(Geology)
in The University of Michigan
2008

Doctoral Committee:
    Associate Professor Todd A. Ehlers, Chair
    Professor Joel D. Blum
    Professor Nikolaos D. Katopodes
    Professor Larry J. Ruff
    Professor Ben A. Van Der Pluijm

"Reality is frequently inaccurate." – *Douglas Adams*

Dedication

I would like to dedicate this dissertation to the following people:

- My wonderful wife Maris and her endless supply of patience, support and home-baked cookies.

- My advisor Todd Ehlers for passing along the skills and thought processes of a scientist.

- The surface process lab, especially Jason Barnes, Greg Stock and Dave Whipp for ideas, comments, discussions, advice and all the rest.

- My committee members, Joel Blum, Nikolaos Katopodes, Larry Ruff and Ben Van Der Pluijm.

- My fellow graduate students and colleagues at the University of Michigan, especially the Finer Wings Club.

- Bruce Wilkinison for help in the early days of my career as a graduate student.

Table of Contents

List of Figures

List of Tables

List of Appendices

Abstract

Quantifying the long-term (~10^6 yrs) denudation history within an orogen is requisite in understanding the evolution of topography and efficacy of various surface processes. Specifically, glaciation is an important process within alpine environments that significantly alters the landscape. However, few studies have evaluated long-term denudation rates in glaciated settings. This dissertation presents an extensive thermochronometer dataset interpreted with multiple numerical methods to constrain long-term rates of denudation in a glaciated orogen, and determine how glaciers affect the topography.

As part of this dissertation, 58 thermochronometer samples were collected within the heavily glaciated Coast Mountains, British Columbia, Canada. Samples were collected over a 60 x 60 km region and span ~4 km of relief. Analyses yielded 58 apatite (U-Th)/He ages, 4 apatite fission track ages, and 9 zircon (U-Th)/He ages, ranging from 1.1 to 15.4 Ma, 6.9 to 39.2 Ma, and 2.4 to 27.3 Ma, respectively. Cooling ages were interpreted in the context of glacial denudation using a standard linear regression technique as well as 1-, 2- and 3-D numerical models. This approach of multiple techniques allows for robust constraints of denudation within the region as well as an evaluation of each technique with respect to a sophisticated 3-D thermal model.

Major results from this study are: (1) an observed pulse of denudation at ~7 Ma interpreted as the onset of glaciation, (2) glacial denudation rates range from ~0.2 to 2.2 mm/yr, more than an order of magnitude less than short-term (10^2 to 10^3 yrs) estimates and ~4 times less than observed long-term rates in southern Alaska, (3) exhumation and cooling within the core of the range occurred rapidly during the last ~7 Myr, perhaps with an increase in the last ~2 Myr associated with the intensification of glaciation during the Pleistocene, (4) glaciers modify the topography in a non-uniform fashion, incising paleo-fluvial networks as well as reworking the local topography by removing peaks and

altering major valley locations. Finally, a sophisticated 3-D thermal model is preferred over 1- or 2-D methods for interpreting large spatial regions with high relief and variable denudation rates.

Chapter 1: Introduction

Topography is the result of competition between tectonics which increases topography and erosion which removes it. Over geologic time the primary agents of erosion are due to the movement of water, wind and ice. One of the most significant agents of erosion is glaciers. Glaciation can significantly alter landscapes and supplant the local fluvial erosion system. This change in dominant surficial process transforms V-shaped interfluves into the characteristic broad, U-shaped valleys of a glaciated terrain. As an example the Coast Mountains, British Columbia, Canada, have been heavily glaciated since the latest Miocene (~6 – 8 Ma) (Fig. 1-1). Various glacial features have been qualitatively described in detail for over 150 yrs (e.g. Agassiz, 1864). However, only recently have studies quantitatively constrained the effects of glaciation and much of this work details processes on decadal to millennial timescales (e.g. Hallet et al., 1996b). A long-standing debate in the geomorphic community is the relative efficiency of a glacial versus fluvial landscape in removing material (e.g. Brozovic et al., 1997; Molnar and England, 1990; Whipple et al., 1999). One way to address this is by quantifying denudation rates of glaciers. Current glacial denudation rate estimates span four orders of magnitude from ~0.01 – >60 mm/yr (e.g. Hallet et al., 1996b). Rates above ~10 mm/yr are not geodynamically feasible over the multiple glacial/interglacial cycles of the last ~2 Ma or longer as they imply exhumation of lower crustal material that is not observed at the surface. Constraining the long-term ($>10^6$ yrs) exhumation history of a glaciated region is necessary to evaluate how landscapes respond to differing denudation environments. Complicating this over-arching question is the fundamental control of how glaciation modifies a landscape: whether denudation is focused within valley bottoms, thereby increasing the local relief, or by removing high peaks in the head-waters and thus limiting the maximum elevation of alpine mountain ranges. The goal of this dissertation is to apply low-temperature thermochronology interpreted with numerical

1

modeling to quantify the long-term evolution of exhumation and denudation within the Coast Mountains, British Columbia.

Denudation, along with normal faulting and ductile thinning is an important process resulting in rock exhumation (Ring et al., 1999). Therefore, quantifying the long-term exhumation rate in a region can reveal the denudation history and perhaps elucidate temporal periods dominated by specific mechanisms. Low-temperature thermochronometers are common tools used to address the long-term evolution of a region (e.g. Ehlers and Farley, 2003; Hodges, 2003; Reiners, 2007). These systems yield information on paleo-exhumation rates as well as the regional thermal field. Many studies have applied these tools to constrain the timing and magnitude of exhumation processes such as faulting (e.g. Ehlers et al., 2003; Stockli et al., 2000), fluvial erosion (e.g. Burbank et al., 2003) and even volcanic eruptions (e.g. Blondes et al., 2007). Traditionally, studies using thermochronology to infer or calculate glacial denudation rates (Berger and Spotila, 2008; Ehlers et al., 2006; Meigs and Sauber, 2000; Shuster et al., 2005; Spotila et al., 2004) use one method to interpret the data, for example analysis of age-elevation profiles or 1-D thermal modeling. This study expands on previous works by analyzing and utilizing a dense thermochronometer dataset within the southern Coast Mountains, British Columbia (Fig. 1-1) interpreted with 1-, 2- and 3-D numerical methods in order to provide robust constraints on denudation and distinguish periods dominated by glacial- and non-glacial processes.

This dissertation constrains exhumation and denudation in the Coast Mountains using low-temperature thermochronology and numerical modeling techniques. Specifically, hypotheses tested are: (1) a pulse of denudation is observable coincident with the onset of glaciation, (2) alpine glaciers are more efficient than streams therefore denudation rates over long periods of time will be higher in glaciated environments, (3) glacial denudation is highly variable across the landscape, even at similar elevations and (4) glaciers modify topography by changing relief initially generated by a fluvial network and therefore do not change the position of valleys and ridges.

Background to methods used:

Thermochronometer cooling ages are a function of the integrated effects of many processes which perturb the crustal thermal field (e.g. Braun, 2002b; Ehlers, 2005; Ehlers et al., 2001; Farley, 2000; House et al., 1998; Mancktelow and Grasemann, 1997b; Stuwe et al., 1994). Heat advected from deep sources such as the mantle or internal heat production from the decay of radioactive elements (namely ^{238}U, ^{235}U, ^{232}Th, and ^{40}K) can increase the near-surface thermal gradient. Additionally, topography of a sufficient wavelength can influence temperatures to depths critical to thermochronology (Braun, 2005) by compressing isotherms beneath valleys and expanding them beneath peaks. High alpine topography can drive fluid flow, redistributing heat and potentially complicating a regions geothermal gradient (Whipp and Ehlers, 2007). Denudation brings warm material towards the surface, while sedimentation buries cooler material to depth. A similar effect occurs due to active faulting, depending on the orientation of slip. Finally, magmatism can cause local perturbations of the thermal field adjacent to intruded bodies. Any of these individual processes can complicate the interpretation of thermochronometer cooling ages.

This dissertation applies low-temperature thermochronology in the heavily glaciated Coast Mountains, British Columbia (Fig. 1-1). This region allows for straightforward interpretation of cooling age data by avoiding some of the complications discussed above. The Coast Mountains have been heavily glaciated for at least the last ~6 Myr (Clague, 1991; Densmore et al., 2007). The lack of major tectonic structures in the core of the range suggests that denudation is the primary mechanism exhuming rocks to the surface (Sweeney et al., 1992). A dense thermochronometer dataset was collected, processed and analyzed in the course of this dissertation. This data has allowed for unique interpretations across individual drainage basins, comparing erosion rates between small tributary and major trunk stream valleys with high peaks within the range. Furthermore, the dense network of samples permits rigorous interpretation using 3-D thermo-kinematic modeling. A major goal of this dissertation is to identify best-fit model parameters to observed cooling ages and evaluate a complex 3-D model with respect to more simplistic 1- and 2-D schemes.

Quantitative methods for data interpretation applied here include a common linear regression technique, forward and inverse modeling, and a sophisticated 3-D thermal model. One of the simplest, most common method for interpreting thermochronometer data is analysis of sample cooling age versus elevation along a vertical profile (Wagner et al., 1977). The best-fit regression line through an age-elevation profile yields an apparent exhumation rate. Additionally, this dissertation utilizes HeFTy, an inverse thermal model (Ketcham, 2005a), to further constrain denudation using aspects of the raw data. This program uses the thermal sensitivity of different thermochronometer systems with raw fission track and (U-Th)/He data to constrain the time-temperature history of a sample. Another simple program is AGE2EDOT (Brandon et al., 1998), a 1-D forward model that constrains denudation rates. This program uses rock thermal properties and knowledge of the thermal field to determine a denudation rate for individual samples. Finally, a 3-D finite element thermo-mechanical model (Braun, 2003) is applied. This powerful code determines the thermal field with respect to denudation, evolving topography, and rock thermal properties. A kinematic field is prescribed and samples are tracked through time to predict cooling ages.

Overview of Chapters and Results

This dissertation is comprised of four main chapters (2 – 5) as well as introduction (1) and conclusion (6) chapters. The main chapters present and interpret data within the southern Coast Mountains, British Columbia. Chapter 2 investigates how glaciation affects the flank of a large glaciated valley in an alpine environment. A 3-D model is used to interpret several samples along an age-elevation profile. In Chapter 3 the scope is expanded to include a large number of samples comprising our entire thermochronometer dataset. Simple 1-D quantitative approaches are evaluated and denudation rates are constrained over a wide region. Chapter 4 extends the temporal scale by including higher temperature thermochronometer systems and findings are compared to previous work throughout the entire Coast Mountains orogen. Here both 1- and 2-D models are evaluated for interpreting a large dataset. Chapter 5 utilizes the full dataset and a sophisticated 3-D model to determine best-fit denudation rates, timing of glaciation, and

whether a simple increase or decrease in relief over present topographic wavelengths is sufficient to fit observed data.

Findings from these chapters address the presented hypotheses that we can distinguish a glacial and preglacial denudation signal, and that glaciers are efficient, dynamic agents of denudation. Indeed, low-temperature thermochronometer data within the southern Coast Mountains does include a signal of pre- as well as syn- and post-glacial denudation. Glaciation appears to increase the long-term denudation rate in a non-uniform pattern across the landscape resulting in areas of focused denudation with increases of 4x from a fluvial environment. Glaciation in the area likely began ~7 Ma and intensified during the last 2 – 4 Myr. Finally, while modeling here does not resolve landscape evolution with respect to increasing or decreasing relief, results show that glaciation does not simply change the amplitude of the paleotopography. Instead, a reworking of topography must have taken place reorganizing drainage patterns, removing peaks and incising valleys where perhaps they previously did not exist.

Publications and Abstracts from this Dissertation

    Publications

Densmore, M.S., Ehlers, T.A., Farley, K.A., Rusmore, M.E., Woodsworth, G.J., 2008, Interpreting thermochronometer cooling ages in a glaciated orogen, to be submitted to *J. Geophys. Res. – Earth Surface.*

Densmore, M.S., Ehlers, T.A., Farley, K.A., Rusmore, M.E., Woodsworth, G.J., 2008, Observed spatial and temporal variations in glacial denudation from thermochronometer data: Coast Mountains, B.C., to be submitted to *J. Geophys. Res. – Earth Surface*.

Densmore, M.S., Ehlers, T.A., Woodsworth, G.J., 2007, Effect of alpine glaciation on thermochronometer age-elevation profiles, *Geophysical Research Letters*, vol. 34. (Chapter 2)

Abstracts

Densmore, M.S., Ehlers, T.A, Farley, K.A., Woodsworth, G.J., 2007, Long-term glacial erosion in the Coast Mountains, British Columbia, Canada from low-temperature thermochronology, Eos Transactions AGU, vol 88., no 52., abstract H53C-1382.

Densmore, M.S., Ehlers, T.A, Farley, K.A., Woodsworth, G.J., 2006, Spatial and temporal variations in topography and glacial erosion from apatite (U-Th)/He thermochronometry, southern British Columbia, Eos Transactions AGU, vol 87., no 52., abstract C33A-1256.

Densmore, M.S., Ehlers, T.A, Farley, K.A., Woodsworth, G.J., 2005, Influence of glacial valley widening and deepening on thermochronometer age-elevation profiles, GSA Abstracts with Programs, vol. 37, no.7.

Densmore, M.S., Ehlers, T.A., Farley, K.A., Woodsworth, G.J., 2004, Quantifying glacial valley widening and deepening with apatite (U-Th)/He thermochronology; Coast Mountains, B.C., Eos Transactions AGU, vol. 85, no. 47., abstract H51A-1100.

Figures

Figure 1-1. Digital elevation model (GTOPO30) and bathymetry (ETOPO5) of the western Canadian Cordillera including political boundaries (thin black line), plate margin interactions (thick black line), major morphogeologic belt (thick dashed line) containing the Coast Mountains (Gabrielse et al., 1991), and maximum Pleistocene ice extent (dashed blue line) (Clague, 1991). Box denotes focus region for this dissertation.
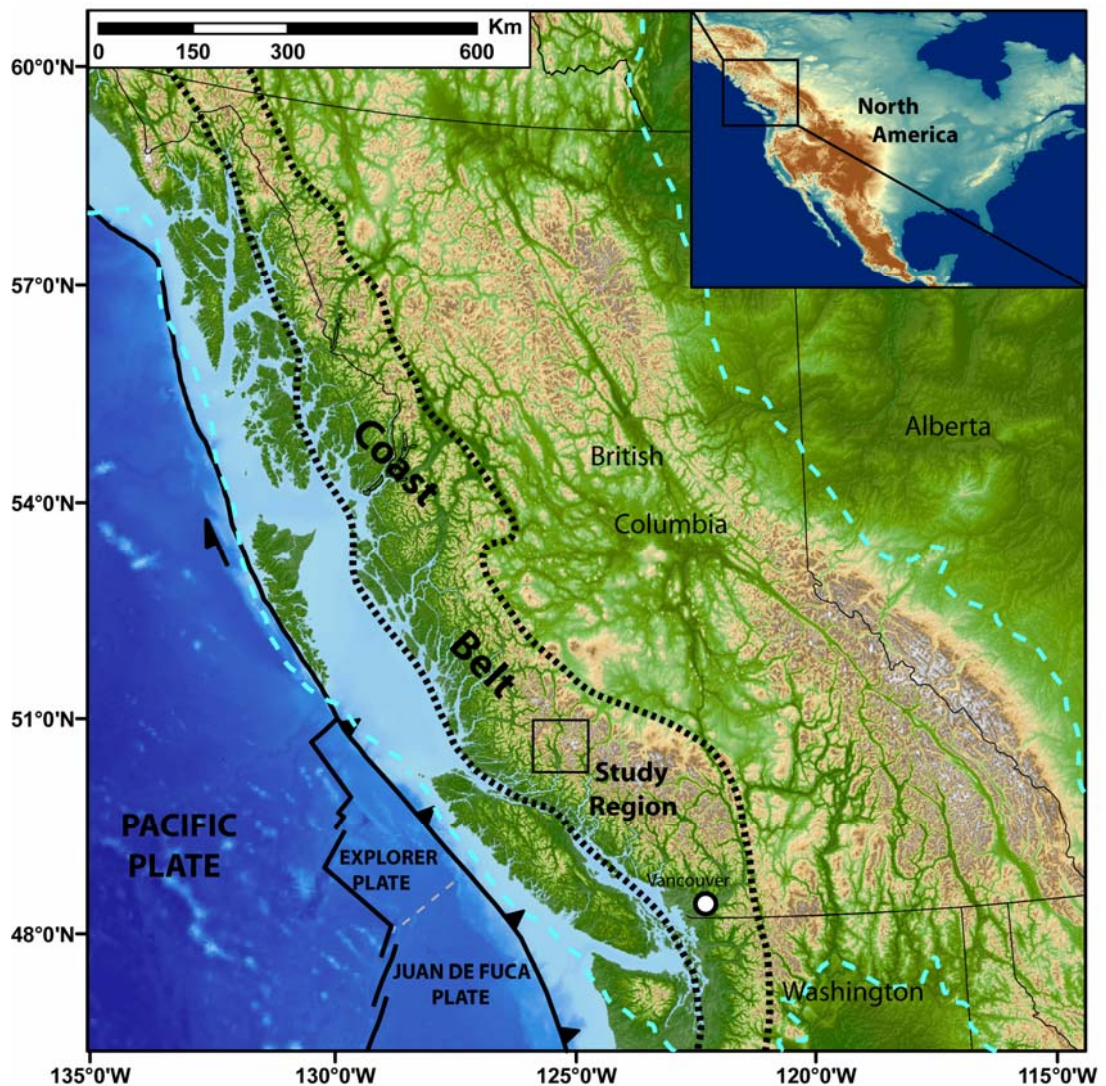
Chapter 2: Effect of Alpine Glaciation on Thermochronometer Age-Elevation Profiles

2.1 ABSTRACT

Low-temperature thermochronometers are widely used to quantify exhumation histories, typically by interpreting sample cooling age-elevation relationships. However, the effects of specific geomorphic processes on age-elevation profiles are seldom considered. We integrate apatite (U-Th)/He [AHe], apatite fission track, and zircon (U-Th)/He thermochronometry with numerical modeling to determine the effect of glacial erosion on an age-elevation profile from the heavily glaciated southern Coast Mountains, British Columbia. AHe data show a distinct break in slope in age-elevation between 1900 – 2100 m. We interpret this break in slope as an acceleration of erosion associated with the onset of alpine glaciation. We use a 3-D thermo-kinematic model to constrain pre- and synglacial erosion rates. Results indicate a preglacial erosion rate of ~0.4 mm/yr that accelerated by a factor of ~2 since ~6 Ma. We propose that glacial valley widening and deepening are responsible for the observed nonlinear AHe age-elevation profile.

2.2 INTRODUCTION

Low-temperature thermochronometers are proven tools for quantifying long-term ($\sim 10^4$ – 10^7 years) exhumation processes (e.g. Hodges, 2003). The most common method for thermochronometer interpretation is analysis of sample cooling age versus elevation (e.g. Wagner et al., 1977). Exhumation rates are calculated from the slope of the best-fit line through an age-elevation profile. Linear age-elevation relationships are interpreted as indicating uniform exhumation. A break in slope suggests a change in exhumation rate, presumably associated with a tectonic or erosional mechanism (e.g.

Fitzgerald et al., 1995). Despite the widespread application of these techniques to tectonic studies, few studies have quantified long-term glacial erosion (e.g. Meigs and Sauber, 2000; Spotila et al., 2004; Thomson, 2002) and no study has examined the effect of a specific geomorphic process on age-elevation profiles.

Glaciers are efficient agents of erosion and should influence erosion rates and thermochronometer age-elevation relationships. Long-term glacial erosion-rate estimates are based primarily on sediment flux data collected over decadal to millennial timescales (max. 2100 yrs), span three orders of magnitude from 0.01 to >60 mm/yr, and hence are highly variable (Hallet et al., 1996a). Erosion rates between 10 – 60 mm/yr are difficult to sustain over the Quaternary because they predict unobserved large magnitudes of erosion (20 – 120 km) and suggest exposure of mantle material.

We use a comparison between numerical model predicted and observed cooling ages from a heavily glaciated valley flank in the Coast Mountains, British Columbia, to quantify the effect of glacial valley widening and deepening on age-elevation profiles.

2.3 GEOLOGIC SETTING

The Coast Mountains are located on the west coast of Canada, extending over 1,000 km from Vancouver to southern Alaska, USA (Fig. 2-1a). Major glaciated valleys traverse the range, with onset of alpine glaciation in the southern Alaskan region inferred to be ~9 Ma from lava flows within tillites (Denton and Armstrong, 1969). Although less clear, glaciation in the southern Coast Mountains is thought to have occurred since the latest Miocene (Clague, 1991).

The Mount Waddington region (Fig. 2-1b) is well suited for applying low-temperature thermochronometry to quantify glacial erosion (Ehlers et al., 2006). This region has been heavily glaciated without significant faulting (Farley et al., 2001; Sweeney et al., 1992), resulting in a purely erosional exhumation mechanism for thermochronometer cooling. The predominantly mid Jurassic to Eocene tonalites and granodiorites (Woodsworth et al., 1991) yield pristine grains for apatite (U-Th)/He [AHe], apatite fission track [AFT] and zircon (U-Th)/He [ZHe] analysis, resulting in reproducible cooling ages (average 1σ error is ~9 % for AHe; Table A-1-1, Appendix 1).

Previous studies have documented the Neogene exhumation history within the Coast Mountains (Fig. 2-1a). AFT and zircon fission-track studies by Parrish (1983) and O'Sullivan and Parrish (1995) characterized the cooling history in the Mt. Waddington region from ~30 – 8 Ma. Shuster et al. (2005) determined ~2 km of erosion since 1.8 Ma by applying ^{4}He/^{3}He thermochronometry to some of the samples presented here. Ehlers et al. (2006) demonstrate that large magnitude and accelerated glacial erosion was pervasive across the southern Coast Mountains. This study complements previous work by addressing how glacial erosion influences thermochronometer age-elevation profiles.

2.4 METHOD AND OBSERVATIONS

Low-temperature thermochronology

Low-temperature thermochronometers record cooling through the upper crust and are sensitive to, among other things, perturbations of the thermal field from topography (Braun, 2005; Ehlers and Farley, 2003). Topography can alter the background thermal field of the upper crust by increasing thermal gradients beneath valleys relative to interfluves (Lees, 1910; Stuwe et al., 1994). Each thermochronometer system is sensitive to a cooling rate dependent closure temperature, so as a sample is exhumed, it will record the time elapsed since passing through this closure temperature (Dodson, 1973). Combining multiple low-temperature thermochronometer systems can provide a robust and detailed exhumation history through the upper crust (Reiners et al., 2003). Because higher temperature systems require more time to be exhumed from their closure temperature to the surface, this multiple systems approach can characterize the exhumation history in this part of the Coast Mountains over ~15 Myr, and therefore capture both the pre- and synglacial erosion regimes.

Data

We present new analyses for twelve samples from a single vertical transect on the western flank of the Klinaklini River Valley (Fig. 2-1b). We sampled the 2300 m vertical extent across a lateral distance of 2500 m. All twelve samples were analyzed for AHe, four were analyzed for AFT, and three for ZHe (Fig. 2-1c; Tables A-1-1 – A-1-3, Appendix 1 for data tables and analytical methods). AHe cooling ages range from 2.3 –

12.0 Ma, with average 1σ error of ~9%. Additionally, the AFT and ZHe cooling ages range from 6.9 – 39.2 Ma, and 10.5 – 21.7 Ma, respectively. Average 1σ errors are 15% for AFT ages and 23% for ZHe.

A distinct break in slope in the age-elevation profile is evident in both the measured AHe and AFT ages. For the AHe data, this break occurs at ~2000 m elevation (Fig. 2-2 a, d), corresponding to a sample age of ~6 Ma, and consistent with estimates for the onset of alpine glaciation in this region. A linear regression through this data yields an apparent exhumation rate of ~0.03 mm/yr prior to ~5.5 Ma, accelerating to ~0.7 mm/yr for the period between 1.98 and ~5.5 Ma. Similarly, the AFT data show a break in slope occurring at 2400 m, corresponding to an age of 12 – 20 Ma (Fig. 2-2 b, e). However, comparison of fission track lengths show long mean lengths (~14.20 ± 0.15 μm) for the three lower samples and shorter lengths (13.26 ± 0.19 μm) for the top sample (Table A-1-2; Appendix 1) suggesting this sample represents the base of an exhumed partial annealing zone (Gallagher et al., 1998) and not a rate increase (see Appendix 1 for detailed discussion of this sample).

Thermo-kinematic model

Quantifying exhumation histories from thermochronometer data can be complicated by temporal and spatial variations in the thermal field samples cool through (Mancktelow and Grasemann, 1997a), which can result from variations in the exhumation rate, and/or topography. We use a 3D thermo-kinematic finite element model to quantify the effect of these perturbations on the thermal field, rock cooling histories, and thermochronometer cooling ages (Braun, 2005; Ehlers and Farley, 2003; Ehlers et al., 2006; Kohl and Hopkirk, 1995). The model solves the 3D advection-diffusion equation with heat production to determine the heat transfer between elements. Details of the modeling approach are given in the Appendix 1 and salient points are summarized here.

The approach followed here is to explore the simplest case of static topography and use differences between predicted and observed thermochronometer ages to infer landscape evolution processes. Future work will use these results to guide simulations that account for the more difficult case of evolving topography. Free parameters in the thermal model include internal heat production (0.8 μW/m^3) and thermal conductivity

(2.7 W/mK) (Lewis et al., 1985). The initial condition of the thermal model is a purely conductive steady-state thermal field (Ehlers et al., 2006) using basal heat flow (20 – 50 mW/m^2) (Lewis et al., 1985) and a constant elevation-dependent surface temperature (T = 4°C at sea level). A transient thermal solution is calculated while samples undergo vertical exhumation at a specified rate for 20 Myr, using a nominal initial age of 50 Ma. Lack of evidence for major active faulting justifies the assumption of purely vertical exhumation.

Simulations were conducted with varying erosion rates from 20 Ma to present. Range of free parameters explored in the kinematic model include pre- and synglacial erosion rates (0.2 – 0.8 and 0.2 – 1.0 mm/yr, respectively), and a variable onset time of glaciation (1.5 – 8 Ma). Particles corresponding to sample locations are tracked backwards through time from the surface into the model interior and the thermal histories are recorded. Using TERRA (Ehlers et al., 2005), each particle time-temperature history is used to predict AHe, AFT and ZHe cooling ages with He diffusion and fission track annealing algorithms.

2.5 RESULTS

We tested 210 combinations of model parameters described above in order to explore two erosional scenarios including: (1) spatially and temporally constant erosion, representing a stable long-term erosional regime, and (2) spatially constant but temporally variable erosion, representing an increase in rate due to glaciation. Rock advection velocities are held constant until a defined threshold time at which point the velocities either remain constant or are increased to represent glaciation. Model output from a given set of free parameters is not unique and represents the tradeoff between variables. Due to this non-uniqueness, we tested across the entire parameter space to identify combinations of parameters that minimize the difference between predicted and observed AHe, AFT, and ZHe ages. We quantified the goodness of fit of each model run with a statistical reduced χ^2 analysis (Ehlers et al., 2003). The χ^2 value is a one-sided distribution, where a value of zero indicates a perfect fit, and higher values represent a progressively worse fit. We calculated χ^2 values for AHe ages only, as there are too few AFT and ZHe ages to compare to model parameters (eq. A-1-2; Appendix 1). Our

criteria for an adequate model are: (1) a χ^2 value below 5.0 (25th percentile), and (2) under-predicting no more than one AHe age.

Scenario 1: Spatially and temporally constant erosion

This scenario considers the simplest case of steady-state erosion. Each simulation explored a different constant erosion rate ranging between 0.2-1.0 mm/yr, for 20 Myr. In the case of exhumation at a constant rate, only rates of 0.6 and 0.8 mm/yr predict cooling ages that adequately fit most of the low-elevation AHe data (Fig. 2-2a). For the higher temperature systems, these rates under-predict all observed cooling ages and generate strictly linear profiles. Although a slower rate of 0.4 mm/yr generates predicted ages that roughly match the AHe data above 2 km, low-elevation ages for all three systems are over-predicted (Fig. 2-2 a – c, squares). Results from this set of models generally yield poor fits to the data with no combinations predicting a break in slope as observed in the AHe data at >2 km elevation. Although some misfit occurs, these model results suggest a long-term (>5 Ma) average erosion rate of roughly 0.4 mm/yr and a short-term (<5 Ma) rate of ~0.6 – 0.8 mm/yr.

Scenario 2: Spatially constant but temporally variable erosion

This scenario evaluates how variations in pre- and synglacial erosion rates influence age-elevation profiles. Several combinations of pre- and synglacial erosion rates, and onset times for glaciation generated an adequate fit to the observed AHe data at elevations below 2 km (Table A-1-4; Appendix 1 for detailed results). Models with an average initial velocity of ~0.4 accelerating to ~0.8 mm/yr at ~4 Ma generated age-elevation profiles close to the data and fall between the triangle and square symbols plotted on Figure 2-2d. The large number of adequately fitting model combinations is reduced when ZHe data is considered by eliminating models with low initial exhumation rates (< 0.4 mm/yr). Predicted ZHe cooling ages require an initial rate of ~0.4 mm/yr to produce enough exhumation to replicate these higher temperature data.

However, no model explored in scenario (2) predicted cooling ages with a break in slope of AHe data similar in magnitude to that observed, although several did produce very subtle breaks in the predicted age-elevation profiles. For example, Figure 2-2d shows two such model runs (triangles and squares) where the top two samples fall slightly off trend from the lower samples. In order to determine the initial rate required

13

to produce a comparable break in slope, an additional model was conducted with an initial exhumation rate of 0.1 accelerating to 1.0 mm/yr at 4 Ma (Fig. 2-2d – f, diamonds). This model predicts AHe cooling ages very similar to those observed at both high and low elevations. However, AFT ages are significantly over-predicted by at least 14 Myr. Furthermore, the predicted ZHe ages poorly fit the data as well, with a 30 Myr misfit. Thus, although an order of magnitude variation between pre- and synglacial erosion rates improves the fit to the AHe data it fails to erode enough material to produce the observed AFT and ZHe ages.

Although implementing temporally variable exhumation in the model does result in similar cooling ages to those observed, the systematic misfit of high-elevation samples suggest that the erosional history is more complex than assumed in these scenarios. To create enough erosion to exhume relatively young AFT and ZHe samples, the long-term erosion rate must be sufficiently high (~0.4 mm/yr). However, in order to produce a significant offset in AHe ages at high elevations, the erosion rate must increase at low elevations while remaining constant or perhaps decreasing at high elevations. This rate change must occur at ~6 Ma to avoid exhumation of AFT and ZHe samples that are younger than we observe. These observations indicate a spatially and temporally variable erosion rate is required in order to reproduce the observed trends in cooling ages.

2.6 DISCUSSION

In this section, we present a scenario whereby glacial erosion can produce a break in slope of an age-elevation profile and compare our results with previous studies in the Coast Mountains.

Spatial variations in glacial erosion

Our results suggest a low pre-glacial erosion rate until ~6 Ma, followed by a factor of ~2 increase in erosion at low elevations (<2000 m). The most likely mechanism for this pattern of erosion is by glacial valley widening and deepening. Hallet (1979) suggested glacial erosion is a function of basal ice velocity. Within the Coast Mountains, ice was thick enough to induce pressure melting at the base of large glaciers (Booth, 1986; Ehlers et al., 2006), therefore increasing basal-sliding velocity and valley bottom

erosion relative to valley walls. Application of this velocity dependent glacial erosion law in numerical models [Habor, 1992] suggests that large, km, scale glacial valley widening and deepening can occur rapidly, and on timescales less than 10^6 yr.

Coupling a glacial landscape evolution and thermal model is an alternative approach to quantifying the effect of glaciation on age-elevation profiles. However, this approach is well beyond the scope of this study and the focus of work in progress. Rather, here we present a conceptual model for the effect of glaciation on low-temperature thermochronometer age-elevation profiles. Figure 2-3 illustrates how glacial valley widening and deepening can influence these profiles. Considering only the effect of valley widening, the topography is modified as glaciers erode the valley wall while not changing the elevation of the valley floor and ridge top (Fig. 2-3a). If erosion outpaces thermal equilibration in the subsurface, excluding the endpoints the distance all samples travel from the closure isotherm to the surface is reduced, decreasing their cooling ages (Fig. 2-3b). In contrast, combined valley widening and deepening causes the valley floor to also be eroded (Fig. 2-3c) so all but the highest elevation sample age is reduced (Fig. 2-3d).

The effects of valley widening and deepening on age-elevation profiles are similar even though they differ in how they spatially distribute erosion within a valley. Both processes produce a break in slope similar to the observed AHe data. However, the primary difference between the resultant profiles is the reduced age of the bottom sample. In our data, this sample yields a relatively young AHe age, implying some component of deepening. However, without knowledge of the preglacial elevations for each sample we cannot quantify the effect of deepening on this lowest sample. Therefore, we suggest that some combination of these effects results in the observed age-elevation profile.

Comparison to previous work

Our finding of an increase in exhumation rates from ~0.4 – 0.8 mm/yr at ~6 Ma is similar to previous exhumation studies in the Coast Mountains (Fig. 2-1a). For example, in the northern Coast Mountains, Farley et al. (2001) document from AHe data an increase in exhumation after ~4 Ma . In the southern Coast Mountains, Mt. Waddington region, O'Sullivan and Parrish (1995) document rapid exhumation at ~5-8 Ma from AFT data and Ehlers et al. (2006) found from bulk AHe ages a minimum 300% increase in

erosion rates starting between 1.5 – 7 Ma. At the same location as this study, Shuster et al. (2005) applied ^{4}He/^{3}He thermochronometry and found a rapid increase in erosion from ~0.5 – 2.5 mm/yr at 1.8 ± 0.2 Ma.   In general, our results are consistent with the previous studies in suggesting an acceleration in Neogene erosion rates. The difference in the magnitude of the acceleration between Shuster et al. [2005] and this study results from the bulk AHe ages used here producing erosion rates averaged over the cooling age of the sample, whereas ^{4}He/^{3}He thermochronometry is sensitive to discrete thermal histories.

2.7 CONCLUSIONS

In this study we suggest that glaciation can significantly alter low-temperature thermochronometer age-elevation relationships. We present AHe, AFT and ZHe cooling ages with distinct breaks in slope of age-elevation profiles corresponding to ~6 Ma for AHe and 12-20 Ma for AFT. We interpret the break in slope of our AHe data to reflect an acceleration of erosion below 2000 m associated with the inception of alpine glaciation in the past ~6 My. By combining 3-D thermal kinematic modeling with low-temperature thermochronometer cooling age data, we explored erosional scenarios of: (1) spatially and temporally constant rates, and (2) spatially constant, but temporally variable rates. We constrain erosion rates from ~0.4 mm/yr, increasing to ~0.8 mm/yr during the early Pliocene. This contrasts with the long-term (>6 Ma) rate of 0.03 mm/yr determined by best-fit regression line. However, neither modeling scenario investigated completely fit the data, suggesting the need for spatially and temporally variable erosion with higher rates at lower (<2000 m) elevations. If erosion rates are higher within valleys compared to adjacent ridges, a break in slope will likely form in the thermochronometer age-elevation relationships. Finally, we suggest that glacial valley widening and deepening are responsible for the nonlinear age-elevation profile in our AHe data and suggest glaciation may have a similar influence on AHe age-elevation profiles collected in other heavily glaciated regions.

2.8 ACKNOWLEDGEMENTS

Official Citation:

Densmore, M.S., Ehlers, T.A., Woodsworth, G.J., 2007, Effect of alpine glaciation on thermochronometer age-elevation profiles: Geophys. Res. Letters, v.34, doi:10.1029/2006GL028371.

2.9 FIGURES

Figure 2-1. Topography and thermochronometer data in the Coast Mountains, British Columbia. (a) Shaded relief DEM with locations of previous studies. (b) Study area in the previously glaciated Klinaklini Valley with a vertical transect of new sample locations and cooling ages. Shaded relief DEM includes snow and ice coverage (stipple pattern). (c) Apatite (U-Th)/He [AHe], apatite fission track [AFT] and zircon (U-Th)/He [ZHe] cooling ages versus sample elevation. 1σ error bars contained within symbol if not visible.

a)

b)

c)
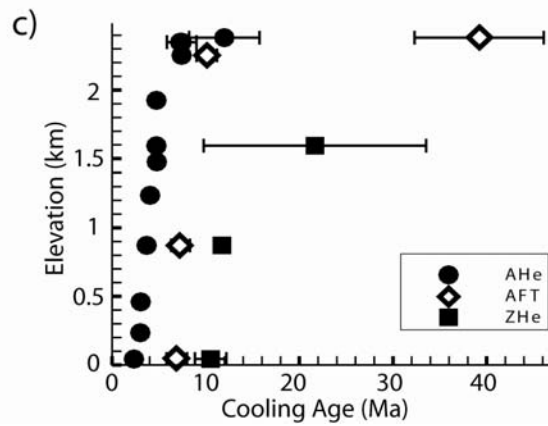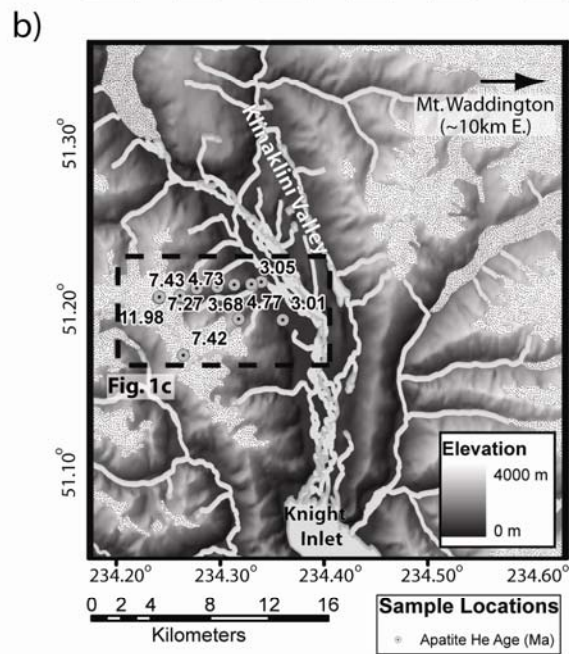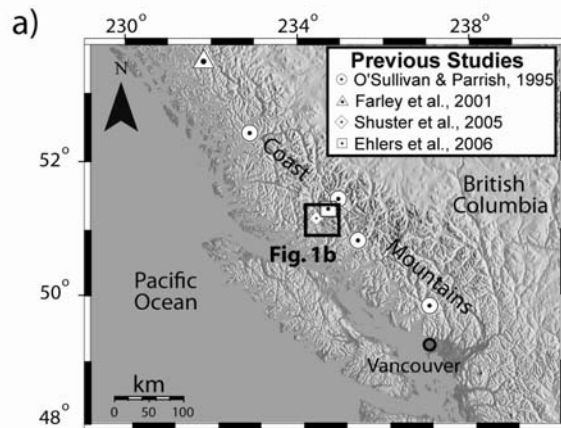
Figure 2-2. Comparison of observed and predicted thermochronometer age-elevation profiles. Observed (filled circles) and predicted (open symbols) cooling ages for uniform (a – c) and temporally variable (d – f) erosion rates: AHe (a & d), AFT (b & e) and ZHe (c & f). 1σ error bars contained within symbol if not visible. Constant erosion-rate models do not predict a break in slope in the AHe data. We highlight three variable erosion models. Two models (open triangles and squares, d – f) bound a region where many parameter combinations yield similar fits (Table A-1-4; Appendix 1). One model (diamonds) fits the AHe data (d), however, the higher temperature systems show significant offset (e & f). Temporally variable erosion models can predict a break in slope but underpredict its magnitude.
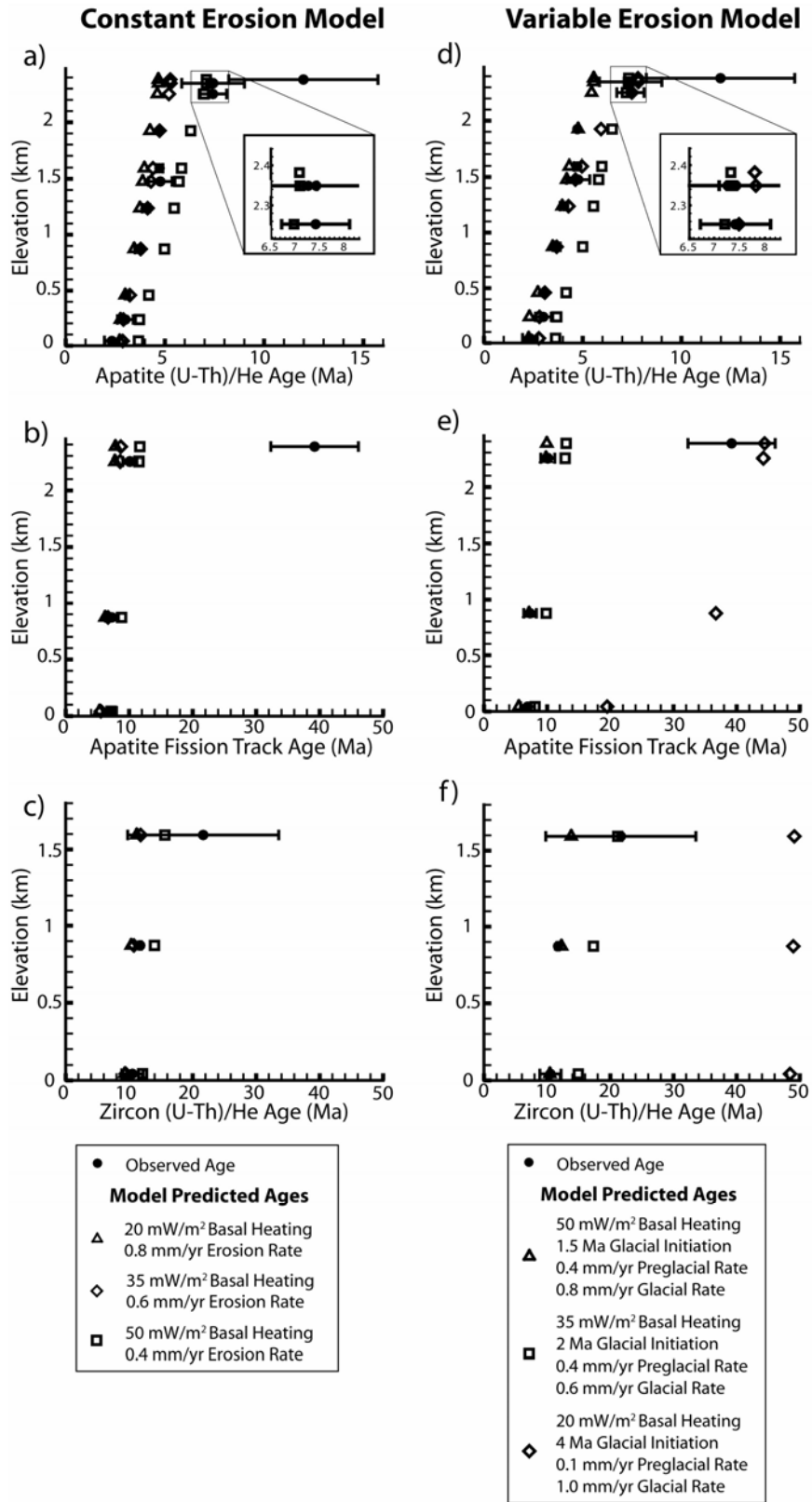
Figure 2-3. Schematic diagram of glacial valley widening and deepening and the effect on thermochronometer age-elevation profiles. Temporal evolution is from initial time t_0 to final time t_2. (a) At all intermediate elevations valley widening reduces the distance traveled from a closure isotherm and (b) decreases the cooling ages. (c) Coupled widening and deepening lowers the valley floor and (d) decreases the corresponding cooling ages. The relative age of the lowest elevation sample may indicate whether (a) widening or (c) coupled widening and deepening is the dominant process.
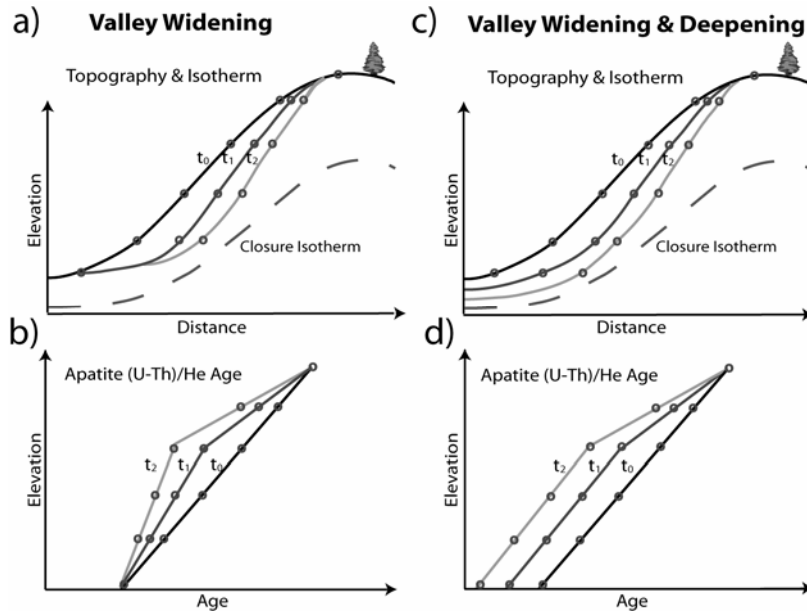
Chapter 3: Quantifying Glacial Denudation with Thermochronology 1: Insights from Apatite (U-Th)/He Thermal Models

3.1 ABSTRACT

Alpine glaciation significantly alters landscapes by eroding broad U-shaped valleys thereby exhuming crustal material. Long-term ($\sim 10^6$ yrs) rates of denudation in glaciated terrains are poorly constrained despite the impact of glaciation on the evolution of mountain topography. Here we quantify the magnitude, rates, and distribution of denudation in the heavily glaciated Coast Mountains, British Columbia, using apatite (U-Th)/He (AHe) thermochronology. Our field area includes the highest peak in the range (Mount Waddington) as well as a major glaciated valley (Klinaklini River Valley) terminating in a steeply sloped fjord encompassing ~4 km of relief. We integrate 44 new and 39 published AHe cooling ages that range from 1.1 – 15.4 Ma. Approaches used to interpret denudation rates from these data include commonly used best-fit regression lines through sample age-elevation profiles and a 1-D thermo-kinematic model. A comparison to more sophisticated 2-D and 3-D approaches is explored in a companion paper. The 1-D thermo-kinematic model uses inputs of the denudation rate, crustal thickness, thermal diffusivity, internal heat production, surface temperature and an estimated initial geothermal gradient. Model outputs include a steady-state solution for

the thermal field and predicted cooling ages. Results from this study include: (1) 1-D thermo-kinematic models indicate denudation rates of 0.2 – 1.5 mm/yr (mean of 0.6 mm/yr). Best-fit regression lines through sample age-elevation plots suggest a denudation rate of 1.0 mm/yr, (2) 1-D model denudation rates generally increase to the northeast through the Klinaklini River Valley with a maximum near a high local peak (Mount Jubilee), (3) breaks in slope of best-fit regression lines indicate an increase in denudation throughout the field region between ~5 and 7 Ma likely associated with the onset of glaciation, (4) calculated denudation rates are highest in intermediate wavelength (peak to peak) valleys of ~5 km, and (5) long-term denudation rates determined here are an order of magnitude lower than short-term (10^2 to 10^3 yrs) rates reported in glaciated southern Alaska.

3.2 INTRODUCTION

Glaciers are significant erosive agents in both temperate and arctic regions. In mid to high latitude mountain ranges they incise broad U-shaped valleys by valley widening and deepening. Historically, studies on glacial denudation have been qualitative, describing distinct features of glaciated landscapes based on observations (e.g. Agassiz, 1864; Gilbert, 1906; Matthes, 1930). In recent studies, links between climate change and tectonics have been hypothesized in coupled landform evolution and numerical models (Beaumont et al., 1992; Koons, 1989; Willett, 1999), motivating more quantitative work addressing the ramifications of different denudation processes on the long-term evolution of orogens (e.g. Brozovic et al., 1997; Champagnac et al., 2007; Herman and Braun, 2006; Herman and Braun, 2008; Molnar and England, 1990; Whipple et al., 1999). Despite these studies, quantifying the effect of glaciation over local and regional scales has not been widely addressed. Work on cross-sectional channel evolution (Harbor, 1992), and hypsometry (Brocklehurst and Whipple, 2004), valley asymmetry (Naylor and Gabet, 2007) and longitudinal profiles of glacial versus fluvial systems (Brardinoni and Hassan, 2006; Brocklehurst and Whipple, 2002; MacGregor et al., 2000) have explored unique aspects of glacial terrains. These studies have primarily focused on trunk-stream evolution over relatively short timescales ($< 10^5$ yrs) as well as

24

characterizing features in 2-D. Transient local and regional features over long timescales ($>10^6$ yrs) have not been similarly examined (Goodfellow, 2007).

Little is known about glacial denudation rates over long timescales. Short-term rate estimates for alpine and continental glaciers span three orders of magnitude (~0.01 to >60 mm/yr) (Hallet et al., 1996b). Extrapolating high rates (>10 mm/yr) over million year timescales is problematic as this implies unreasonable and unseen magnitudes of exhumation in glaciated terrains. In the case of alpine glaciers, current denudation rates are likely dominated by recent rapid deglaciation that are not necessarily representative of the long-term rates (Church and Ryder, 1972; Koppes and Hallet, 2002; & 2006) making it difficult to estimate long-term rates from short-term data (Harbor and Warburton, 1993). Several techniques are available for constraining these glacial denudation rates. A mass balance approach can be applied by measuring the volume of sediment deposited at a river's base level and relating it to drainage basin area (Hebbeln et al., 2007; Milliman and Syvitski, 1992). This approach integrates all sediment derived from a catchment and therefore determines a basin-wide average denudation rate. Cosmogenic radionuclide concentrations can improve on mass balance methods by requiring only a small sample for analysis (Balco and Stone, 2005). Studies have utilized these techniques to constrain the amount of material removed during the last glaciation (e.g. Staiger et al., 2005; Yingkui et al., 2005). However, the ephemeral nature of snow and ice coverage and the duration of glacial/interglacial cycles deters the use of cosmogenic nuclides in glaciated settings (Bierman and Nichols, 2004; Hallet and Putkonen, 1994; Schildgen et al., 2005). This study compliments previous work by addressing long-term rates of glacial denudation using low-temperature thermochronology.

Low-temperature thermochronometers are common tools used to quantify rates of denudation that result from surface processes such as glaciation (e.g. Ehlers, 2005; Hodges, 2003; Reiners and Brandon, 2006), predominantly by interpreting sample cooling age versus elevation (Wagner et al., 1977). These systems provide important information on spatial and temporal variations in long-term denudation. For example various studies have applied low-temperature thermochronometers, such as apatite (U-Th)/He (AHe), to constrain long-term rates of glacial denudation (Berger and Spotila,

2008; Densmore et al., 2007; Ehlers et al., 2006; Farley et al., 2001; Meigs and Sauber, 2000; Shuster et al., 2005; Spotila et al., 2004; Stock et al., 2006; Thomson, 2002).

We complement previous work by integrating 44 new and 39 published AHe samples collected from the heavily glaciated southern Coast Mountains, British Columbia. We interpret the data from this region using two different techniques including conventional regression lines through age-elevation profiles and a 1-D numerical model. This approach allows us to: (1) analyze spatial variations in cooling ages with respect to topography, (2) calculate spatial variations in denudation between these 1-D thermal models, and (3) compare denudation rates with short term ($\sim 10^2$ yrs) estimates. The high density of samples in this study provides insight into the variability in timing and magnitude of glacial denudation across a $\sim$60 x 60 km region. In a companion paper we present (1) a comparison to denudation rates calculated by 1-D approaches here with more sophisticated 2- and 3-D approaches, and (2) estimates of orogen-wide denudation over longer (>10 Ma) timescales from higher-temperature thermochronometer systems (Densmore, 2008c). Thus, the emphasis of this study is the presentation of new data and a quantification of sample exhumation histories from conventional 1D thermal modeling approaches.

3.3 BACKGROUND

The Coast Mountains of British Columbia are a region of dramatic relief ($\sim$4 km) composed of primarily intrusive rocks situated within the greater Canadian Cordillera. Here we present the geologic setting of the Cordillera and the recent regional and local glacial history of the Coast Mountains.

3.3.1 Geology

The Canadian Cordillera is separated into 5 major morphogeologic belts, reflecting the integrated tectonic and geomorphic history of each region (Gabrielse et al., 1991). From east to west, they are the Foreland, Omineca, Intermontane, Coast and Insular Belts (Fig. 3-1). The Foreland Belt forms the easternmost foothills of the

Cordillera and is composed primarily of Paleozoic and early Mesozoic folded clastic assemblages. These sedimentary strata thin to the west where they underlie the Omineca Belt, a product of Mesozoic and early Cenozoic accretion and crustal shortening. This region is characterized by uplifted imbricated thrust sheets of metasedimentary rocks (Gabrielse et al., 1991). Continuing westward is the allochthonous Intermontane belt, defined by its subdued topography and low-grade metamorphism. Next is the Coast Belt, an area of high relief encompassing the Coast Mountains and the northern Cascade Mountains. This narrow belt consists primarily of Late Mesozoic and Early Cenozoic granitic and lesser metamorphic rocks of the Coast Plutonic Complex and has the greatest concentration of plutonic rocks within the Cordillera (Woodsworth et al., 1991). The Coast Belt is a mix of migmatite and gneisses with NW-SE trending elongated discrete and coalescing plutons, predominantly composed of quartz diorite, granodiorite and diorite (Roddick and Hutchison, 1974; Woodsworth et al., 1991). K-Ar and Rb-Sr age determinations in the central Coast Mountains indicate plutonic emplacement during Late Cretaceous through Paleocene (Harrison et al., 1979, and references therein). Finally, the Insular Belt occurs just offshore from the mainland and is comprised of volcanic arc and exotic terranes (Gabrielse et al., 1991).

3.3.2 Neogene Glacial History

Present day topography of the Coast Mountains is characterized by large U-shaped valleys that traverse the range and terminate in steep fjords. Recent glaciations are widely correlative to northern hemisphere events, however onset of glaciation in the Canadian Cordillera is poorly constrained. In this section we highlight the known glacial history in the Coast Mountains. Dated tillites in easternmost Alaska indicate the onset of glaciation ~9 Ma (Denton and Armstrong, 1969) and scattered evidence from dropstones, and ice-contact volcanic deposits suggest glaciation near Queen Charlotte Island during the late Miocene (~5 – 7 Ma) (Higgs, 1991), within the Yukon Territory sometime before 1 Ma (Naeser et al., 1982), and in British Columbia ~1 – 3 Ma (Mathews and Rouse, 1986; Souther et al., 1984). Finally, apatite (U-Th)/He (Densmore et al., 2007; Ehlers et al., 2006) and $^{4}He/^{3}He$ (Shuster et al., 2005) thermochronometer data within the southern

Coast Mountains (Waddington region) indirectly suggest an inception of glaciation ~6 Ma with intense denudation occurring at 4 – 1.8 Ma.

Terrestrial Quaternary deposits in the Cordillera generally record Wisconsinan (~10 – 75 ka) and Holocene events, with Sangamonian (~75 – 125 ka) and earlier deposits either covered by thick tills or completely removed by subsequent glaciations (Clague, 1991). Marine oxygen isotope and magnetic stratigraphy data from central Pacific Ocean deep-sea sediments record eight major glacial cycles since 800 ka, each lasting ~100 ka, with many more frequent but less intense events prior to 800 ka (Clague, 1986; Shackleton and Opdyke, 1973).

The Coast Mountains were the source area for Cordilleran ice and each glacial highstand dramatically increased ice thickness and flow through the region. The earliest record of ice-sheet glaciation in southern British Columbia occurred ~130 ka (Armstrong, 1981; Shackleton and Opdyke, 1973). The Cordilleran ice sheet covered most of British Columbia and repeatedly formed ice domes centered within or to the east of the Coast Mountains that dictated the direction of ice flow (Clague, 1991, and references therein). Two intense glaciations have been identified since ~100 ka, the penultimate, during the early to middle Wisconsinan, and the last (Fraser) glaciation during the late Wisconsinan (Fulton, 1984). These events were similar although penultimate glacial deposits lie beyond Late Wisconsinan glacial limits (Clague, 1991 and references therein). During the Fraser Glaciation, ice expanded beyond the limits of the Coast Mountains, Olympic Mountains and Cascade Range. Alpine glaciers coalesced to form piedmont ice lobes that extended to the continental shelf to the west, into eastern British Columbia where they may have merged with the Laurentide ice sheet, south into the Puget lowlands and eastern Washington, and as far north as southern Alaska and Yukon (Booth et al., 2004; Clague, 1991). The maximum extent of ice during this time appears to have lagged behind that of the Laurentide Ice-Sheet by a few thousand years, growing rapidly at ~18 ka (Clague et al., 1980).

By ~15 ka, the ice began to retreat very rapidly (Blais-Stevens et al., 2001; Kovanen and Easterbrook, 2001; Mosher and Moran, 2001). Limited evidence suggests a brief cooling trend correlative with the Younger Dryas period (Friele and Clague, 2002; Mathewes et al., 1993) before glaciers receded to their final positions today in the

highlands of the Coast Mountains. Presently, large glaciers and ice fields sit adjacent to the high peaks, especially in the Mount Waddington region (Fig. 3-1, box).

3.3.3 Previous Thermochronology Studies

Low-temperature thermochronology studies within the Mount Waddington region provide estimates of the long-term (10^6 yrs) denudation history. Here we present local studies while additional work from throughout the range is summarized in Densmore et al. (2008c, and references therein). Parrish (1983) determined zircon and apatite fission track (ZFT & AFT) ages ranging from 18.6±1.8 – 99.9±3.8 Ma and 5.2±0.6 – 88.3±8.1 Ma, for ZFT and AFT respectively. From this, Parrish concluded there were 3 distinct periods of apparent Cenozoic denudation: intense Paleocene-Eocene (>40 Ma) denudation in the central and eastern regions, subdued denudation during the middle Cenozoic (~10 – 30 Ma) through the axial part of the range, and rapid Pliocene (~5 Ma) to recent denudation in the southern area. This AFT data was reexamined by O'Sullivan and Parrish (1995) for the effect of apatite composition on fission track data, though the overall interpretations remained similar. Densmore et al. (2007) and Ehlers et al. (2006) used ZHe, AFT and a subset of AHe data presented here from the Mount Waddington region. Cooling ages from these studies range from 2.4±0.4 to 27.3±1.4 Ma for the ZHe, 6.9±1.1 to 39.2±6.9 Ma for AFT ages, and 1.5±0.1 to 15.4±2.8 Ma for AHe ages. Results from these studies demonstrate acceleration in denudation rates from ~6 to 2 Ma attributed to glaciation. Finally, Shuster et al. (2005) applied ^{4}He/^{3}He thermochronometry to constrain removal of ~2 km of material in the last 1.8 Myr +/- 0.2 Ma. The 1.8 Ma onset of rapid exhumation in the southern Coast Mountains suggests that glaciation at this time may have intensified. This interpretation awaits verification from sparsely available marine records or future ^{4}He/^{3}He thermochronometer studies.

3.4 METHODS

3.4.1 Apatite (U-Th)/He Thermochronometry

The analytical procedure used here for determining AHe cooling ages follows that of House et al. (2000), with analyses preformed at the California Institute of Technology

laboratory. Rock processing and mineral separation were preformed by Apatite to Zircon, Inc. using standard heavy-liquid separation techniques. Apatite grains were selected using standard microscopy under crossed-polarized filtered transmitted light to identify grains that meet the following criterion: each grain must have (1) an Ft value of >0.70 (Farley et al., 1996), (2) no inclusions of U, and Th rich mineral phases, and (3) a morphology as near to a complete hexagonal prism as possible. Each grain was loaded in a platinum tube, laser step-heated with the evolved helium measured on a quadrupole mass spectrometer using isotope dilution, then digested and analyzed for ^{238}U, ^{232}Th and ^{147}Sm using an inductively coupled plasma mass spectrometer again using isotope dilution. The amount of daughter product (^{4}He) is related to the parent (^{238}U, ^{232}Th or more rarely ^{147}Sm) to determine a sample cooling age. Analytical error associated with this method is typically low, around 2% (House et al., 2000). A minimum of three grains for each sample were run as replicates to determine age reproducibility. Errors presented here are 2σ deviation from the average age for each sample, with an average of ±1.0 Ma (17.4%) for all samples.

A thermochronometer age records the time since the sample was at a particular cooling rate dependent temperature, commonly referred to as the effective closure temperature (Dodson, 1973). In the specific case of AHe, this temperature is ~70°C for a cooling rate of 10°C/Myr (Farley, 2002). Above this temperature, ^{4}He derived from α-decay of ^{238}U, ^{232}Th and ^{147}Sm can readily diffuse out of the crystal lattice as quickly as it is produced. At temperatures between ~45 – 75°C, helium is partially retained (the He partial retention zone, or PRZ) and below 45°C all ^{4}He produced is trapped within the grain. The low closure temperature of the AHe system lends itself to constraining rock cooling through upper crustal temperatures and quantifying near surface disturbances to the thermal field (e.g. from topography and surface processes).

Interpreting AHe data in the context of glacial denudation can be problematic due to exhumation complexities such as intense fluvial denudation or faulting. Measured AHe ages average the integrated cooling history from the closure temperature to the surface. Using a single cooling age we cannot distinguish between different exhumational processes, such as glacial versus fluvial and hillslope denudation. However, exhumation from other processes in the study area is likely subsidiary to

glacial denudation given the protracted and intense glacial history of the range. The Mount Waddington region has not had significant fault activity since at least the late Miocene (Sweeney et al., 1992), and today continuous and undeformed lateral and end moraines are present in the Waddington region suggesting little to no recent faulting. Furthermore, although fluvial and hillslope processes have certainly been active since the glaciers receded, glaciation has likely been the dominant control on the modern morphology of the range.

3.4.2 Estimation of Denudation Rates from 1-D thermal model

Thermochronometer cooling ages are commonly used to estimate the magnitude and rate of exhumation (Ring et al., 1999). Cooling ages are dependent on the thermal history during exhumation. The background thermal field is influenced by a number of factors, including heat flow into the base of the crust, rock thermophysical properties, topography, erosion and sedimentation, fluid flow, and faulting (Ehlers, 2005). The simplest approach we use to interpret exhumation rates is to take the slope of a best-fit regression line through a plot of sample age versus elevation. This approach is commonly used in thermochronometer studies due to its simplicity. A second approach used here involves a 1-D thermal model that accounts for advective and conductive heat transfer. Here, we use AGE2EDOT (Brandon et al., 1998; Ehlers et al., 2005) to estimate cooling ages from samples exhumed with an assumed steady and constant denudation rate. This program uses input parameters of layer thickness (km), thermal diffusivity (km^2/Myr), uniform internal heat production (°C/Myr), surface temperature (°C), and an initial near-surface thermal gradient for no denudation (°C/km) (Table 3-1) to solve for a steady-state thermal field (Reiners and Brandon, 2006):

Equation 3.1:

$$T(z) = T_s + (T_L - T_S + \frac{H_T L}{\dot{\varepsilon}}) \frac{1 - e^{\dot{\varepsilon} z / \kappa}}{-e^{-\dot{\varepsilon} L / \kappa}} - \frac{H_T z}{\dot{\varepsilon}}$$

where T_S is the surface temperature, T_L the temperature at the base, H_T the heat production, L the layer thickness, $\dot{\varepsilon}$ the denudation rate, z the depth, and κ the thermal

diffusivity. Using this approach, cooling ages for any given thermochronometer system can be related to a denudation rate (Fig. 3-2).

Using a 1-D advective thermal model provides a more robust estimate of the denudation rate than the age-elevation method due to the age-elevation assumptions of a constant exhumation rate for all samples, and that all samples pass through the closure temperature at the same depth (Fitzgerald et al., 1995; Reiners and Brandon, 2006). Using a regression line technique necessitates a vertical transect of samples collected over a short horizontal distance. A 1-D thermal model eliminates the need for vertical transects and can provide denudation rate information on a single sample.

Caveats to our 1-D steady-state modeling approach are that it does not account for the effects of topography, elevation, or thermal transients on sample cooling ages. AHe cooling ages vary with elevation and samples collected at high elevations should be older than those collected at low elevations. This elevation relationship is not incorporated in a 1-D calculation, although it can be corrected for as discussed later. In a companion paper (Densmore, 2008a) we apply a 3-D transient thermo-kinematic model to the same samples and document differences in calculated denudation rates from these various methods. Additionally, the AHe closure temperature is dependent on radiation damage within an apatite grain (Shuster et al., 2006), correlating with the effective uranium concentration (eU). Grains presented here have an eU of ~28 ppm, equating to an AHe closure temperature of ~64 °C (Shuster et al., 2006). This effect is not accounted for using AGE2EDOT. Consequently, predicted cooling ages using a sophisticated 3-D thermal model (Densmore, 2008a) indicate ~10% difference between assumed Durango kinetics and grains with an eU of 61.8 ppm, resulting in a minor (<5 %) difference in predicted denudation rates. Here we report what can be used from a quantitative analysis and a step-wise increase in model complexity compared to the common approach of a regression line through data in age-elevation space.

3.5 RESULTS

3.5.1 AHe Data

We report new analyses from 44 samples along with 39 published AHe cooling ages covering the Mount Waddington region of the Coast Mountains (Fig 3-3). Compiled ages range from 1.1 – 15.4 Ma (Table 3-2). Samples were collected over a ~60 x 60 km area spaced at ~4 km intervals. Sample elevations cover nearly 4 km of relief from the peak of Mount Waddington (4019 m, highest peak in B.C.) to near sea level at Knight Inlet over a distance of ~40 km. Between these two points stand Mount Jubilee (2263 m) and the Klinaklini Valley, a broad U-shaped valley ~15 km wide between ridges and with 2000 m of relief over a horizontal distance of ~7 km.

3.5.2 Age-Elevation Profiles

Subsets of the data are presented in Figure 3-4 to highlight variations in sample age versus elevation and distance across the study area. Data was grouped into four transects with the best fit regression line through each transect yielding the apparent denudation rate over the last ~6 Ma (Figs. 3-4c – f). Samples near the valley bottom (< 400 m) were grouped for comparison of low-elevation samples versus distance up-valley. A denudation rate cannot be calculated from a simple regression line in this subset as these samples are not arranged as a vertical profile and cover a large horizontal distance.

Transect 1. This transect (Fig. 3-4c) represents the most densely sampled region in our field area. Ages range from 2.3±0.7 – 12.4±6.7 Ma. Relief in this region is over 2300 m from 43 to 2382 m over a horizontal distance of ~8 km. The best-fit regression line yields an apparent denudation rate of 0.8 mm/yr for the last ~6 Ma. This profile has a distinct break in slope at ~2000 m, corresponding to a cooling age of ~6 Ma.

Transect 2. On the eastern flank of Mount Waddington, ages along Transect 2 (Fig. 3-4d) range from 4.0±0.3 to 14.1±0.8 Ma. Sampling here spans the greatest relief of all transects from 750 to 4000 m over ~18 km horizontal distance. The age-elevation profile is steep for the recent history (< 8 Ma) with a calculated denudation rate of 1.1 mm/yr. This profile has a break in slope at ~3000 m, corresponding to a cooling age of ~8 Ma.

33

Transect 3. Transect 3 (Fig. 3-4e) spans from the Klinaklini Valley to the peak of Mount Jubilee with ages ranging from 1.7±0.1 – 4.0±0.7 Ma. This region consists of steep slopes and high relief from the valley floor at 251 m to the peak of Mount Jubilee at 2418 m over a short horizontal distance of ~7 km. In contrast to other presented transects, the age-elevation profile here does not display a break in slope. Instead, ages follow a linear trend with an apparent denudation rate of 1.1 mm/yr.

Transect 4. The final transect (Fig. 3-4f) is off-valley from the Klinaklini Valley, just north of Knight Inlet. Here, ages range from 4.6±5.0 to 14.3±5.8 Ma. Relief spans >2100 m from 165 to 2367 m, over a horizontal distance of ~16 km. The best-fit regression line yields a denudation rate of 1.0 mm/yr. However, large error (>100%) associated with the lowest elevation data point, limits our ability to report a meaningful denudation rate. A slight break in slope may occur in this profile as well, however due to high error (~40%) we do not extend our interpretation beyond ~8 Ma for this transect.

Valley Bottom Samples. Cooling ages from low-elevation (< 400 m) samples near the valley bottom were compared to resolve spatial variations within the Klinaklini Valley. These samples range from 1.7±0.1 to 4.8±0.6 Ma over a lateral distance of ~35 km. In general, AHe cooling ages decrease from south to north upvalley. The youngest age in the suite (1.7 Ma), sample 01MR-59, is roughly halfway through the section coinciding with the base of Transect 3.

Interpretation of Age-Elevation Profiles. Age-elevation relationships provide information on the duration and rate of denudation. Apparent denudation rates determined from these profiles over the last ~8 Ma range from 0.8 to 1.1 mm/yr. Some transects presented here have a break in slope of age versus elevation above ~2000 m corresponding to ~5 to 10 Ma, with the exception of one, Transect 3 (Fig. 3-4) for which samples are not available above ~2400 m. Higher temperature AFT data from O'Sullivan and Parrish (1995) and Densmore et al. (2007) exhibit a break in slope at ~10 – 15 Ma which may suggest exhumation in the region began at this time. A break in slope is commonly interpreted to be indicative of an increase in the denudation rate. In the absence of documented recent faulting in this region and no change in plate motions over this time interval we interpret the break in slope as due to the onset of glaciation. Therefore, we infer that glaciation within the central Coast Mountains began ~6 Ma and

was most intense at elevations below ~2000 m. However, the break in slope in AHe ages apparent in Transect 2 occurs above ~3000 m and may indicate an exhumed PRZ. This implies exhumation of samples from near the ~70°C isotherm and not necessarily a change in rate. The relatively high elevation of the break in slope and older cooling ages along this flank of Mount Waddington suggests a lower amount of total denudation in the region. O'Sullivan and Parrish (1995) report a similar interpretation in AFT data in the same region where they identify a partial annealing zone (PAZ) of fission tracks occurring at ~2200 m. This lower elevation is expected as the AFT system is sensitive to a higher closure temperature and therefore occurring lower in the section. Our AHe data support an exhumed PAZ and suggest all other transects explored have experienced more intense glaciation that has removed this older signal of cooling. Finally, Transect 3 has no break in slope in age versus elevation. We infer this is due to high rates of denudation causing very young cooling ages, even at elevations above 2000 m, completely overprinting the signal of previous cooling history. This indicates the record of cooling near Mount Jubilee records only recent and very rapid exhumation between 2 – 4 Ma.

3.5.3 Horizontal Swath Profiles of Cooling Ages

We minimize the effect of topography on cooling ages by evaluating samples along different horizontal swath profiles (Fig. 3-3) with samples grouped into bins based on their elevation (Figs. 3-5 and 3-6). Each profile is 10 km wide, roughly twice the critical wavelength the AHe system is sensitive to (Braun, 2002a). In some cases, samples within 2km of a swath were considered to fill data gaps. Cooling ages are divided into bins based on elevation: low elevation (< 1000 m), high elevation (>1000 m), and a set of similar elevation samples within each profile (within 400 m) to highlight variations across the profile.

Northern and Southern Klinaklini Valley Profiles. The profiles across the Klinaklini Valley illustrate the high relief and rugged topography of this region (Fig. 3-5a and b). Cooling ages in the southern profile average 4.2 Ma for samples below 1000 m and 9.4 Ma for samples above 1000 m (Fig. 3-5c). There is no apparent trend in cross-valley samples as cooling ages are roughly equivalent within error across the Klinaklini Valley. Similar elevation samples near 2000 m are also comparable on either side of the

valley. There is no obvious spatial pattern within this grouping other than cooling ages are generally older at higher elevations.

Cooling ages from samples in the northern profile average 2.9 and 6.6 Ma for samples below and above 1000 m, respectively (Fig. 3-5d). Samples from similar elevations along both the northern and southern profiles generally have ~2 Ma younger ages on the east side of the valley compared to the west. Samples west of the valley axis show a strong correlation between older ages and higher elevations. On the east side of the valley near Mount Jubilee, samples above 1500 m are younger than or equal to samples below 1000 m elsewhere in the profile.

Waddington Profiles. The Waddington profiles do not include the deep Klinaklini Valley but instead incorporate cooling ages along the flanks of Mount Waddington (Figs. 3-6a and b). Samples along the NE profile average 4.2 and 5.4 Ma below and above 1000 m, respectively (Fig. 3-6c). The average cooling age for samples above 1000 m is the lowest of all profiles presented. Additionally, all cooling ages on the southwest end of the profile near Mount Jubilee are very low regardless of elevation. This trend is also apparent in similar elevation samples that reveal a marked low near Mount Jubilee.

Finally, most samples along the NW Mount Waddington profile were collected at similar elevations with none collected below 1000 m. Cooling ages along this profile range from 3.8 to 14.1 Ma. Similar elevation samples near ~1700 m exhibit a concave up pattern of ages with an average of 6.3 Ma (Fig. 3-6d).

Interpretation of Swath Profiles. The previous spatial variations in cooling ages are interpreted here. Within the southern Klinaklini Valley, comparable ages on both sides of the valley indicate similar magnitudes and rates of denudation. In comparison, the northern profile yields consistently younger cooling ages within each elevation bin indicating a higher rate of denudation. The presence of many young AHe ages near Mount Jubilee suggests focused denudation in this region since ~4 Ma. This is in agreement with the findings of Ehlers et al. (2006) who suggested a paleotopographic high has been removed between Mount Jubilee and Mount Waddington using a number of the same samples here. Finally, samples along the NW Mount Waddington profile display a concave up pattern of cooling ages. This pattern is typical of a large

topographic high that perturbs isotherms causing the thermal field to adjust and mimic a damped version of topography. Consequently, samples that cool directly beneath the topographic high will have the lowest ages, as seen here. Furthermore, this pattern suggests near uniform exhumation across the profile.

3.5.4 Denudation Rate Estimates

Using AGE2EDOT (Brandon et al., 1998; Ehlers et al., 2005) we calculate a denudation rate for each sample and compare this with sample elevation (Fig. 3-7) and spatial position (Figs. 3-8 and 3-9). Here we analyze the calculated rates by grouping the data into subsets along the valley bottom and across multiple topographic profiles as above. We look at variations in denudation rate at different elevations along each profile to identify spatial variations as a function of the topography.

All Data. Calculated denudation rates for the entire dataset span 0.2 to 1.5 mm/yr with an average of 0.6 mm/yr (Fig. 3-7a). A higher AHe cooling age results in a lower calculated denudation rate, and in general these rates are inversely correlated with AHe age versus elevation. The line shown on Figure 3-7a is a best-fit regression through the data. A clear correlation exists between elevation and denudation rate with samples from higher elevations generally yielding a lower denudation rate. However, the low R^2 value (0.322) indicates that this is not a perfect relationship and suggests that although elevation does affect the calculated rates, a signal of variable denudation rate at different elevations is present. Comparing samples of similar elevation reduces the relative influence of this elevation dependence.

Valley Bottom Data. Valley bottom samples in Figure 3-4g show an increasing denudation rate south to north up valley from 0.6 to 0.9 mm/yr (Fig. 3-7b). However, the maximum rate of 1.3 mm/yr is roughly halfway through the suite of samples at the base of Mount Jubilee. Again, samples in this group vary in elevation by ~300 m and therefore the influence of elevation on calculated denudation rates is minimal.

Northern and Southern Klinaklini Valley Profiles. Along the southern profile of the Klinaklini Valley denudation rates range from 0.2 to 0.9 mm/yr with an average 0.5 mm/yr (Fig. 3-8c). The highest calculated denudation rate is near the valley axis corresponding to the lowest elevation sample. Similar elevation samples near ~2000 m

average 0.3 mm/yr with a maximum of 0.5 mm/yr on the east side of the valley. As with cooling ages within this profile, no clear correlation exists between denudation rate and distance from valley center. Calculated rates from samples above and below 1000 m are consistent within this profile, averaging ~0.3 and 0.7 mm/yr, respectively.

In the northern Klinaklini Valley profile calculated rates range from 0.2 to 1.3 mm/yr, with an average of 0.6 mm/yr (Fig. 3-8d). Again the highest calculated rate is near the valley bottom at the base of Mount Jubilee. Similar elevation samples near ~2200 m average 0.4 mm/yr with a maximum of 0.7 mm/yr near the crest of Mount Jubilee. In general, denudation rates are higher on the east side of the Klinaklini Valley than on the west. Furthermore, denudation rates are more varied within each elevation range unlike the southern profile.

Waddington Profiles. The highest and lowest calculated rates from any point are along the NE Waddington profile. Here rates span 0.2 to 1.5 mm/yr with an average of 0.7 mm/yr (Fig. 3-9c). Note that this highest rate is from a sample at >1700 m elevation while the lowest rate is from the peak of Mount Waddington at 4000 m. Similar elevation samples of ~1500 m average 0.8 mm/yr. However, a very pronounced group of samples near Mount Jubilee yield significantly higher rates. Samples immediately adjacent to Mount Jubilee have an average denudation rate of 1.0 mm/yr, nearly a factor of two higher than the mean rate of all samples. The wide range of denudation rates for samples from >1000 m is likely the result of the large elevation range (3750 m) captured in this profile that is not present in any other profile.

Finally, rates along the NW Waddington profile range from 0.2 to 0.7 mm/yr, with an average of 0.5 mm/yr (Fig. 3-9d). Note the 0.2 mm/yr denudation rate is again the lowest in the entire dataset and occurs at the highest elevation. Similar elevation samples near ~1600 m average 0.5 mm/yr with an increase in rate nearing Mount Waddington and a maximum of 0.7 mm/yr.

Regional Patterns in 1D Rates. Patterns in calculated denudation rates follow the interpretations from AHe cooling-age profiles above. Calculated rates from low-elevation (<1000 m) samples reinforce the idea that denudation increases upvalley and is focused near Mount Jubilee. Average denudation rates from samples below 1000 m are ~0.7 (Fig. 3-8c) and 0.9 mm/yr (Fig. 3-8d) for the southern and northern profiles,

respectively. Additionally, denudation rates are generally higher on the east side of the Klinaklini Valley than on the west with average rates of ~0.9 and 0.8 mm/yr (Figs. 3-8c and d) over the same elevation range. These observations suggest focused glacial intensity in the northeast of the field region, with a maximum near Mount Jubilee.

In addition to spatial variations in denudation, a positive correlation appears between denudation rate and glacial basin size. We again compare rates determined at low (<1000 m) elevations for consistency and to reduce the influence of elevation. In smaller tributary valleys we find generally low denudation rates averaging ~0.6 mm/yr, as seen in the southern region of the valley (Fig. 3-10). However, larger valleys currently occupied by glaciers, such as the Franklin Glacier, exhibit very high denudation rates averaging ~0.9 mm/yr. Lastly, the large Klinaklini Valley has moderate calculated denudation rates on the valley walls, averaging ~0.8 mm/yr. Again, these findings support focused denudation along the flanks of Mount Jubilee.

3.6 DISCUSSION

In this section we discuss spatial variations in denudation, relate our findings to previous work in the region, and compare denudation rate estimates derived from best-fit regression lines and a 1-D thermal model.

3.6.1 Spatial Variations in Denudation

The southern region of our study area is characterized by relatively low denudation rates at all elevations, from 0.2 to 0.6 mm/yr, with lower rates with increasing distance from the valley axis (Fig. 3-10). This section of the field area has many smaller tributary valleys that drain in to the Klinaklini. Due to their small size, these valleys likely did not contribute much to the total ice flux through the Klinaklini River Valley and therefore experienced lower denudation rates and magnitude of exhumation.

Traversing north through the valley, denudation rates are fairly uniform on the western slope near the valley axis. Here, rates average ~0.7 mm/yr across the valley flank from just north of Knight Inlet over 20 km to the Klinaklini Glacier (Fig. 3-10).

Within the valley, rates are generally high compared to other low-elevation samples (~0.9 mm/yr vs. 0.6 mm/yr). These observations indicate elevated denudation within the major valley compared to most tributaries.

Denudation rates from the east slope of the Klinaklini valley are anomalous. Samples in this region have higher calculated denudation rates than any other at similar elevations. This is especially true approaching Mount Jubilee and continuing eastward to the Franklin Glacier where the average denudation rate is 1.1 mm/yr. Calculated rates here are higher than anywhere within the field region for any elevation set. It is unclear whether this represents an increase in ice flux due to an input from the flanks of Mount Waddington or perhaps the removal of material and reorganization of the paleotopography, a focusing coincident with the confluence of ice, or differing degrees of erodability.

Continuing northeast past the Franklin Glacier toward Mount Waddington, calculated denudation rates decrease higher in the catchment, from 0.8 – 0.6 mm/yr (Fig. 3-10). The summit and east flank of Mount Waddington have a moderate rate, averaging 0.5 mm/yr.

Finally, we address the magnitude of rate change over small spatial distances for similar elevation samples (Figs. 3-8 and 3-9). We neglect the northern profile which appears to have two distinct populations of ages (Fig. 3-8d). The southern (Fig. 3-8c) and NW Waddington (Fig. 3-9d) profiles have very similar trends in terms of magnitude of change in calculated denudation rates. In the southern profile, denudation rates change by ~0.2 mm/yr over a distance of ~40 km while along the Waddington profile rates differ by ~0.3 mm/yr over ~50 km. These profiles capture significant features in the landscape, namely the Klinaklini River Valley and Mount Waddington, respectively. These large, long-wavelength topographic features alter the subsurface thermal field, which is not accounted for in 1-D calculations. In contrast, rates along the NE Waddington profile (Fig. 3-9c) should have a component of this effect, but are completely dominated by denudation near Mount Jubilee. Along this profile the range of rates is ~0.9 mm/yr over ~20 km. This amplitude and wavelength are significantly different than that caused by large topographic features. This analysis supports the previous assertion of increased denudation near Mount Jubilee.

3.6.2 Comparison with Previous Work

The long-term average denudation rates presented here are comparable to previous studies within the Mount Waddington region but are significantly less than sediment flux data from modern glacial systems in Alaska. Our 1-D thermal model rates range from ~0.3 to 1.2 mm/yr for the last ~10 Myr. These are comparable to those reported by Densmore et al. (2007) who found rates of ~0.4 – 0.8 mm/yr along Transect 1 in this work. Additionally, Farley et al. (2001) documented exhumation of ~0.4 mm/yr within the last 4 Ma in the central Coast Mountains. However, Spotila et al. (2004) found long-term denudation rates nearly an order of magnitude higher (~3 mm/yr) in southern Alaska. This difference may be caused by a number of factors including variations in lithology, tectonic complications or glacial processes. Lithologies sampled by Spotila et al. within the Chugach-St. Elias Mountains included sandstones, gneisses and graywackes among others. These may provide a more erodible substrate than the crystalline, predominantly granodiorite rocks found in the Coast Mountains. Additionally, this region of Alaska is tectonically active and results may reflect the effect of tectonic uplift increasing slopes and accelerating denudation. Lastly, many of the glaciers in the Chugach-St. Elias Mountains are tidewater glaciers and may be subject to higher rates of glacial sliding and ice flux. Our findings of locally enhanced denudation near Mount Jubilee support that of Ehlers et al. (2006) who identified a paleotopographic high ~16 km southwest of Mount Waddington that has been removal by accelerated glacial denudation.

Short-term denudation rate estimates from Alaska far out-pace long-term averages calculated here. Sediment flux studies in southern Alaska indicate rates 2 orders of magnitude higher than those found here, up to ~64 mm/yr (Hallet et al., 1996b). Koppes and Hallet (2006) find an average denudation rate of ~9 mm/yr when revised to allow for an increase rate of sediment discharge during rapid retreat. Figure 3-11 compares the glacial denudation rates of Hallet et al. (1996b) with results of this study and Spotila et al. (2004). Long-term rates derived from thermochronology are at least 50% less than minimum short-term estimates, and more than an order of magnitude less than typical reported rates. Short-term estimates of glacial denudation rates are likely governed by

transient events such as glacial surges and retreats that are averaged out in thermochronometer data, or represent sediment evacuation from local sinks and are not representative of long-term rates.

3.6.3 Comparison of Denudation Rates

Average denudation rates calculated using AGE2EDOT are lower than those determined using regression lines for samples < ~6 Ma. The rates calculated by these two methods differ by 15 – 275%. Calculated rates for Transect 1 range between 0.2 – 1.0 mm/yr, averaging 0.7 mm/yr. This average rate is ~15% lower than determined from the best-fit regression line (0.8 mm/yr). Transect 2, on the east flank of Mount Waddington, spans 0.4 – 0.6 mm/yr with an average of 0.4 mm/yr. This mean value is lower by more than a factor of 2 than that determined using a regression line (1.1 mm/yr). Near Mount Jubilee calculated rates for Transect 3 span 0.7 – 1.3 mm/yr with an average of 0.9 mm/yr. This rate is ~20% lower than the best-fit regression line indicates (1.1 mm/yr). Finally, in the southern region of the valley Transect 4 spans 0.3 – 0.6 mm/yr with an average of 0.4 mm/yr. Again, this rate is lower by more than a factor of 2 than the best-fit regression line rate of 1.0 mm/yr.

The regression-line method assumes all samples pass through the closure isotherm at a constant depth below the surface. This assumption is problematic when samples are spread over a large (>10 km) horizontal distance. The regression line method can lead to an over-prediction of calculated denudation rates and may account for the observed difference. In this section we address each transect individually and discuss the agreement between analyses. Vertical transect 1 (Fig. 3-4c) has good agreement between the two methods primarily due to samples being collected over a relatively short horizontal scale.

Transect 2 (Fig. 3-4d) requires a more in depth investigation in order to resolve rate estimates. Samples along this transect are separated by ~20 km horizontal distance which may introduce error in the regression line analysis. Furthermore, the majority of samples here are at low elevations and it is more appropriate to use the median elevation to determine a rate from our 1-D model. This yields 0.4 mm/yr, very little change from the averaged model estimate. We tested whether the model input parameters were valid

42

in this region of the field area or may be the cause of misfit. We found the rates could not be reconciled even using a 3 fold increase in thermal diffusivity (99 vs. 32 km^2/Myr) or internal heat production (21 vs. 6.8 °C/Myr). On the other hand, using a lower near-surface geothermal gradient (8 vs. 19 °C/km) does predict a rate closely matching the regression-line estimate (median ~0.9 mm/yr). However, this change, as well as 3 fold increases in diffusivity or heat production over a short horizontal distance in a predominantly homogenous pluton, is geologically unreasonable. The model was run using 30% changes in all 3 values allowing for small-scale variations. This model output denudation rates ranging from 0.3 to 0.8 mm/yr with an average of 0.6 mm/yr, still well below the regression-line prediction. One physical explanation that could account for the offset may be a transient local denudation pattern. The rapid denudation suggested by the steep age-elevation profile combined with comparatively older AHe cooling ages may indicate exhumation occurred rapidly from ~8 to 5 Ma then decreased significantly after 5 Ma. If this is the case, comparing all transects would suggest rapid denudation in the region that migrated west/southwest with time. More recent (<5 Ma) exhumation has been focused within the Klinaklini Valley and near Mount Jubilee while the northeast flank of Mount Waddington has experienced relative stability. In the context of glaciation, this would imply that significant glaciation in the region began in the late Miocene and, due perhaps to drainage reorganization or focused denudation, migrated to the flanks of the Klinaklini River Valley.

From the comparison above we comment on the relative value of denudation rate estimates determined from simple regression-lines and the 1-D model employed here. The regression-line method has the distinct advantage of requiring only the cooling age and elevation of a sample with no knowledge of the thermophysical rock properties. On the other hand, a simplifying assumption of the thermal field must be made and samples need to be collected within a narrow horizontal range to extract a meaningful result. Using a 1-D thermal model such as AGE2EDOT provides information on individual samples. However, the elevation dependence shown above indicates that determined rates are best interpreted across the landscape from samples at similar elevations. A companion paper to this uses a coupled 3-D thermo-kinematic model that incorporates topography, variable exhumation and measured rock properties to predict

thermochronometer cooling ages. A detailed comparison between denudation rates from 1-, 2- and 3-D thermal models is presented in that paper. An important finding from this comparison is that at moderate denudation rates (0.6 mm/yr) predicted ages from 1-D and 2-D methods fall within ~20% of average cooling ages calculated using a sophisticated 3-D method. However, 1-D thermal modeling overemphasizes short-wavelength, high-amplitude features in the topography.

3.7 CONCLUSIONS

We report 44 new and 39 published apatite (U-Th)/He cooling ages from the heavily glaciated Coast Mountains, British Columbia. We interpret this dataset in the context of glacial modification of the landscape using a combination of approaches: (1) best-fit regression lines through vertical transect age-elevation profiles, (2) topographic profiles to compare samples with respect to topography, and (3) a 1-D thermal model that relates cooling ages to denudation rates. From this, we determine the following:

- Cooling ages from a ~60 x 60 km region including ~4 km of relief range from 1.1 – 15.4 Ma with an average 2σ error of 17.4%.

- Denudation rates estimated from best-fit regression lines range from 0.8 to 1.1 mm/yr, with an average of 1.0 mm/yr. Rates increase throughout the field area at ~5 – 7 Ma, interpreted to indicate onset of significant glaciation during this period, altering the landscape most intensely below 2000 – 3000 m.

- Denudation rates estimated from a 1-D thermal model (AGE2EDOT) range from 0.2 – 1.5 mm/yr, with an average rate of 0.6 mm/yr.

- Calculated denudation rates are highest in large valleys (~3 – 5 km wide) currently occupied by glaciers, averaging ~0.9 mm/yr at low elevations. The largest valleys (>10 km wide) tend to have lower denudation rates, averaging ~0.8 mm/yr at low elevations. Consequently, small tributary valleys have the lowest denudation rate average of 0.6 mm/yr, presumably due to lower ice flux. However, it is difficult to distinguish whether these findings are a consequence of geographic location (e.g. near Mount Jubilee) rather than valley size.

- Denudation generally (1) increases south to north upvalley from Knight Inlet, (2) is slightly higher within the valley than on the flanks, (3) increases west to east across the Klinaklini Valley, and (4) is focused near the summit of Mount Jubilee. These results indicate glaciation was most intense near Mount Jubilee suggesting a long-term pattern of ice flux over a present-day topographic high. Cooling ages from the northeast flank of Mount Waddington may indicate accelerated denudation between 5 to 8 Ma that has since migrated to the southwest.

- These denudation rates are significantly lower than short-term rates determined using sediment yield data from basins in Alaska irrespective of elevation, basin size and spatial position. The range of rates presented here from all methods (0.2 – 1.5 mm/yr) is nearly an order of magnitude less than the lowest short-term rate from Alaska, and at least half that found by Spotila et al. (2004) using AHe thermochronology in southern Alaska.

Finally, calculated denudation rates from the applied thermal model and more simplistic approaches yield mutually consistent average long-term rates. However, model calculated rates are 15 to 275% lower than estimated rates from regression-lines possibly due to regression lines over-predicting apparent denudation, the topographic and elevation dependence of 1-D model estimates, and samples spacing not evenly distributed through vertical transects. Each method requires a unique sampling strategy to properly utilize and interpret results.

Citation:

Densmore, M.S., Ehlers, T.A., Farley, K.A., Rusmore, M.E., Woodsworth, G.J., 2008, Observed spatial and temporal variations in glacial denudation from thermochronometer data: Coast Mountains, B.C., to be submitted to *J. Geophys. Res. – Earth Surface*.

3.8 FIGURES

Figure 3-1. Shaded relief digital elevation model (DEM) of British Columbia, Canada, with major morphologic belts and relative plate motions. Ex. Plate= Explorer Plate, J.D.F. Plate = Juan de Fuca Plate. Box denotes area shown in subsequent figures.
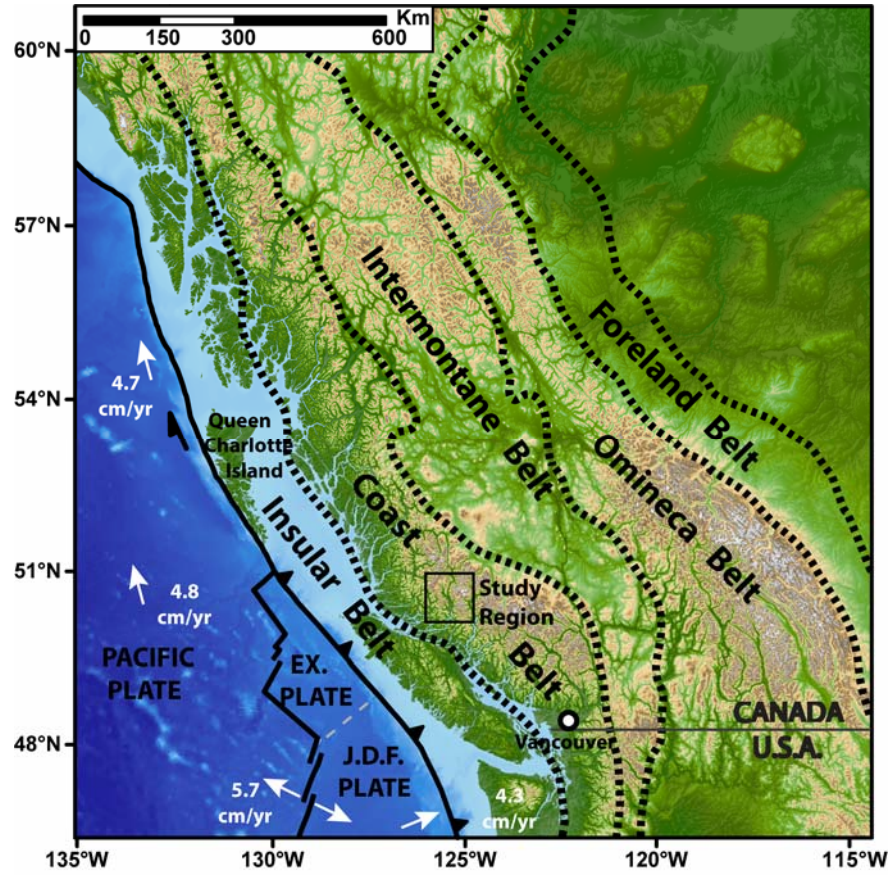
Figure 3-2. Cooling age versus denudation rate calculated using 1-D thermal model. Multiple thermochronometer systems used for comparison.
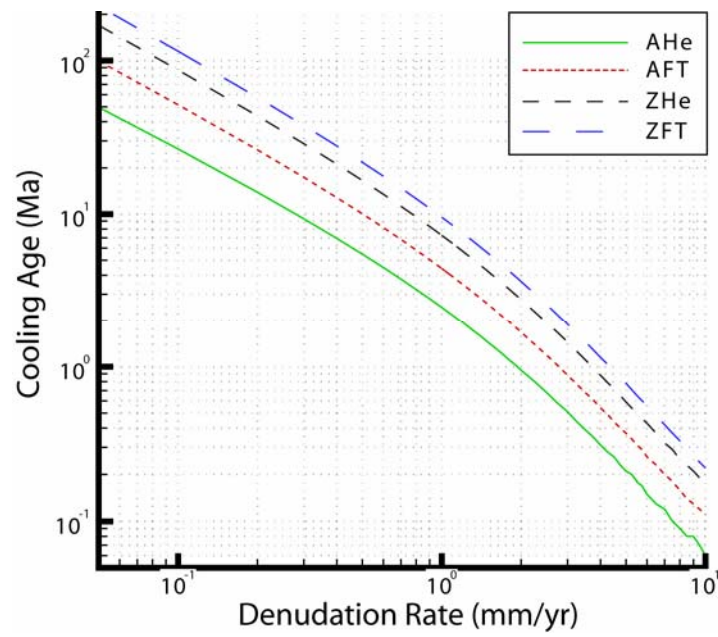
Figure 3-3. Shaded relief DEM with sample locations and AHe cooling ages (Ma) and coverages for present day glacial extent (white) and vegetation (light grey). Major geographic features as well as data profiles shown in subsequent figures are highlighted.
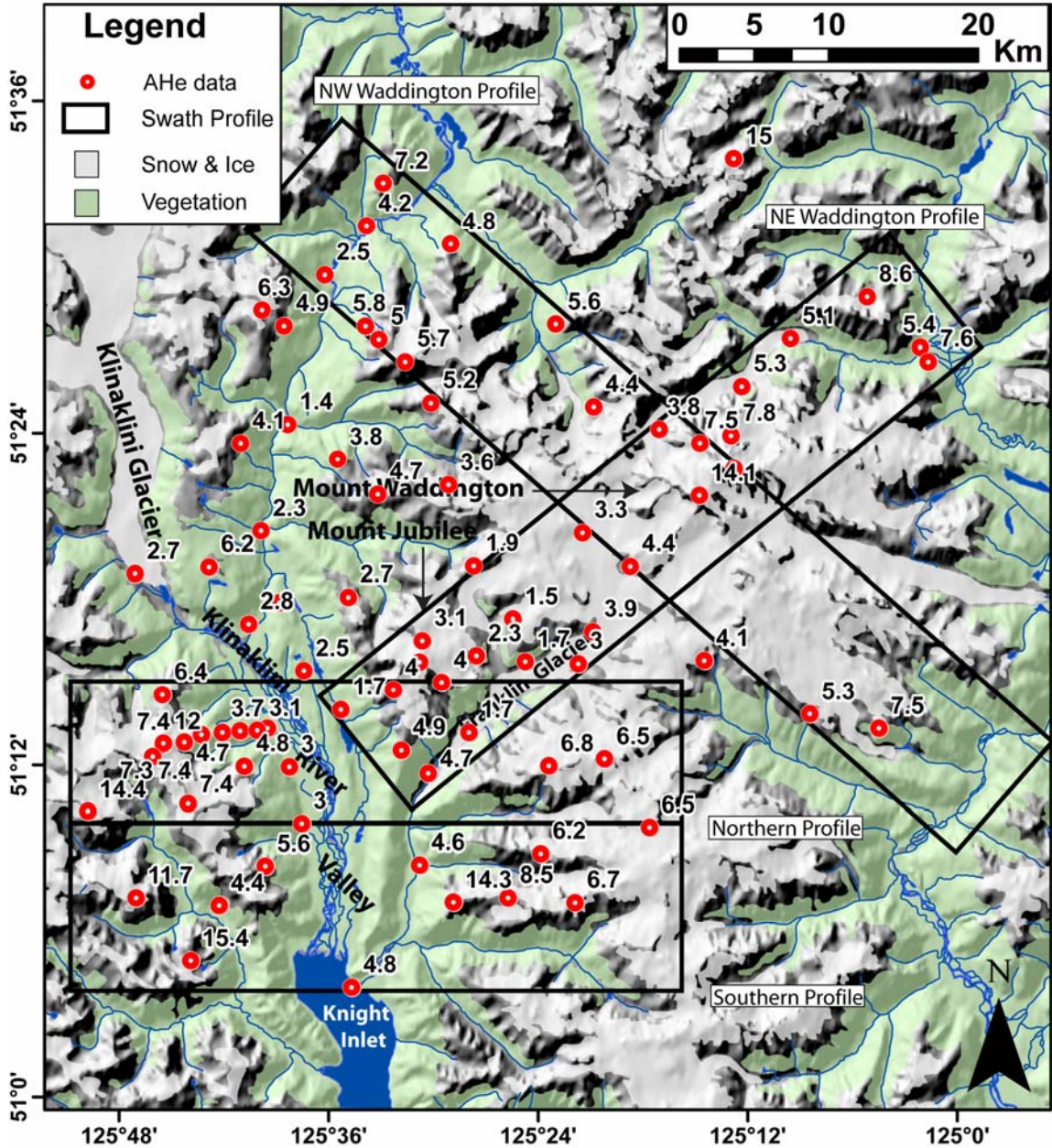
Figure 3-4. Location and denudation rates for data transects. Rates calculated using best-fit regression line. A: Shaded relief DEM with boxes denoting sample locations used for vertical transects (squares) as well as low-elevation valley bottom samples (diamonds). B: All AHe cooling age data in age versus elevation. Error bars are 2σ and contained within data point if not visible. C: Transect 1 on west slope of Klinaklini Valley. Note even distribution of samples with elevation and bend in age-elevation relationship at ~5-8 Ma, corresponding to ~2000 m. D: Transect 2 on northeast slope of Mount Waddington. Here, cooling ages tend to be older than samples at similar elevations elsewhere in the field region. E: Transect 3 on the east slope of the Klinaklini Valley including Mount Jubilee. Cooling ages here are generally very young even at high elevations (>2000 m). F: Transect 4 on the east slope of the Klinaklini Valley including smaller tributary streams but no major glaciers. The calculated denudation rate here is dependent on a single low-elevation sample with poor reproducibility (error ~100%) and is included for completeness. G: All samples within the Klinaklini Valley at <400 m. No denudation rate can be calculated, although a northward younging trend is apparent.

A) Sample Locations
- ○ AHe Data
- ◇ Valley Bottom Samples
- ▢ Transect Samples

B) All Data

C) Transect 1 — 0.8 mm/yr

D) Transect 2 — 1.1 mm/yr

E) Transect 3 — 1.1 mm/yr

F) Transect 4 — 1.0 mm/yr

G) Valley Bottom Samples (< 400 m elevation)
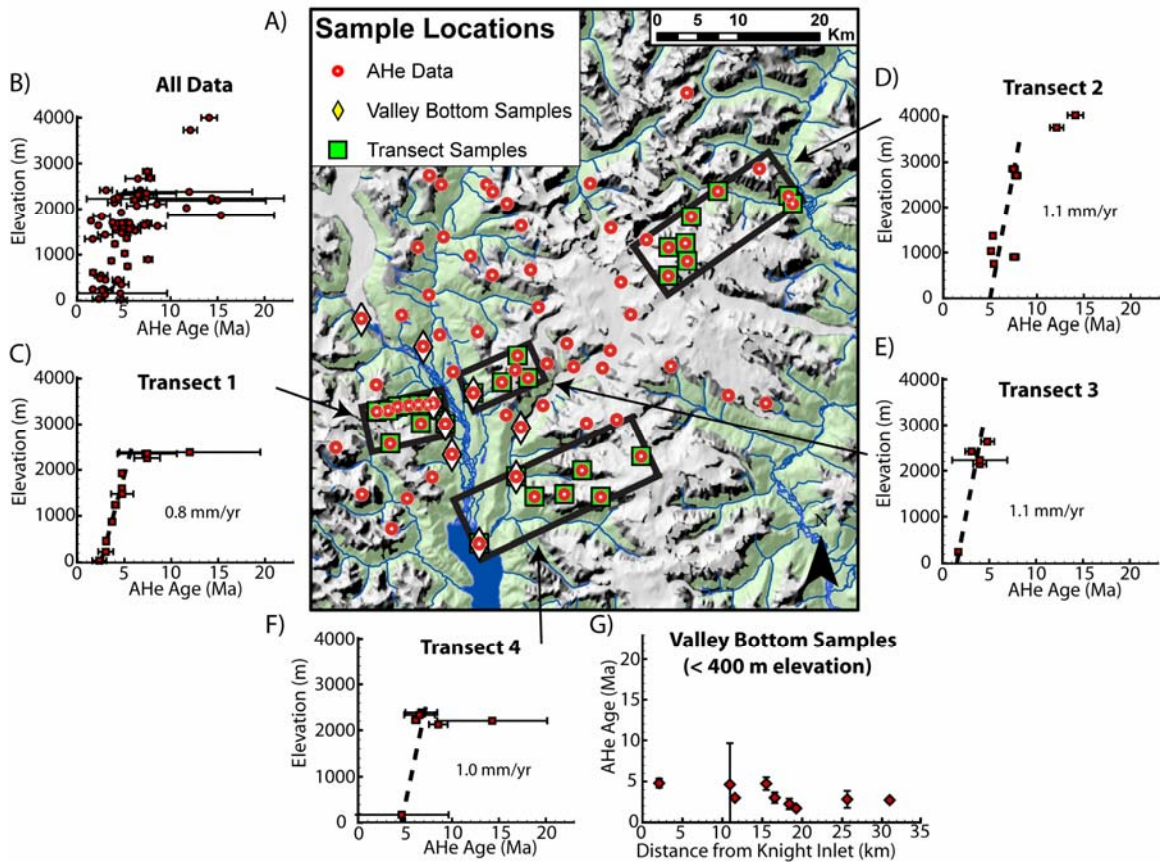
Figure 3-5. Horizontal swath profiles for the Klinaklini Valley with projected sample locations and cooling ages. These and subsequent profiles are 10 km wide with samples projected from a ~12 km wide region. This as well as small errors in GPS resolved elevation accounts for minor offset of some samples above or below max and min profiles. Regions defined in Figure 3-3. Diamonds correspond to samples at or below 1000 m, circles are above 1000 m and open circles are samples at similar elevations (within ~400 m) for comparison. A: Min (light grey)- mean (medium grey)- max (dark grey) elevation profile with projected samples from the southern Klinaklini Valley. Valley axis marked for reference. Similar elevation samples in this transect at ~2300 m. B: Min-mean-max profile for northern Klinaklini Valley. Neighboring peaks highlighted for reference. Similar elevation samples in this profile occur near ~2100 m. C: Samples from (A) in cooling age with 2σ error versus distance along profile. D: Samples from (B) in age versus distance.

51
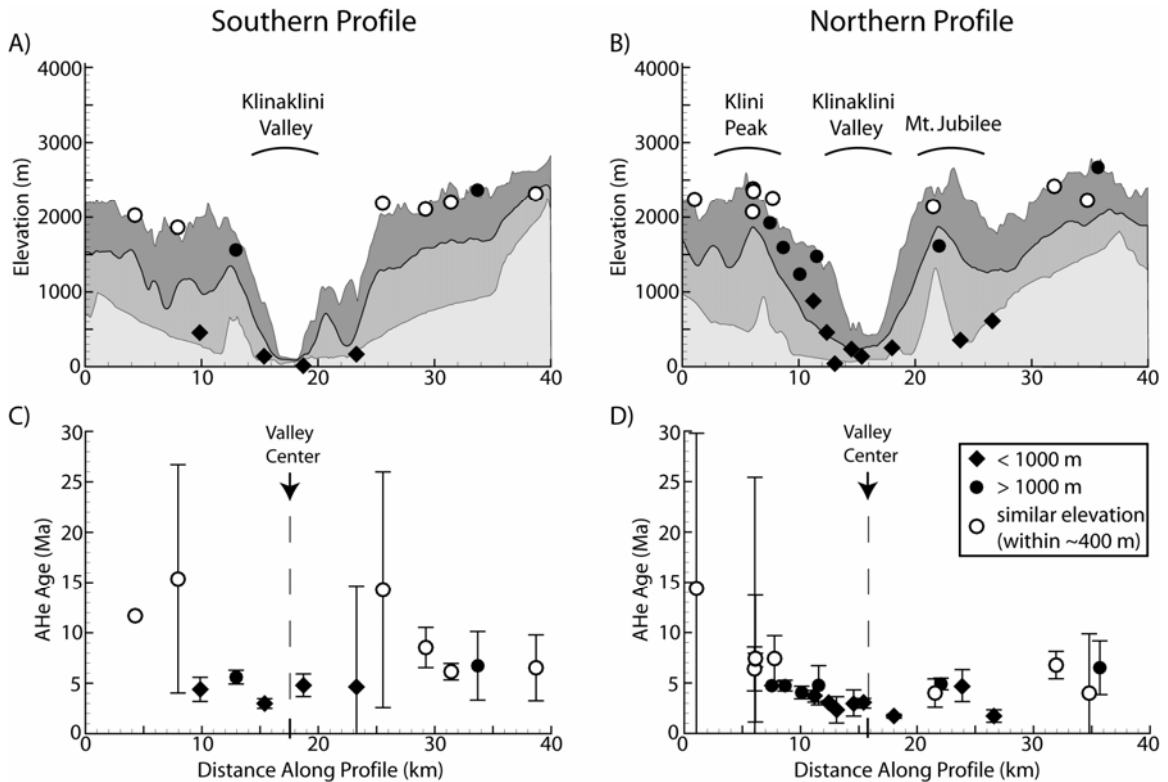
Figure 3-6. As figure 3-5, horizontal swath profiles for Mount Waddington region. A: NE trending min-mean-max profile across Mount Waddington. Similar elevation samples in this region are at ~1600 m. B: NW trending profile through Mount Waddington with samples near ~1700 m highlighted. C: Age versus distance for samples in (A). Note low cooling ages of samples at all elevations near Mount Jubilee. D: Samples from (B) in age versus distance.
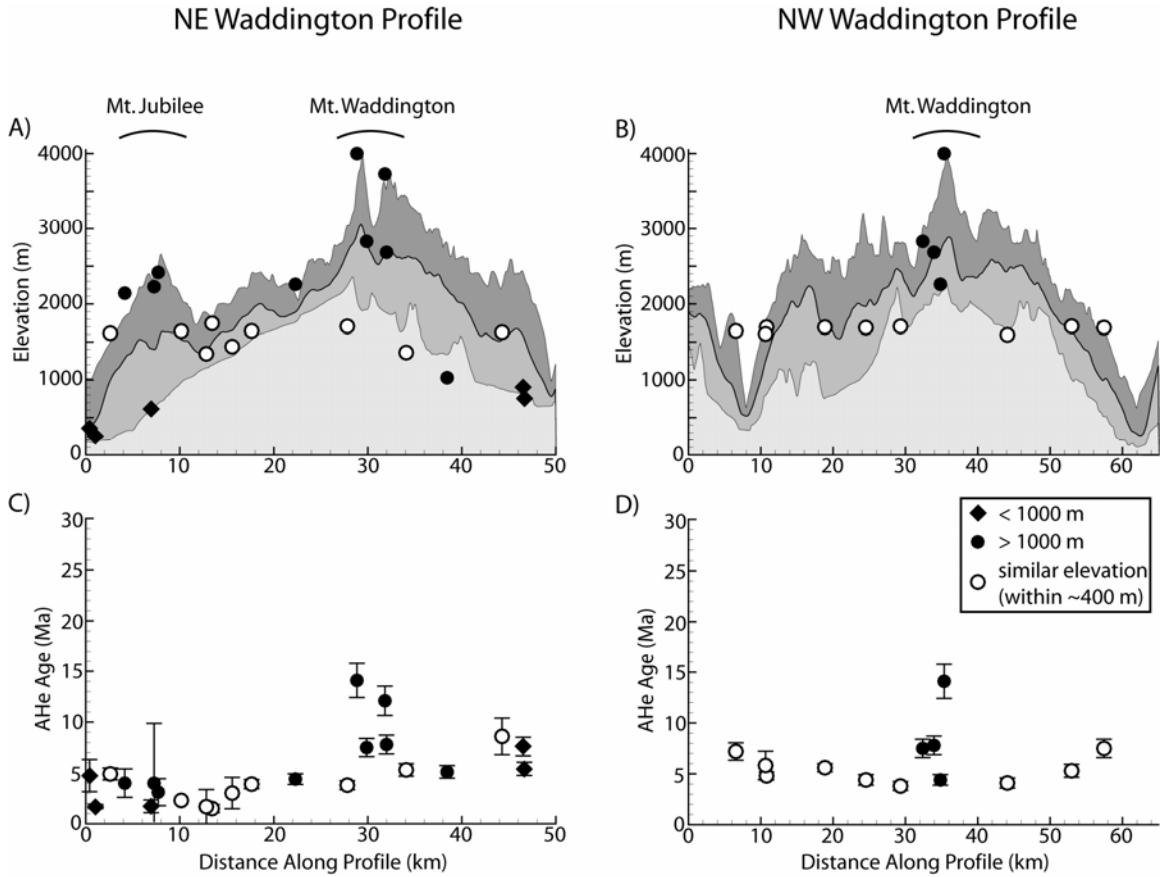
Figure 3-7. Calculated denudation rates from 1-D thermal model relative to spatial position. A: All samples in elevation versus calculated denudation rate. Error bars are derived by inputting sample ages at 2σ extent of cooling ages and determining denudation rates. Symbols are consistent from previous figures with diamonds below 1000 m and circles above. Best-fit trend line and corresponding R^2 is used to identify elevation dependence on calculated denudation rates (see text). B: Calculated denudation rate versus distance up-valley for all samples below 400 m elevation.
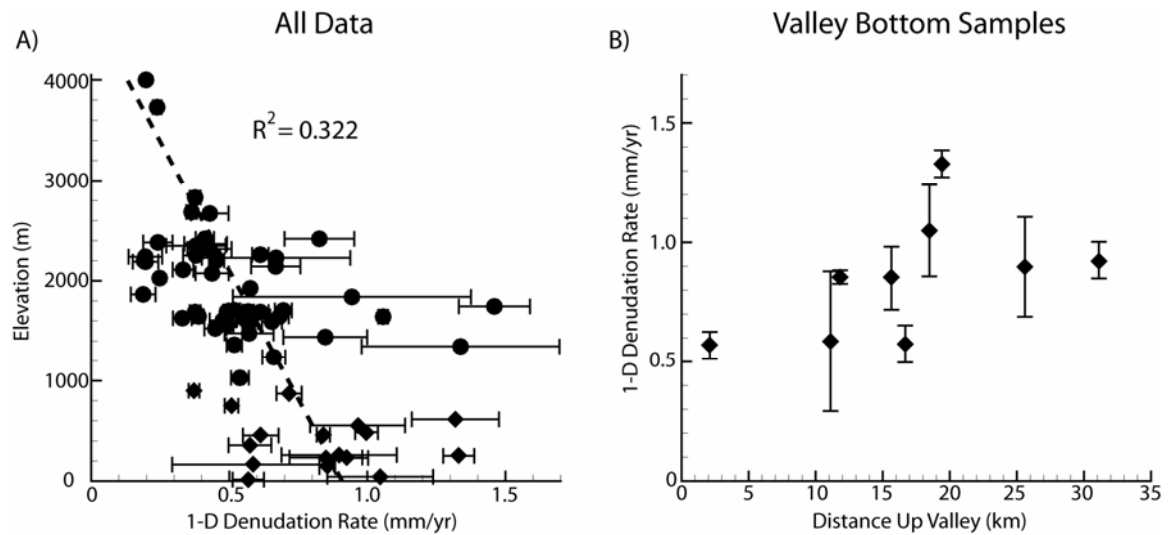
Figure 3-8. Horizontal swath profiles as figure 3-5 with calculated denudation rates. A: Min-mean-max profiles for the southern region of the Klinaklini Valley. B: Min-mean-max profile of northern Klinaklini Valley. C: Calculated denudation rate versus distance along profile from samples in (A) with 2σ error. D: Denudation rate versus distance for samples in (B).
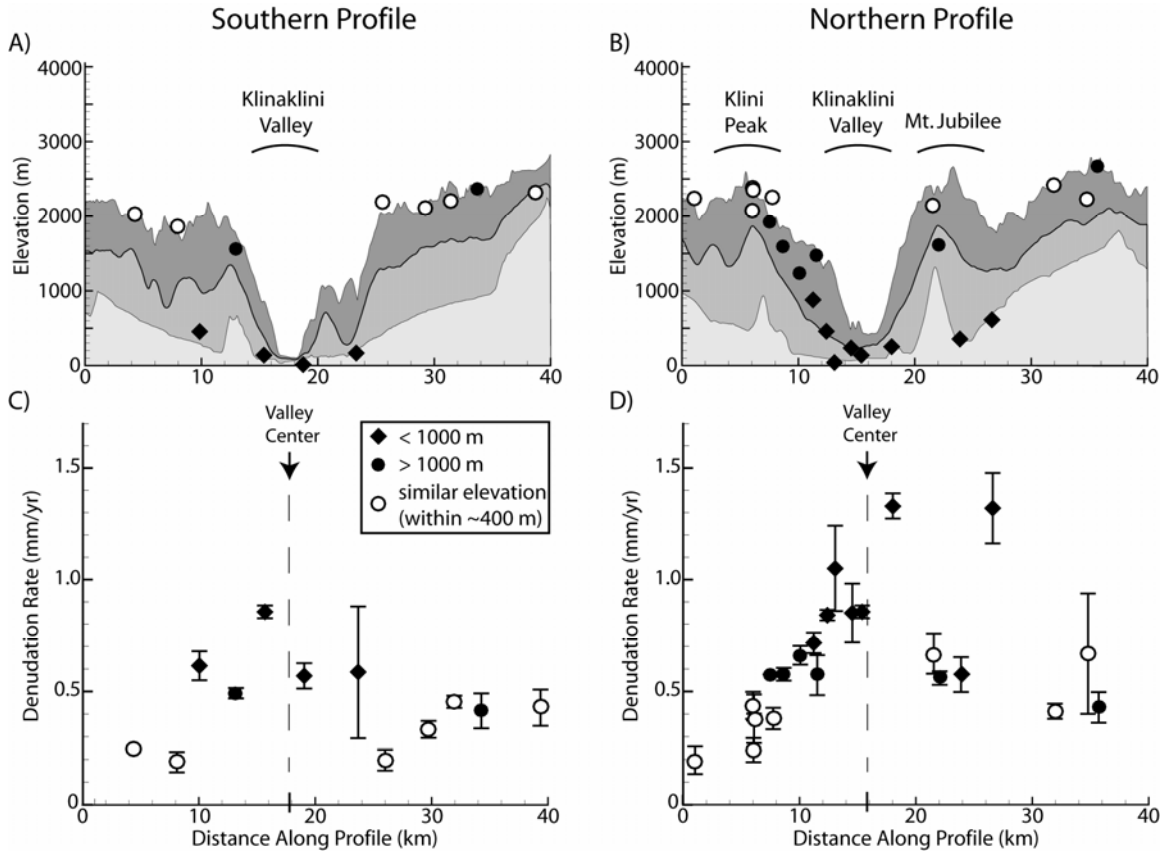
Figure 3-9. Horizontal swath profiles as figure 3-6 with calculated denudation rates. A: Min-mean max profiles trending NE across Mount Waddington. B: Min-mean max profiles trending NW across Mount Waddington. C: Denudation rate versus distance for samples in (A) with 2σ error. Note very high calculated rates of denudation near Mount Jubilee. D: Denudation rate versus distance for samples in (B).
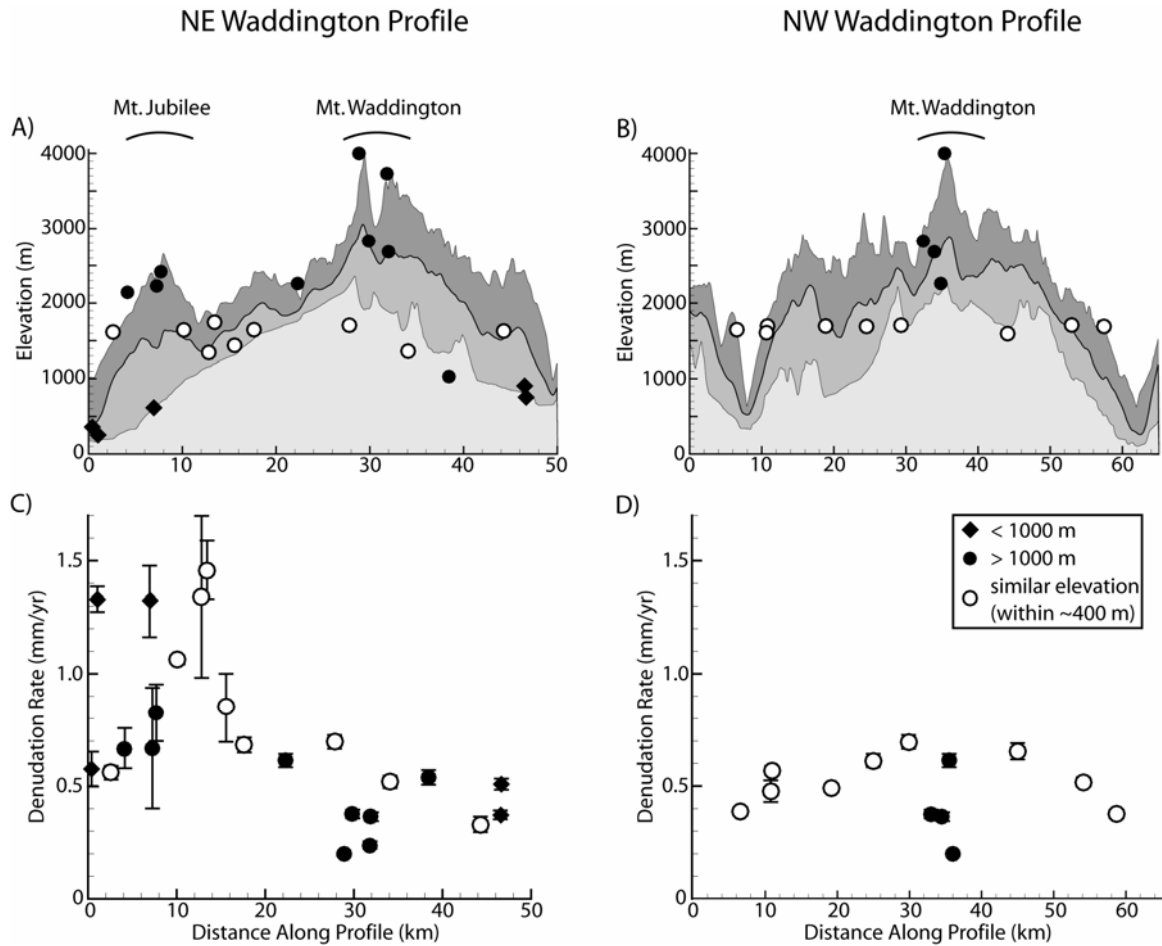
Figure 3-10. Shaded relief DEM with thermal model calculated denudation rates (mm/yr). Symbols consistent with previous plots with diamonds below 1000 m, circles from 1000 – 2000 m and squares >2000 m.
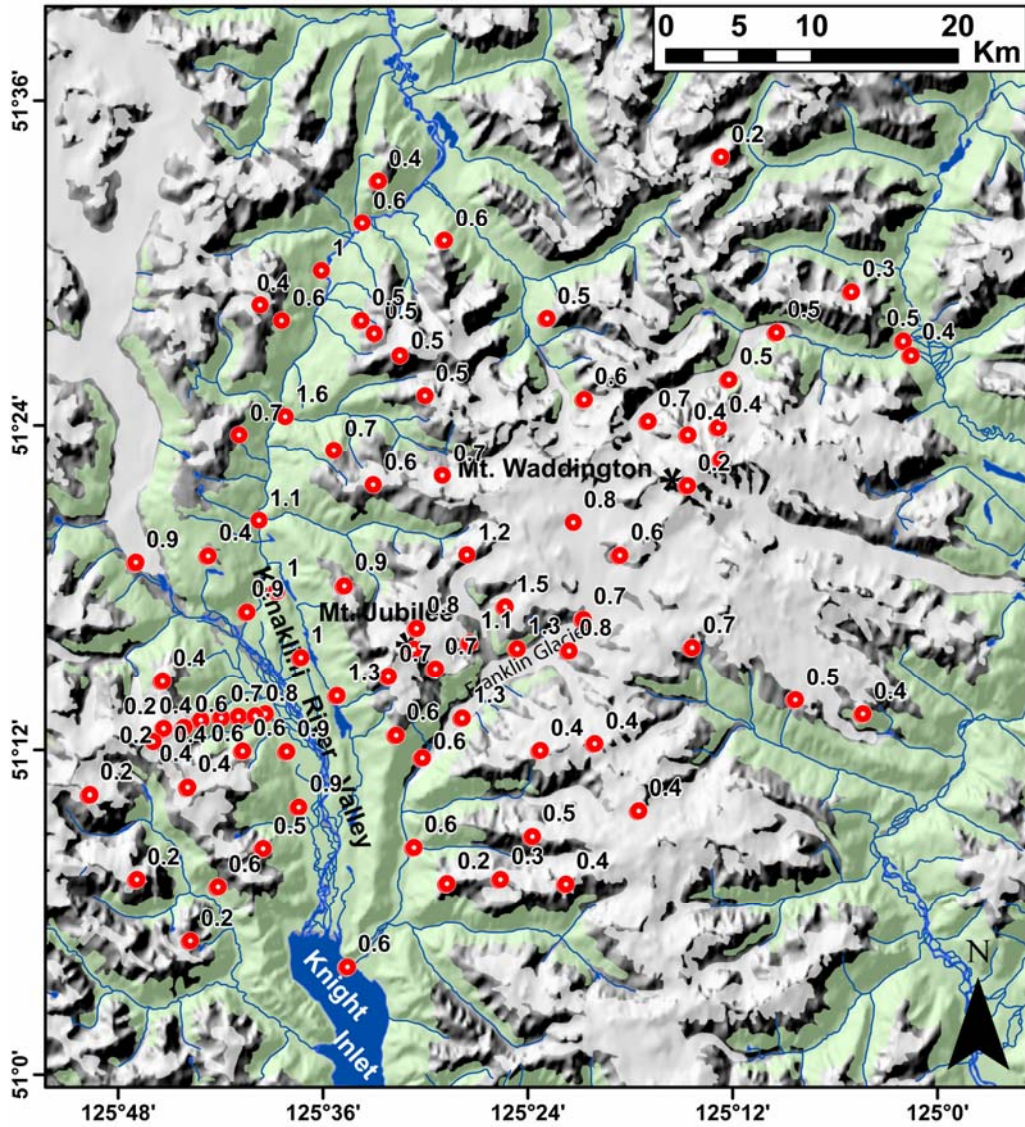
Figure 3-11. Reproduction of Hallet et al., (1996b) figure 2 with Alaska data highlighted (diamonds) from all other samples (circles) and including estimated long-term rates of denudation from this paper (filled square) and Spotila et al. (2004) (open square). Note, basin size for these long-term rates is estimated from small tributaries but rates are applicable over a range of areas.
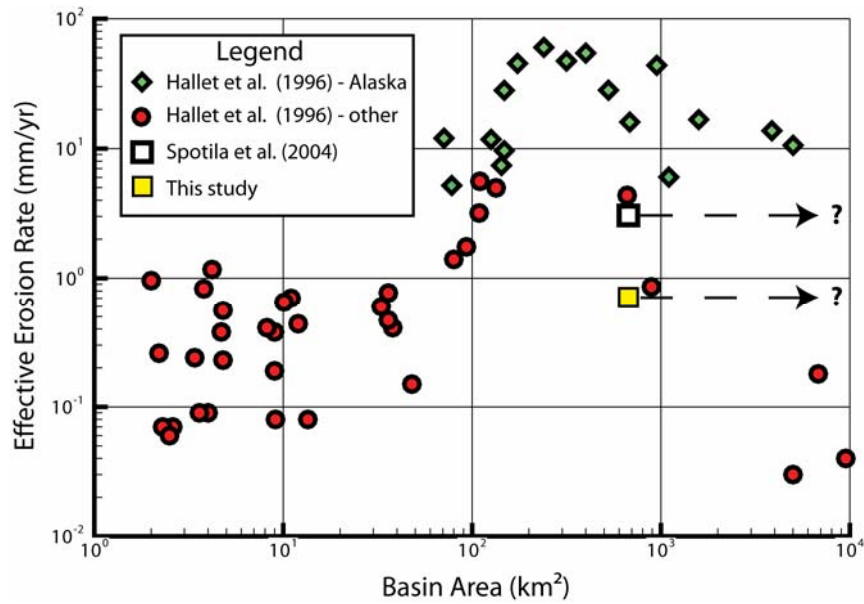
Table 3-1. Thermal model variables and justification. Diffusivity and heat production were measured on rock samples within field region, surface temperature from Ehlers et al. [2006], thermal gradient with no denudation from 3-D thermal model at steady state of Densmore et al. [2007] and depth to Moho (constant temperature boundary) from Hammer and Clowes (1997).

Constant	Value	Reference
Thermal Diffusivity	31.81 km^2/Myr	See Appendix 2
Internal Heat Production	6.76 °C/Myr	See Appendix 2
Surfact Temperature	4.0 °C	Ehlers et al., 2006
Surface Thermal Gradient (no erosion)	19 °C/km	Densmore et al., 2007
Depth to Constant Temperature	35 km	Hammer and Clowes, 1997

Table 3-2. Apatite (U-Th)/He cooling age data analyses from single grain analyses.
UTM coordinates use North American Datum 1983. FT Corr. is the fraction of alpha
particles retained, and Corr. Age the FT corrected age.

SAMPLE ID		Elev. (m)	UTM Easting (M)	UTM Northing (m)	MASS (µg)	U ppm	TH ppm	He (nmol/g)	FT Corr.	Raw Age (Ma)	Corr. AGE (Ma)	Avg. Age (Ma)	Std. Dev. (Ma)
TEKI001	A	2190	325955	5666842	3.6	34.4	62.0	3.1	0.72	11.6	16.2	14.3	2.9
	B				5.6	43.4	74.2	2.6	0.77	7.8	10.2		
	C				3.9	26.7	44.5	2.4	0.73	12.1	16.5		
TEKI002	A	2110	329634	5667146	6.0	14.3	15.7	0.6	0.77	6.2	8.1	8.5	0.5
	B				2.9	18.2	39.3	1.0	0.73	6.7	9.2		
	C				2.4	25.5	39.0	1.1	0.69	5.7	8.3		
TEKI003	A	2367	334093	5666835	4.4	17.1	15.1	0.7	0.76	6.0	7.8	6.7	0.9
	B				2.1	34.5	13.1	0.8	0.69	4.0	5.7		
	C				3.1	20.2	18.8	0.6	0.73	4.8	6.6		
TEKI004	A	2317	339097	5671849	5.5	44.7	5.1	1.2	0.78	4.9	6.3	6.5	0.8
	B				5.2	39.2	7.4	1.3	0.76	5.8	7.6		
	C				2.7	65.5	7.6	1.5	0.71	4.0	5.7		
TEKI005	A	2203	331810	5670106	4.2	39.2	48.2	1.2	0.76	4.5	6.0	6.2	0.2
	B				3.8	44.9	63.6	1.5	0.75	4.5	6.1		
	C				3.2	41.0	61.4	1.4	0.73	4.7	6.4		
TEKI006	A	2418	332342	5675928	6.0	15.8	41.5	0.7	0.78	5.2	6.6	6.8	0.3
	B				4.8	15.2	39.2	0.7	0.76	5.5	7.2		
	C				5.5	17.7	44.9	0.8	0.78	5.0	6.5		
TEKI007	A	2671	336092	5676407	5.3	77.4	59.1	2.1	0.77	4.3	5.6	6.5	0.7
	B				2.6	214.6	115.1	6.9	0.73	5.3	7.2		
	C				3.5	61.7	58.0	2.1	0.75	5.0	6.7		

	A				2.4	26.8	21.0	0.4	0.69	2.1	3.0		
TEKI008	B	1439	334317	5682815	3.8	48.4	68.6	0.9	0.76	2.7	3.5	**3.0**	**0.4**
	C				1.9	72.6	80.7	0.9	0.69	1.8	2.6		
	A				2.8	25.9	28.3	0.2	0.72	1.3	1.8		
TEKI009	B	1345	330773	5682934	3.1	15.9	7.4	0.2	0.75	1.6	2.2	**1.7**	**0.4**
	C				3.7	7.9	0.6	0.0	0.75	0.9	1.1		
	A				4.8	9.9	3.4	0.1	0.77	1.4	1.8		
TEKI010	B	615	327002	5678185	2.1	16.4	4.1	0.1	0.71	1.1	1.5	**1.7**	**0.2**
	C				3.4	10.7	3.4	0.1	0.75	1.4	1.9		
	A				3.0	1.4	0.2	0.0	0.74	3.9	5.2		
TEKI011	B	357	324283	5675443	3.7	1.5	1.1	0.0	0.72	3.4	4.7	**4.7**	**0.4**
	C				3.9	1.1	0.0	0.0	0.76	3.2	4.2		
	A				6.1	27.5	56.9	0.5	0.76	2.2	2.9		
TEKI012	B	165	323678	5669348	4.6	34.9	82.6	1.8	0.76	6.2	8.2	**4.6**	**2.5**
	C				5.3	33.7	74.6	0.6	0.77	2.1	2.8		
	A				4.9	20.0	29.3	0.5	0.76	3.4	4.5		
TEKI014	B	2143	321944	5681045	3.2	21.4	10.3	0.3	0.73	2.7	3.7	**4.0**	**0.3**
	C				3.2	13.3	11.1	0.2	0.73	2.8	3.9		
	A				2.0	9.3	6.2	0.2	0.69	4.2	6.1		
TEKI015	B	2228	325182	5681534	2.8	3.4	3.7	0.0	0.72	2.0	2.8	**4.0**	**1.5**
	C				2.9	4.2	4.7	0.1	0.74	2.3	3.1		
	A				4.7	5.4	0.5	0.1	0.77	2.7	3.4		
TEKI016	B	2418	323861	5684352	2.5	7.7	0.8	0.1	0.72	1.9	2.7	**3.1**	**0.3**
	C				3.3	5.7	0.7	0.1	0.75	2.4	3.2		
	A				2.1	4.6	1.1	0.0	0.71	1.5	2.2		
TEKI017	B	1840	318911	5687263	5.1	3.6	1.6	0.0	0.78	2.0	2.5	**2.6**	**0.5**
	C				4.7	3.7	0.9	0.1	0.77	2.5	3.3		

TEKI018	**A**	554	314268	5686900	4.7	40.8	37.6	0.4	0.75	1.6	2.1	**2.6**	**0.3**
	B				4.5	47.7	67.4	0.7	0.77	2.1	2.8		
	C				8.5	46.1	37.3	0.7	0.80	2.3	2.9		
TEKI019	**A**	260	312221	5685482	7.0	46.5	30.3	0.6	0.80	2.1	2.7	**2.8**	**0.5**
	B				5.2	74.2	49.8	0.8	0.76	1.7	2.3		
	C				7.1	48.0	22.4	0.8	0.80	2.8	3.5		
TEKI021	**A**	230	304606	5688840	4.2	11.1	11.6	0.1	0.75	1.9	2.5	**2.7**	**0.1**
	B				2.8	11.7	14.9	0.2	0.72	1.9	2.7		
	C				5.0	6.5	5.1	0.1	0.77	2.2	2.9		
TEKI022	**A**	1525	309592	5689284	5.3	7.7	15.5	0.3	0.77	4.6	6.0	**6.2**	**0.3**
	B				5.7	14.6	17.4	0.5	0.77	5.1	6.6		
	C				3.9	13.8	16.5	0.4	0.75	4.5	6.0		
TEKI025	**A**	2253	308159	5673448	6.2	9.2	7.3	0.3	0.80	5.3	6.6	**7.4**	**0.6**
	B				4.8	7.3	7.4	0.3	0.77	6.0	7.8		
	C				2.5	10.6	10.3	0.4	0.71	5.5	7.8		
TEKI028	**A**	140	315797	5672100	5.3	17.7	34.9	0.3	0.76	2.3	3.1	**3.0**	**0.1**
	B				3.9	19.0	38.1	0.3	0.74	2.3	3.1		
	C				3.0	18.9	39.4	0.3	0.73	2.1	2.8		
TEKI029	**A**	1865	308352	5662899	3.0	9.0	5.0	0.5	0.74	9.4	12.7	**15.4**	**2.8**
	B				4.7	7.9	5.1	0.7	0.76	14.7	19.3		
	C				4.6	8.8	6.4	0.6	0.77	10.8	14.1		
TEKI039	**A**	454	310255	5666633	4.3	7.6	4.2	0.2	0.76	3.5	4.6	**4.4**	**0.3**
	B				3.3	2.2	2.5	0.0	0.72	3.3	4.6		
	C				8.7	3.2	2.1	0.1	0.80	3.2	4.0		
TEKI040	**A**	2027	304677	5667133	3.6	40.4	44.0	2.4	0.75	8.7	11.7	**11.7**	**0.0**
	B				4.7	26.6	34.0	1.7	0.76	8.9	11.7		
	C				3.3	33.9	46.5	2.1	0.73	8.6	11.7		

TEKI041	**A**				4.5	88.3	78.1	4.8	0.76	8.2	10.8	
	B	2239	301455	5672928	5.1	79.5	78.3	5.2	0.77	9.7	12.6	**14.4** **3.8**
	C				3.9	82.0	96.1	8.3	0.74	14.7	19.7	
TEKI045	**A**				2.0	75.4	81.4	1.6	0.69	3.1	4.5	
	B	1737	318192	5696518	2.7	17.6	6.7	0.2	0.74	2.2	2.9	**3.8** **0.7**
	C				2.9	53.9	37.1	1.0	0.72	2.9	4.0	
TEKI046	**A**				1.9	28.3	23.3	0.6	0.68	3.4	5.0	
	B	2143	320907	5694158	4.7	22.5	18.6	0.5	0.76	3.5	4.6	**4.7** **0.2**
	C				2.3	32.7	32.7	0.7	0.70	3.1	4.4	
TEKI047	**A**				2.3	16.5	7.6	0.1	0.71	1.3	1.8	
	B	2063	327322	5689351	4.7	11.2	14.7	0.1	0.77	1.5	2.0	**1.9** **0.1**
	C				2.3	20.5	10.9	0.2	0.70	1.3	1.9	
TEKI051	**A**				4.5	84.8	73.6	1.0	0.76	1.8	2.4	
	B	487	315921	5682323	6.3	75.6	86.1	1.0	0.77	1.9	2.4	**2.5** **0.1**
	C				3.9	71.0	47.9	0.9	0.75	1.9	2.6	
TEKI052	**A**				2.2	19.7	15.9	0.2	0.69	1.3	1.9	
	B	220	313051	5691701	3.1	6.6	11.3	0.1	0.73	1.8	2.5	**2.3** **0.3**
	C				2.1	100.8	78.6	1.1	0.70	1.7	2.5	
TEKI053	**A**				2.8	13.7	32.7	0.1	0.71	0.8	1.1	
	B	297	314840	5698872	1.9	6.3	15.1	0.1	0.69	1.1	1.7	**1.4** **0.2**
	C				1.9	6.0	19.2	0.1	0.68	0.9	1.3	
TEKI054	**A**				4.6	34.7	64.6	0.8	0.73	3.0	4.1	
	B	1350	311703	5697593	2.5	35.9	66.5	0.9	0.70	3.1	4.4	**4.1** **0.3**
	C				3.5	37.4	68.9	0.8	0.73	2.7	3.7	
TEKI058	**A**				8.4	6.3	0.9	0.1	0.81	2.4	3.0	
	B	395	317333	5708891	3.1	4.0	0.9	0.0	0.73	1.7	2.2	**2.5** **0.3**
	C				2.3	4.2	0.9	0.0	0.69	1.5	2.2	

TEKI060	**A**	401	320152	5712187	5.0	45.8	7.8	0.8	0.75	3.0	4.0	**4.2**	**0.4**
	B				1.9	29.6	6.3	0.4	0.69	2.7	3.8		
	C				2.7	54.2	4.9	1.0	0.69	3.3	4.8		
TEKI061	**A**	1927	334607	5691575	3.8	1.5	2.3	0.0	0.75	2.1	2.9	**3.3**	**0.4**
	B				4.5	1.7	2.5	0.0	0.76	2.4	3.1		
	C				4.6	0.9	1.2	0.0	0.76	2.9	3.9		
TEKI062	**A**	1912	325638	5694794	3.2	85.6	81.5	1.5	0.73	2.6	3.5	**3.6**	**0.3**
	B				4.6	75.3	60.1	1.4	0.75	2.9	3.9		
	C				5.3	62.0	17.4	0.9	0.79	2.6	3.3		
TEKI064	**A**	2330	324434	5700316	5.2	5.4	2.9	0.1	0.77	3.4	4.5	**5.2**	**0.6**
	B				8.4	6.0	2.1	0.1	0.79	4.2	5.3		
	C				1.7	16.5	21.5	0.5	0.69	4.1	5.9		
TEKI066	**A**	2548	322734	5703071	1.7	7.9	3.1	0.2	0.68	3.6	5.4	**5.7**	**0.3**
	B				2.9	15.3	3.8	0.4	0.73	4.4	6.0		
	C				2.9	11.3	3.0	0.3	0.74	4.1	5.6		
TEKI067	**A**	2556	305791	5676560	3.5	1.4	2.2	0.0	0.73	2.8	3.8	**5.4**	**1.1**
	B				1.7	2.4	3.2	0.1	0.67	4.3	6.4		
	C				1.7	2.2	2.4	0.1	0.69	3.5	5.1		
	D				2.8	2.4	3.7	0.1	0.73	4.7	6.4		
TEKI068	**A**	2666	323699	5682925	9.3	5.1	11.6	0.1	0.72	3.0	4.2	**4.4**	**0.2**
	B				15.5	11.6	30.2	0.3	0.75	3.4	4.6		
TEKI071	**A**	2070	313116	5706502	2.5	44.1	1.9	1.1	0.72	4.7	6.6	**6.3**	**0.6**
	B				4.0	54.7	4.0	1.6	0.76	5.3	7.0		
	C				2.9	29.0	1.5	0.6	0.74	4.0	5.5		
TEKI072	**A**	1422	314612	5705443	2.6	28.1	11.0	0.6	0.72	3.4	4.7	**4.9**	**0.4**
	B				4.1	178.4	69.9	4.2	0.73	4.0	5.4		
	C				2.7	20.4	4.5	0.4	0.70	3.2	4.6		

	A				2.0	84.1	69.1	2.0	0.69	3.7	5.4		
TEKI073	**B**	1606	320071	5705440	4.0	22.9	6.5	0.6	0.75	4.7	6.2	**5.8**	**0.4**
	C				6.1	32.8	9.1	0.9	0.78	4.5	5.9		
	A				3.7	5.6	6.7	0.1	0.75	3.8	5.0		
TEKI074	**B**	2092	320960	5704553	2.3	8.5	4.3	0.2	0.70	3.5	5.0	**5.0**	**0.1**
	C				2.9	21.5	4.1	0.5	0.74	3.8	5.1		

Chapter 4: Quantifying Glacial Denudation with Thermochronology 2: Cenozoic Exhumation History from Thermochronometer Data

4.1 ABSTRACT

Miocene to recent denudation of the southern Coast Mountains, British Columbia, has been driven by a variety of processes, most recently by orogen wide glaciation. Prior to glaciation, plate tectonic processes generated topographic relief whereas fluvial and hillslope processes eroded topography. This study uses low-temperature thermochronology to quantify transients in rock cooling histories associated with these phases of denudation, with an emphasis on the rates of pre-glacial denudation of the range. Low-temperature thermochronometers are interpreted using numerical modeling techniques to quantify long-term ($>10^6$ yrs) denudation within the southern Coast Mountains. We utilize 6 new and 20 previously published apatite and zircon (U-Th)/He (AHe and ZHe) and apatite and zircon fission track (AFT and ZFT) samples collected over a 60 x 30 km region in order to characterize spatial and temporal variations in long-term denudation. Cooling ages range from 5.2 to 39.2 Ma for AFT samples, 2.4 to 27.3 Ma for ZHe, and 18.6 to 55.2 Ma for ZFT. We use an inverse model to quantify sample cooling histories as a function of measured fission track length distributions and (U-Th)/He cooling ages, and a 1-D thermo-kinematic model to estimate denudation rates. From these, we identify phases of cooling within the southern Coast Mountains including

a period of subdued denudation rates (~0.2 mm/yr) during most of the Miocene (~30 to 10 Ma), increased denudation rates (~0.2 to 0.4 mm/yr) during the latest Miocene (~7 Ma) and a likely increase to very rapid rates (~1.0 mm/yr) within the last ~4 Myr. We interpret these phases as related to pre-glacial erosion and the inception and further intensification of glaciation.

4.2 INTRODUCTION

The Coast Mountains of the Canadian Cordillera have some of the highest topographic relief in North America (~4 km) and span over 1000 km from SE Alaska, USA, to SW British Columbia, Canada. The range has experienced Mesozoic and Cenozoic plutonic emplacement, surface uplift and denudation including significant alteration due to intense glaciation from alpine glaciers as well as the Cordilleran Ice Sheet. Controversy exists concerning the evolution of the range due in part to overprinting of structural and geomorphic evidence by accretionary, plutonic and glacial processes. The timing and mechanism of surface uplift to present elevation is ambiguous and has been postulated as the result of early to mid Miocene (~14 Ma) extension (e.g. Rohr and Currie, 1997), thermal buoyancy due to the passage of the Anahim hotspot during the Miocene (~10 Ma) (e.g. Parrish, 1983), or Pliocene (~2.5 Ma) isostatic uplift associated with continental and alpine glaciation (e.g. Farley et al., 2001). Additionally, the timing of inception of glaciation is poorly constrained. Here, we address the long-term ($>10^6$ yr) evolution of the Coast Mountains by applying low-temperature thermochronology in order to evaluate the long-term denudation history of the range. We emphasize quantifying rates of rock cooling and denudation pre and post glaciation.

Denudation is a common mechanism for rock exhumation (Ring et al., 1999) and low-temperature thermochronometers are proven tools for quantifying the time-temperature history of rocks (Hodges, 2003; Reiners et al., 2005). Exhumation rates can be resolved from thermochronometer cooling ages with knowledge of the subsurface thermal field. Previous studies within the Coast Mountains have applied thermochronology in order to quantify aspects of the exhumation and denudation history (Fig. 4-1) (Densmore et al., 2007; Ehlers et al., 2006; Farley et al., 2001; Hickes, 2001; O'Sullivan and Parrish, 1995; Parrish, 1983; Shuster et al., 2005). We augment these

studies by combining apatite and zircon (U-Th)/He (AHe and ZHe) with apatite and zircon fission track (AFT and ZFT) cooling ages and interpret the data using numerical models to quantify the exhumation of rocks from ~250 to 70 °C over the last ~40 Myr. Furthermore, we compare our findings to previous studies to compile an orogen-scale history of denudation and identify temporal variations in rock exhumation related to different phases of orogen denudation (i.e. glacial vs. pre-glacial). For a detailed study of local variations in AHe cooling ages used here, see Densmore et al., (2008b).

4.3 GEOLOGIC SETTING

4.3.1 Morphogeologic Belts of British Columbia

The Canadian Cordillera is separated into 5 major morphogeologic belts, each the product of differing tectonic and geomorphic processes (Gabrielse et al., 1991). From east to west, they are the Foreland, Omineca, Intermontane, Coast and Insular Belts (Fig. 4-1a). The Foreland Belt forms the easternmost foothills of the Cordillera and is composed primarily of Paleozoic and early Mesozoic (>540 – ~180 Ma) clastic assemblages. These sedimentary strata thin to the west where they underlie the Omineca Belt, a product of Mesozoic and early Cenozoic (~160 – 55 Ma) accretion and crustal shortening. Continuing westward is the allochthonous Intermontane belt, defined by its subdued topography and low-grade metamorphism. This belt consists of an amalgam of terranes accreted during the ~mid to late Mesozoic (~220 – 100 Ma). Following is the Coast Belt, an area of high relief encompassing the Coast Mountains and the northern Cascades. This narrow belt consists primarily of Late Mesozoic and Early Cenozoic (~150 – 55 Ma) granitic and lesser metamorphic rocks of the Coast Plutonic Complex and has the greatest concentration of plutonic rocks within the Cordillera (Woodsworth et al., 1991). The Coast Plutonic Complex is a matrix of migmatite and gneisses with NW-SE trending elongated discrete and coalescing plutons, predominantly composed of quartz diorite, granodiorite and diorite (Roddick and Hutchison, 1974; Woodsworth et al., 1991). Finally, the Insular Belt occurs just offshore from the mainland and includes the present day continental margin as well as Vancouver and Queen Charlotte Islands.

4.3.2 Cordilleran Tectonic History

The tectonic framework of the Cordillera represents the integrated effects of rifting, passive margin sedimentation, convergence, accretion, and volcanism since ~2.0 Ga. A detailed discussion is available in Gabrielse and Yorath (1991) with salient points summarized here. Much of the Proterozoic through Late Paleozoic (~1.85 Ga – 370 Ma) history is dominated by various local episodes of continental rifting with associated volcanism, compression, and ubiquitous passive margin deposition forming miogeoclinal sequences (Thorkelson et al., 2001). By Middle Triassic time (~230 Ma), allochthonous terranes of island arc and Asian (Tethyan) affinity began accreting on the autochthonous continent (Johnston and Borel, 2007; Monger, 1993). During the Jurassic, ocean basins created during earlier rifting began to close, changing the style of accretion from smaller, discrete bodies to large superterranes (Colpron et al., 2007; Nokleberg et al., 2000) forming much of the morphogeologic belts discussed above. These exotic terranes continued to add material to the continent as well as create topography, volcanism, and associated syntectonic deposition in adjacent foredeeps. By the end of the Mesozoic, the Omineca Belt had become an uplifted metamorphic province, the Insular Belt had converged with the Intermontane resulting in significant crustal shortening, and the Coast Belt had developed as a plutonic complex obscuring the suture zone between the Insular and Intermontane Belts (O'Leary et al., 1993).

The termination of subduction of the Kula plate in the mid Eocene (~40 Ma) led to a reorganization of the plate margin along the entire coast (Atwater and Stock, 1998; Engebretson et al., 1984), resulting in strike-slip faulting (Hyndman and Hamilton, 1993; Irving et al., 2000), and a pulse of volcanism, uplift and extensional faulting in the Coast and Omineca Belts. Climatic evidence suggests the Coast Mountains were not a significant topographic and orographic feature at this time (Rouse and Mathews, 1979). Neogene tectonics has been dominated by interactions between the Pacific, Juan de Fuca, and North American plates. Contraction and uplift in the Coast and Insular Belts created high, mountainous topography and shed sediments into accretionary prisms offshore, the exact timing and mechanism of which is unresolved. Concurrently, the Explorer Plate separated from the Juan de Fuca Plate in the late Pliocene (~2 Ma) (Riddihough and

Hyndman, 1991) and subduction has slowed as the present Explorer Ridge may be reorganizing southward (Braunmiller and Nabelek, 2002; Dziak, 2006).

4.4 PREVIOUS WORK

4.4.1 Geochronology

Several studies have applied various geochronology techniques to constrain the plutonic emplacement history of the Coast Mountains (Fig. 4-1b). In the southernmost part of the range, Friedman and Armstrong (1995, and references therein) documented a general west to east younging trend of emplacement and cooling through the Middle Jurassic to Late Cretaceous (~160 – 65 Ma) using U-Pb and whole rock K-Ar and Rb-Sr ages. Similarly, K-Ar and Rb-Sr determinations in the central Coast Mountains yield Late Cretaceous through Eocene ages (~65 – 50 Ma) (Harrison et al., 1979, and references therein). However, a few Triassic (215 Ma) and older plutons have been recognized in this region and are interpreted as entrained exotic material (Gehrels et al., 1991a). Finally, in the northern region U-Pb dates indicate a migration of plutonism from west to east during the Late Cretaceous and Paleocene (~80 – 55 Ma) (Gehrels et al., 1991b; van der Heyden, 1989).

4.4.2 Thermochronology

High- and low-temperature thermochronology studies within the Coast Mountains have constrained emplacement and unroofing of intrusions as well as estimates of long-term (10^6 yrs) denudation and exhumation (Fig. 4-1c). Biotite K-Ar ages in the southern region range from 16±1 to 103±5 Ma (Richards and McTaggart, 1976). Parrish (1983) determined zircon and apatite fission track (ZFT & AFT) ages throughout the Coast Mountains, ranging from 18.6±1.8 to 99.9±3.8 Ma and 5.2±0.6 to 88.3±8.1 Ma for ZFT and AFT respectively. Of note, all low-temperature cooling ages significantly postdate emplacement ages derived from high-temperature thermochronology and geochronology studies. These low-temperature cooling ages do not correspond to plutonic intrusion but rather to exhumational events. This distinction justifies interpretation of ages in the context of denudation environments. Parrish interpreted cooling-age data as indicating

there were three distinct periods of Cenozoic denudation: intense Paleocene-Eocene denudation in the central and eastern regions, subdued during middle Cenozoic through the axial part of the range, and rapid Pliocene to recent in the southern section. These AFT data were reexamined by O'Sullivan and Parrish (1995) for apatite chemical variability and many of the previous ages were amended, though the overall interpretations of events remained similar. Hickes (2001) applied ZHe and AHe in the northern Coast Mountains with ages ranging from 40.8±3.3 to 52.1±4.2 and 7.0±0.4 to 34.7±2.1 Ma, respectively. Hickes documented rapid cooling at ~45 Ma, relative thermal stability between 38 and ~7 Ma, and rapid cooling after 7 Ma. This most recent cooling pulse was interpreted to relate to late Neogene global cooling and climatic instability. These findings are corroborated by AHe data in the central part of the range that indicate little to no exhumation from 30 to 10 Ma, steady exhumation between 10 and ~4 Ma, and rapid denudation after ~2.5 Ma (Farley et al., 2001). Various studies in the Mount Waddington region have recognized rapid cooling from ~8 to 1.8 Ma, likely associated with the inception of intense glaciation in the region. For a detailed discussion of these data see Densmore et al., (2008b).

4.5 METHODS

4.5.1 Low-Temperature Thermochronology

Low-temperature thermochronometers record the time since a rock resided at a specific temperature, commonly known as the closure temperature (Dodson, 1973). Each mineral system utilizes a known parent-daughter relationship, for example He produced from the α-decay of U and Th, to determine a cooling age. The cooling age represents the cumulative effect of many processes acting to advect rocks to the surface and can be directly equated to an exhumation history with some knowledge of the subsurface thermal field and the kinematic setting of the sample. Combining multiple thermochronometers exploits the sensitivity of each system to discrete temperature ranges and enables the reconstruction of a time-temperature history through the upper crust (Reiners et al., 2005). Here we combine AHe, AFT, ZHe and ZFT to constrain cooling and exhumation in the Coast Mountains from ~250 to 70 °C (Brandon et al., 1998;

Farley, 2000; O'Sullivan and Parrish, 1995; Reiners et al., 2002). We assume that all samples have been exhumed to the surface vertically, implying no lateral motion from faulting. This assumption is justified based on a lack of evidence for active faulting in the region during or after the time of sample cooling. The core of the range has not been tectonically active since the late Miocene (>10 Ma) (Farley et al., 2001; Sweeney et al., 1992) and widespread undeformed Quaternary moraines indicate no recent deformation. We infer our assumption of vertical sample exhumation due to erosional unroofing is valid, although pre-Miocene faulting data is sparse.

4.5.2 Analytical Procedure

New ZHe ages (Table 4-1) were analyzed at the California Institute of Technology laboratory. Grains were chosen using standard microscopy under cross-polar filtered transmitted light. Each selected grain was documented and measured along the a, b and c-axis to determine the α-emission correction (Farley et al., 1996). These grains were loaded into platinum packets and thermally degassed by laser step-heating. Radiogenic helium released in this process was measured versus a spike of ^{3}He as a ^{4}He/^{3}He ratio on a quadrapole mass spectrometer. The remaining grain material was then digested, spiked with ^{235}U and ^{230}Th and analyzed for ^{238}U and ^{232}Th using isotope ratios determined from an inductively coupled plasma mass spectrometer (ICP-MS). Two aggregate packets of four grains each were run for every sample.

4.5.3 Inverse Thermal Modeling

Previous fission track studies within the Coast Mountains did not have modern modeling techniques available to constrain the thermal history. Here we employ the inverse thermal model HeFTy (Ehlers et al., 2005; Ketcham, 2005b) to resolve time-temperature histories for all four mineral systems considered. This program uses diffusion properties of helium, the annealing behavior of fission tracks, raw sample data and input thermal constraints to calculate sample cooling histories. Required inputs in this model are dependant on the thermochronometer system of interest. Fission track models require measured fission track length data, number of spontaneous and induced

tracks, and etch-pit widths (D_{par}) while (U-Th)/He models require measured grain radius, cooling age and sample error. Our modeling approach follows that of Barnes et al. (2006) and begins with an open-ended model with limited thermal information, to which we progressively add thermal restraints based on sample cooling ages and closure temperatures. Up to 5 thermal constraints are imposed depending on sample availability at each modeled location. We begin with an initial temperature condition of 350 – 400 ºC between 50 – 80 Ma from the emplacement history of the Coast Mountains. This initial temperature is sufficiently above the highest temperature sensitivity (ZFT) in order to completely reset any age signal for all samples. Higher temperatures over a longer period of time yield no changes in model results and validate our choice of the imposed initial condition. Conservative thermochronometer sensitivity windows used here are: (1) 175 – 250 ºC from ZFT (Brandon et al., 1998), (2) 140 – 220 ºC from ZHe (Reiners et al., 2002), (3) 60 – 160 ºC from AFT (O'Sullivan and Parrish, 1995), and (4) 40 – 85 ºC from AHe (Farley, 2000). These temperature windows combined with the range of sample cooling ages define regions within the time-temperature history that predicted paths must pass through. Each model is run using a Monte Carlo simulation with 20,000 paths. Segments along each t-T path varied using a monotonic consistent scheme and were halved 5 times (5E) between data constraints and 2 times (2E) between emplacement and highest temperature thermochronometer (Ketcham, 2005b). Models are evaluated using the commonly used merit value, or probability measure of goodness of fit. Models defined as good fits (merit = 0.5) have a 50% probability of a worse fit to the data, while acceptable fitting models (merit = 0.05) have a 5% probability of a worse fit (Ketcham et al., 2000).

4.5.4 Forward Thermo-kinematic Modeling

The 1-D forward thermal model AGE2EDOT is applied (Brandon et al., 1998; Ehlers et al., 2005) to determine a thermal field with respect to denudation. This estimates cooling ages based on the assumption of a constant exhumation rate and thermal steady state. Program inputs include the denudation rate (mm/yr), thermal diffusivity (km^2/Myr), internal heat production (°C/Myr), surface temperature (°C) and a

near-surface thermal gradient with no denudation (°C/km) (Table 4-2). Model outputs include cooling ages for different thermochronometer systems as a function of the denudation rate, which was treated as the primary free parameter in our analysis. Observed cooling ages were compared to predicted AHe, AFT, ZHe and ZFT ages to identify the range of acceptable denudation rates (Fig. 4-2). Alpha-radiation damaged ZFT ages are calculated for comparison (Garver et al., 2005) although samples within the southern Coast Mountains tend to have young cooling ages and relatively low amounts of uranium and thorium minimizing this effect.

In general cooling ages increase in age with increasing sample elevation. This relationship introduces a bias in 1-D modeling which do not account for topography, causing calculated denudation rates to be lower at higher elevations. In order to apply a 1-D model in an alpine environment this effect must be corrected for. We apply an elevation correction similar to Brandon et al. (1998, appendix A2) and Reiners et al. (2003). Ages are corrected using the following:

Equation 4.1:

$$\text{Age}_{corr} = Age_{samp} - ((Elev_{samp} - Elev_{mean}) / \dot{E}_{rec})$$

where Age_{corr} is the corrected age, Age_{samp} the sample cooling age, Elev_{samp} sample elevation, Elev_{mean} local mean elevation and $\dot{E}_{rec}$ the recent denudation rate. To first order this has the effect of projecting all samples to a plane at the mean elevation. Denudation rates are then calculated using these corrected ages.

4.6 RESULTS

4.6.1 Thermochronometer Data

Our thermochronometer data set is composed of 6 new ZHe samples (Table 4-4.1) combined with 11 AFT, 3 ZHe and 6 ZFT published samples (Fig. 4-3). Additionally, we use all 83 AHe samples reported in Densmore et al. (2008b) to provide context and extend the thermal history to lower temperatures of ~70 ˚C. Samples were collected over a ~40 x 50 km region with a ~4 km range of elevation, including the highest peak in the

range Mount Waddington (4016 m), and the mouth of Knight Inlet near sea level (Fig. 4-3).

AHe cooling ages (Fig. 4-4a) are described in detail in Densmore et al. (2008b). Ages range from 1.4 to 15.4, with an average of 5.2 Ma. Average error (2σ) is 1.0 Ma (17.4%). In general, AHe ages increase with increasing elevation, although there is a wide range in the distribution. Variability in the age-elevation relationship is due in part to the large spatial area over which the samples were collected.

AFT ages (Fig. 4-4b) range from 5.2 to 39.2 Ma and have an average 2σ error of 22%. These ages display a clear age-elevation relationship with older ages at higher elevations. A slight break in slope is apparent at ~2400 m. This feature combined with shortened fission track lengths has been attributed to the exhumation of a partial annealing zone (O'Sullivan and Parrish, 1995).

Both zircon systems do not display a positive correlation in age-elevation (Figs. 4-4c and d). For ZHe, sample ages are variable across the elevation range even though collected over a relatively narrow horizontal distance (~25 km). Cooling ages range from 2.4 to 27.3 Ma with an average error (2σ) of 27.2%.

Finally, ZFT ages (Fig. 4-4d) range from 18.6 to 55.2 Ma with an average error (2σ) of 13%. With the exception of one young sample, these ages fall within a narrow range of ~40 to 50 Ma. This outlying age is from a sample ~12 km south of Mount Waddington, removed from the main line of transect traversing Mount Waddington.

All samples are projected onto a swath-averaged elevation profile (Fig. 4-5) in order to compare cooling ages across the study area. This swath is 25 km wide and 85 km long, encompassing the full range of elevations within the Coast Mountains as well as all samples used here. Minimum, mean, and maximum lines of elevation (Fig. 4-5a) reflect the rugged topography and high relief over a short horizontal distance. Additionally, the field area is divided into three regions, namely the Klinaklini Valley (KV) at 0 – 37 km, Mount Jubilee (MJ) at 37 – 50 km and Mount Waddington (MW) at 50 – 85 km distance along profile. These regions are generally characterized by intermediate, young, and old cooling ages, respectively. In the KV region, AFT ages are generally ~10 Ma and ZHe samples range from 13.4 to 26.6 Ma. The most striking feature seen in the data are the remarkably young cooling ages within the MJ region (~40

74

km distance along the profile). AFT and ZHe samples are at a minimum in this area at 5.2 ± 1.2 and 2.4 ± 0.7 Ma, respectively. The MW region has generally older AFT ages that range from 11.7 to 27.4 Ma, and ZFT ages of ~45 Ma. Comparing similar elevation samples reduces the topographic effect on cooling ages. Both low (~1000 m) and high (~2500 m) elevation AFT samples display a younging trend along profile toward the MJ region with a subsequent increase in age in the MW region (Fig. 4-5c).

4.6.2 HeFTy Modeling

Our HeFTy modeling defines variations in sample cooling histories across the field region (Fig. 4-6). All samples modeled are generally consistent, displaying fairly monotonic cooling from ~160 °C since 30 – 10 Ma. Furthermore, many, but not all samples indicate a pulse of rapid exhumation within the last ~8 Myr. Subsets of the data were grouped together into three vertical transects to minimize lateral variations in our models: (1) the western slope of the heavily glaciated Klinaklini Valley, (2) the western flank and summit of Mount Jubilee, and (3) the northeast flank and summit of Mount Waddington (Fig. 4-6). The following sections describe results from the top and bottom sample of each transect. Additional intermediate samples were also modeled but display little change and for brevity are not discussed.

Transect 1. This transect includes models on the flank of the Klinaklini Valley with input time-temperature constraints of AHe, AFT, and ZHe for the upper and lower samples (Fig. 6a and b). Acceptable model fits along this transect indicate a wide range of time-temperature paths until ~10 Ma where rapid cooling occurred from ~100 °C (Fig. 4-6a and b). However, no model along this transect yielded a good fit to the data. Moreover, the lowest sample (TEKI038, Fig. 4-6b) produced no acceptable fits when ZHe, AFT and AHe constraints were integrated into the model. Figure 4-6b shows two model results using only ZHe & AFT and only ZHe & AHe. The disconnect in the cooling envelops from these models occurs at ~5 Ma where they do not overlap. Regardless of the specific sample position at ~5 Ma, cooling in this region from ~140 °C appears to have been relatively rapid since ~15 Ma. Models of this transect limit rapid cooling from ~100 °C to 7 – 18 Ma in the upper sample, and 5 – 9 Ma in the lower

sample. Best-fit results indicate relatively monotonic cooling from ~150 ºC in the upper sample and more rapid, stepwise cooling from ~180 ºC in the lower sample.

Transect 2. Here, we model the cooling history near Mount Jubilee with imposed constraints from ZHe and AHe samples (Fig. 4-6c and d). Samples record cooling within the last 10 Myr for the upper, and 27 Myr for the lower sample (Fig. 4-6d). The models along this transect exhibit many good-fits to the data and a tightly constrained recent (<15 Ma) cooling history. Good-fitting models constrain cooling as very rapid and monotonic from 160 ºC in the last 3 – 11 Myr in the upper sample (Fig. 4-6c), and 10 – 26 Myr in the lower sample (Fig. 4-6d). The best-fit model for both samples predicts very rapid cooling since ~5 Ma from >80 °C. The large error in ZHe cooling age of the upper sample limits precision, however very rapid cooling along transect 2 from ~200 ºC likely occurred since ~10 – 15 Ma.

Transect 3. The final transect is along the northeast flank of Mount Waddington and incorporates AHe, AFT and ZFT data for both samples modeled (Fig. 4-6e and f). Model results display moderate rates of cooling from 100 ºC since 27 Ma in the upper sample (Fig. 4-6e) and 15 – 17 Ma in the lower sample (Fig. 4-6f). The predicted cooling path is well constrained but only fit by a small number of model results (3 good fits) and may be stepwise or monotonic. Monotonic cooling is implied from 100 ºC since ~20 Ma for both samples, with a marked increase in the last 3 – 5 Ma where rapid cooling from 50 ºC may have occurred. Average cooling and exhumation rates appear to be comparatively lowest along this transect than in others modeled.

All three transects imply a period of rapid cooling in the last 25 Ma: Transect 1 indicates a pulse of exhumation between 5 – 18 Ma from temperatures of 100 ºC, Transect 2 between 3 – 25 Ma from 160 ºC, and Transect 3 in the last 5 Ma from 50 ºC. These pulses of rapid cooling correspond to cooling rates of 5.6 – 20 ºC/Ma along Transect 1, 6.4 – 53.3 ºC/Ma along Transect 2, and 10 ºC/Ma for Transect 3.

4.6.3 AGE2EDOT Modeling

Spatial trends in denudation are identified by estimating rates using elevation corrected cooling ages and AGE2EDOT. Observed age-elevation relationships suggest

an elevation correction of AHe and AFT ages is required, while no clear correlation preclude the need for correcting ZHe and ZFT data. We use an average elevation of 1300 m through 50 km along profile (near Mount Jubilee) and 1900 m for the remainder (near Mount Waddington). Recent denudation rates derived from AHe age-elevation profiles in Densmore et al. (2008b) are 0.8 mm/yr within the KV region, 1.1 mm/yr near the MJ region, and 1.1 mm/yr in the MW region. A denudation rate of 0.6 mm/yr is used to correct AFT ages. This rate is derived from an age-elevation profile in Parrish (1983) near Mount Waddington. Our elevation correction adjusts ages +100/-33% for AHe and +30/-12% for AFT ages. These ages were input in AGE2EDOT to determine corrected sample denudation rates.

Calculated denudation rates are similar between all thermochronometers here, ranging from 0.2 to 2.2 mm/yr (Fig. 4-7b). Rates from AHe ages range from 0.2 to 1.8 mm/yr with an average of 0.6 mm/yr. These rates increase with increasing distance along profile reaching a maximum near Mount Jubilee (~40 km along profile), averaging 0.8 mm/yr within the MJ region. In the MW region, calculated AHe rates decrease to an average of 0.5 mm/yr, slightly below the AHe average.

Denudation rates derived from higher temperature thermochronometer systems (AFT, ZHe and ZFT) follow a similar trend to AHe calculated rates but are slightly lower with an average of 0.5 mm/yr. In general, rates from AFT, ZHe and ZFT ages increase with increasing distance along profile. Of note, rates from AFT ages are very similar to those calculated from neighboring AHe samples through most of the profile. Rates derived from higher temperature chronometers reach a regional maximum within the MJ region at 2.2 mm/yr. This calculated rate is derived from a ZHe cooling age and consequently incorporates no elevation correction. However, this sample is ~50 m above the local mean (1300 m) and would produce a negligible change in calculated denudation rate. Finally, AFT, ZHe and ZFT calculated denudation rates decrease with distance through the profile near Mount Waddington, averaging 0.4 mm/yr.

4.7 DISCUSSION

4.7.1 Total Denudation Magnitude

The denudation history of the southern Coast Mountains can be constrained by estimating the magnitude of material removed from the landscape. Here, our calculated denudation rates are combined with thermochronometer cooling ages to estimate the total magnitude of denudation for each of the defined regions (Fig. 4-8). Average cooling ages are used from each region in order to smooth local variations and characterize the regional extent of exhumation. Instances of a single cooling age from a mineral system within a region is omitted to avoid over-emphasizing any one data point. Of note, these are not volume estimates and are independent of drainage basin area. The total denudation magnitude is the product of the highest temperature thermochronometer system available (ZHe or ZFT) and the corresponding calculated denudation rate. These estimates are 9.2, 8.8 and 11.5 km for the KV, MJ and MW regions, respectively. All three are of comparable order, however timing over which this denudation was accomplished varies dramatically. In the KV region, 9.2 km was removed over 20.9 Myr (from ZHe, denudation rate of 0.4 mm/yr) while within the MJ region removal of 8.8 km took less than 7 Myr (from ZHe, denudation rate of 1.3 mm/yr). In the MW region the 11.5 km was removed over 28 Myr (from ZFT, denudation rate of 0.4 mm/yr). This average ZFT age is heavily influenced by one age (18.6 Ma) significantly younger than the remaining four. For consistency we report the average age but emphasize that ZFT ages in this region are generally older and therefore our estimate may under predict the amount and duration of denudation recorded. Regardless, in comparison to MW the MJ region has experienced ~75% total denudation in less than 25% time.

Next, we determine denudation magnitudes for lower-temperature thermochronometers (AHe and AFT) and compare these values to HeFTy time-temperature constraints. Each region is discussed in detail below.

KV Region. The amount and duration of denudation from average AFT and AHe ages are 7.2 km since 15.4 Ma, and 3.3 km since 6.5 Ma, respectively. Average denudation rates are 0.5 mm/yr for both AFT and AHe cooling ages. These values along with calculated ZFT denudation rate (0.4 mm/yr) indicate consistent, steady denudation

over the 20.9 Ma time span recorded in all three thermochronometer systems here. We cannot constrain a distinct cooling history using these results and our HeFTy models which yield no good fits. However, steady, moderate exhumation (~0.4 mm/yr) does fit the range of HeFTy predicted thermal histories (e.g., Fig. 4-6a).

MJ Region. The area near Mount Jubilee exhibits the highest average denudation across the entire topographic profile. Here, AHe ages suggest over 3.4 km of material have been removed in the last 3.4 Myr. This amount combined with the total for the region suggests rapid denudation (>1.0 mm/yr) since at least ~7 Ma. Denudation in this region removes nearly an equal amount of material as in the KV region in significantly less time. Furthermore, we have no age constraints near Mount Jubilee older than 10 Ma and therefore these estimates represent a lower boundary. Rapid denudation in this region is consistent with the best-fit HeFTy results which indicate a high cooling rate, therefore a high denudation rate (>0.8 mm/yr) since ~ 8 Ma (e.g., Fig. 4-6c).

MW Region. In the MW region 5.7 km of material has been removed since 21.2 Ma (from AFT, denudation rate of 0.3 mm/yr) and 3.1 km since 7.3 Ma (from AHe, denudation rate of 0.4 mm/yr). Modeled cooling histories in this region are not well constrained but are broadly consistent with calculated denudation rates and magnitudes (e.g., Fig. 4-6f). The largest discrepancy between denudation estimates and modeled time-temperature history is derived from HeFTy results that suggest increasing or at least stable cooling rates between 20 and 10 Ma. However, our calculated denudation rates do fall within the range of acceptable-fit models.

Our calculated denudation rates and magnitudes incorporate pre- and syn- and post-glacial regimes within the field area. In general, average long-term rates of denudation are temporally consistent throughout each region however some variation does exist. Most notably, rapid denudation within the MJ region indicates focused exhumation since at least ~7 Ma. Slight increases in denudation rates may be present at ~7 Ma in the KV and MW regions but are difficult to resolve within sample error. Regardless, these observations suggest that the long-term transition from primarily fluvial and hillslope denudation to a glacial environment induces varying responses across the topography. In particular, our findings indicate in the last ~7 Myr denudation magnitudes differing by >6 km over a horizontal distance of ~20 km. This reveals significant local

variations in denudation within the study area. The dramatic change in material removed over a short distance cannot be accommodated by crustal flexure alone and therefore necessitates some component of a temporally variable landscape. The major implication of this is the MJ region must have featured greater relief than present day, likely with an expanded ridge-line continuing along the western flank of Mount Waddington. Assuming the modification of the local terrain near Mount Jubilee was coincident with intense alpine glaciation, this would most likely require one of two possible scenarios: increased ice flux and focused denudation originating from (1) Mount Waddington, or (2) the Klinaklini Valley. Cirque retreat from the walls of the paleotopography may have joined ice sourced from Mount Waddington, eroding the landscape over a number of glacial/interglacial cycles. Alternatively, Mount Jubilee may have functioned as a nunatak during glacial highstands, bisecting and diverting ice flow through the Klinaklini Valley. Unfortunately, modern topography in the region does not clearly differentiate between these two scenarios. However, both cases require drainage reorganization and fluvial reworking during interglacial times to establish present day morphology. Finally, this major reworking is not laterally continuous emphasizing the irregular distribution of denudation over glacial/interglacial cycles.

A major caveat of the timing and duration here is rapid, recent (<4 Ma) denudation may be averaged out over a longer period of time. In looking at regional trends in the data over long periods of time we lose resolution of small-scale (both spatial and temporal) features. Results from Ehlers et al. (2006) and Shuster et al. (2005) indicate increased denudation rates in the last ~4 and 1.8 Myr, respectively. This recent increase in denudation is in agreement with our good-fitting HeFTy time-temperature models. However, this signal cannot be distinguished within our average denudation rates. Additionally, an identified denudation rate increase captured by AHe and AFT data in this region (Densmore et al., 2007; Ehlers et al., 2006) is not reflected in our average denudation rates. This is a result of the spatially variable nature of glacial denudation as well as averaging cooling ages within each region. The three defined regions here encompass high relief and large spatial areas therefore averaged cooling ages incorporate different topographic features. For example, samples located within small tributary valleys as well as the main trunk of the Klinaklini River Valley are

integrated into a single age. For a detailed investigation into these small scale features using AHe cooling ages, see Densmore et al. (2008b).

4.7.2 Mid-Late Cenozoic Denudation History (~30-0 Ma)

We present an integrated history of cooling and denudation within the southern Coast Mountains to compare with previous thermochronologic work throughout the orogen (Fig. 4-9). Our calculated long-term denudation rates average 0.4 mm/yr between 28.1 and 7.3 Ma where there is a marked increase, especially in the Mount Jubilee region, to an average of 0.9 mm/yr. This recent, rapid denudation indicates effective long-term rates must be lower prior to ~10 Ma (~0.2 mm/yr) in order to accommodate the high rates earlier in the record. Best-fit HeFTy models indicate fairly monotonic cooling (~4 °C/Myr) from ~160 °C since 20 Ma with an increase to more rapid cooling (~5 – 10 °C/Myr) at ~10 Ma perhaps followed by a very recent pulse within the last 3 to 5 Myr (~10 – 15 °C/Myr). Assuming an average geothermal gradient of 25 °C/km, these cooling rates suggest denudation rates of ~0.2 mm/yr for <20 Ma, increasing to 0.2 – 0.4 mm/yr at 10 Ma with an additional recent increase to ~0.4 – 0.6 mm/yr. Studies by Hickes (2001), O'Sullivan and Parrish (1995), and Farley et al. (2001), primarily in the lower relief northern and central Coast Mountains, indicate a denudation history defined by a sustained episode of relative quiescence from ~35 through 10 Ma (~0.1 – 0.2 mm/yr), a pulse of rapid denudation between ~5 – 10 Ma (~0.4 mm/yr) and perhaps a further increase within the last 4 Myr (~0.4 – 0.8 mm/yr).

Overall, the similarity in the southern, northern and central Coast Mountains implies that the identified phases of denudation in local studies are broadly relevant. This indicates the orogen experienced similar episodes of exhumation and denudation along strike, regardless of variations in plate boundary deformation to the west (Fig. 4-1). However, local variations in timing and magnitude exist between most of the datasets. For example, the timing of rapid recent denudation ~1.0 mm/yr in the MJ region is observed in the central Coast Mountains, while the magnitude is somewhat lessened. With respect to glaciation, this emphasizes the temporal and spatial variability of glacial denudation on both a local and regional scale.

We interpret these identified phases of denudation in terms of mountain building and glaciation. As suggested by Parrish (1983) the initial pulse of exhumation during the mid to late Paleogene may be related to orogenesis and deformation associated with the collision of the Pacific Plate and North America. The decrease to subdued rates during Miocene likely represents a period of gradual (mostly fluvial) erosion of the orogen. The onset of more rapid denudation in the late Miocene is linked to the onset of glaciation in the region, perhaps ~7 – 6 Ma, thus changing the major mechanism of denudation from fluvial and hillslope to glacial. This signal appears to be ubiquitous throughout the range and not confined to the southern region with the highest topography. Recent denudation rates appear highest in the southern Coast Mountains, perhaps owing to the high topography encouraging more intense glaciation. This increase in denudation is variable on a local scale indicating that not all regions are similarly affected by glacial denudation. Finally, an increase in denudation during the Pleistocene may be present but is difficult to directly test using conventional thermochronology.

4.8 CONCLUSIONS

We present a synthesis of new and previously published AHe, AFT, ZHe and ZFT thermochronometer data from the southern Coast Mountains, British Columbia. This data was interpreted with inverse and forward thermal modeling techniques to provide independent and straightforward quantitative methods for constraining denudation over long periods of time ($>10^6$ yrs). Our findings from this approach are:

- Thermochronometer cooling ages from AFT, ZHe and ZFT range from 5.2 – 39.2 Ma, 2.4 – 27.3 Ma, and 18.6 – 55.2 Ma, respectively. Errors (2σ) for these systems are generally between 15 – 25%.

- Cooling ages generally follow a positive age-elevation relationship but show wide variability, as ZHe and ZFT data do not exhibit a clear age-elevation relationship. There is a pronounced minimum in cooling ages near Mount Jubilee (MJ region) indicating focused exhumation in this region associated with greater denudation relative to other regions of the study area.

- Inverse modeling of fission track and (U-Th)/He ages for sample cooling histories indicates a general pattern of monotonic cooling from ~160 ºC since 30 – 10 Ma and more rapid exhumation within the last ~8 Myr. Specifically, 3 vertical transects modeled indicate distinct cooling envelopes: (1) steady cooling from ~140 ºC in the last ~15 Ma (~0.4 mm/yr) along the western slope of the Klinaklini Valley, (2) rapid cooling from ~200 ºC since 10 – 15 Ma (>0.6 mm/yr) near Mount Jubilee, and (3) relatively slow cooling that may be stepwise or monotonic from ~100 ºC since ~20 Ma (~0.25 mm/yr) on the northeast flank of Mount Waddington.

- Denudation rates determined from cooling age data using the 1-D model AGE2EDOT range from 0.2 – 2.2 mm/yr with an average of ~0.5 – 0.6 mm/yr for all thermochronometer systems. We divide the region into 3 areas correlating with distinct patterns of denudation: (1) the Klinaklini Valley with rates slightly increasing to the east/northeast, (2) Mount Jubilee with generally high rates of denudation, and (3) Mount Waddington with subdued denudation rates below the calculated average.

- Calculated denudation magnitude, or the total amount of material removed from our 3 regions is 9.2, 8.8 and 11.5 km since 20.9, 6.9, and 28.0 Ma, respectively.

This chronology of exhumation indicates spatially and temporally variable denudation for the southern Coast Mountains since at least 30 Ma. These findings along with previous work throughout the range suggest 3 major phases of denudation: (1) relatively high during the mid – late Paleogene (>30 – 20 Ma), perhaps associated with the early phases of subduction off shore, (2) a period of subdued denudation during most of the Miocene (~20 – 7 Ma), and (3) an increase to fairly rapid rates from the latest Miocene (~7 Ma) to the present, presumably due to the onset of extensive glaciation. These findings are consistent throughout the orogen, although local variations in rates and timing do occur. Finally, only AHe samples sufficiently capture the most recent period of cooling. Therefore, in this region some combination of higher temperature thermochronometers (AFT, ZHe or ZFT) and AHe must be used in order to characterize the most recent signal of cooling, and specifically the onset of glaciation.

4.9 ACKNOWLEDGEMENTS

Citation:

Densmore, M.S., Ehlers, T.A., Farley, K.A., Rusmore, M.E., Woodsworth, G.J., 2008, Observed spatial and temporal variations in glacial denudation from thermochronometer data: Coast Mountains, B.C., to be submitted to *J. Geophys. Res. – Earth Surface*.

4.10 FIGURES

Figure 4-1. Shaded-relief digital elevation model (DEM) of the Canadian Cordillera. Numbers in boxes show general age ranges for groups of samples. A: General features of the terrain including plate boundaries (EX.= Explorer, J.D.F.= Juan de Fuca), and major morphogeologic belts. Black box is study area shown in subsequent figures. B: Sample locations from previous geochronologic studies within the Coast Mountains. W.R. K-Ar= whole rock ^{40}K-^{39}Ar, W.R. Rb-Sr= whole rock Rb-Sr. C: Sample locations from previous thermochronometer studies. AHe= apatite (U-Th)/He, AFT= apatite fission track, ZHe= zircon (U-Th)/He, ZFT= zircon fission track, Bio K-Ar= biotite ^{40}K-^{39}Ar, Hb K-Ar= hornblende ^{40}K-^{39}Ar.
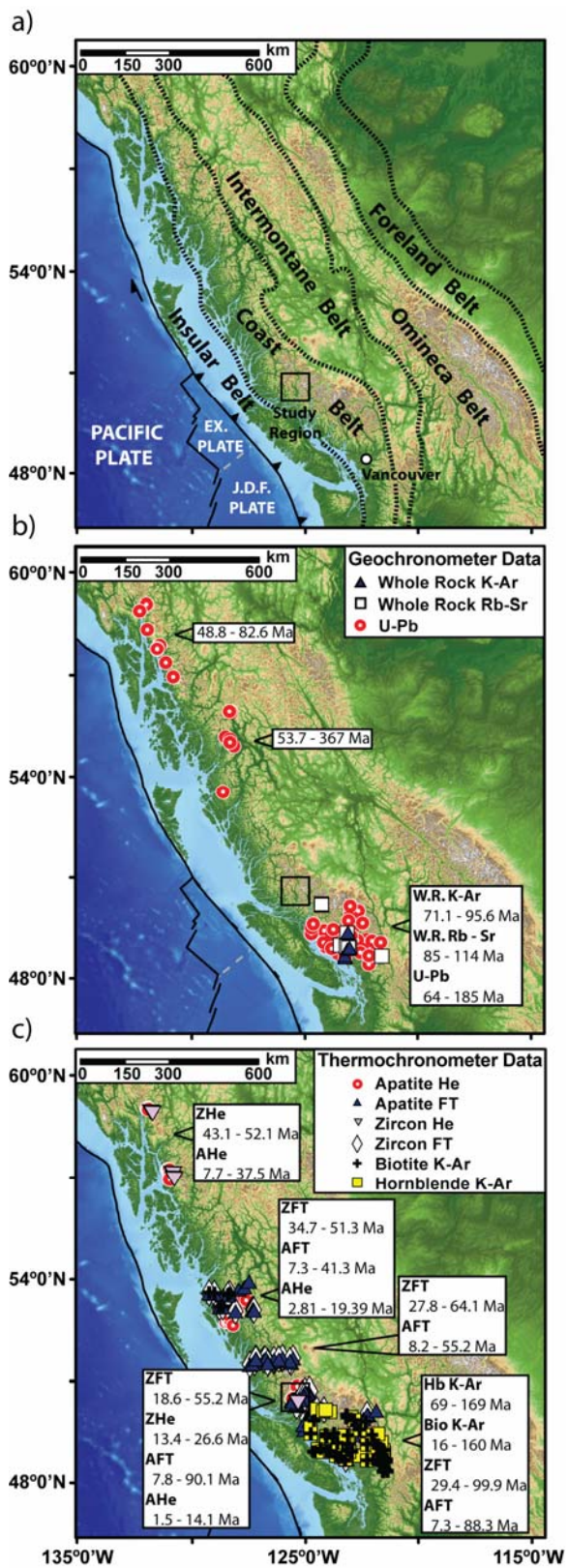
Figure 4-2. AGE2EDOT model results for all thermochronometer systems applied here, showing how cooling ages are uniquely related to erosion (denudation) rates.
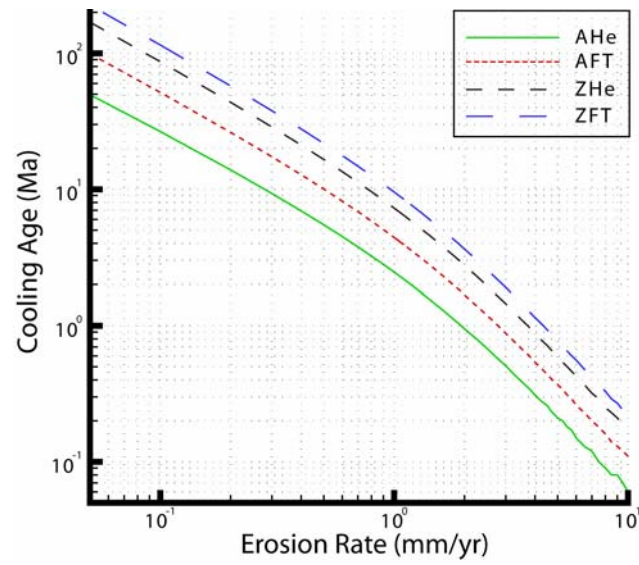
Figure 4-3. Shaded relief DEM of Mount Waddington region showing present-day extents of snow and ice (white) and vegetation (light grey), as well as sample locations from all thermochronometers. Rectangle represents swath used for min-mean-max elevation profile in subsequent figures, dashed lines separate specific regions (KV= Klinaklini Valley, MJ= Mount Jubilee, MW= Mount Waddington) and solid lines are quasi-vertical transects used in HeFTy modeling (see Fig. 4-6). AHe= apatite (U-Th)/He, AFT= apatite fission track, ZHe= zircon (U-Th)/He, ZFT= zircon fission track.
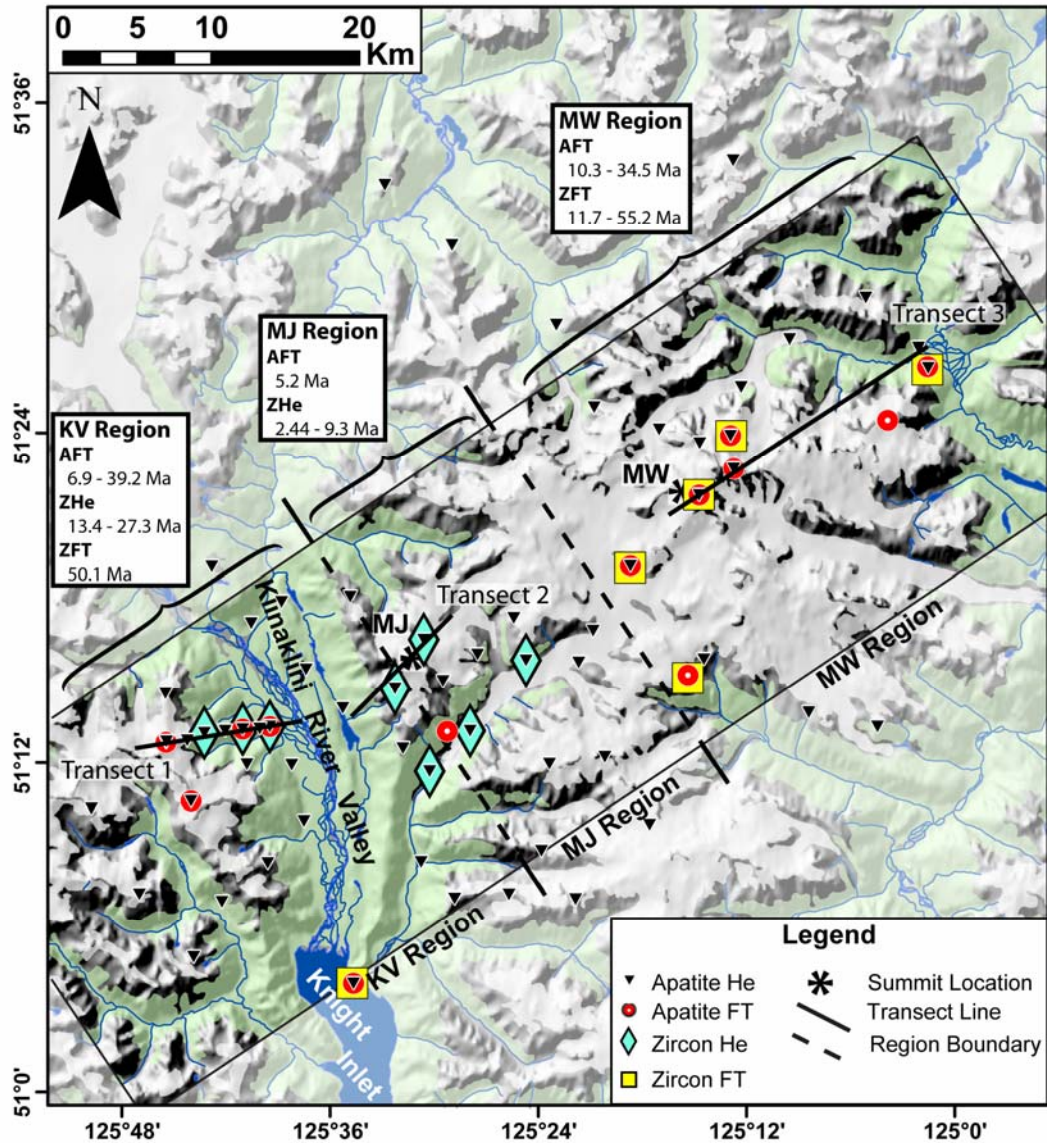
Figure 4-4. Thermochronometer cooling ages versus sample elevation. Error (2σ) is based on age reproducibility and is contained within symbols if not visible. A: Apatite (U-Th)/He ages (Densmore, 2008b) included for comparison but we highlight higher temperature thermochronometers here. B: Apatite fission track ages – note X-axis change. C: Zircon (U-Th)/He ages. D: Zircon fission track ages – note X-axis change.
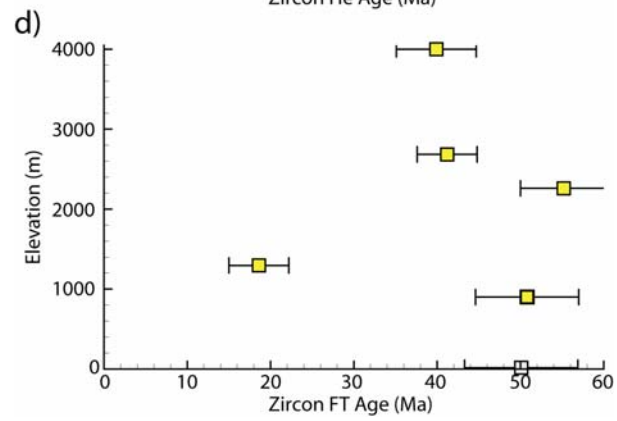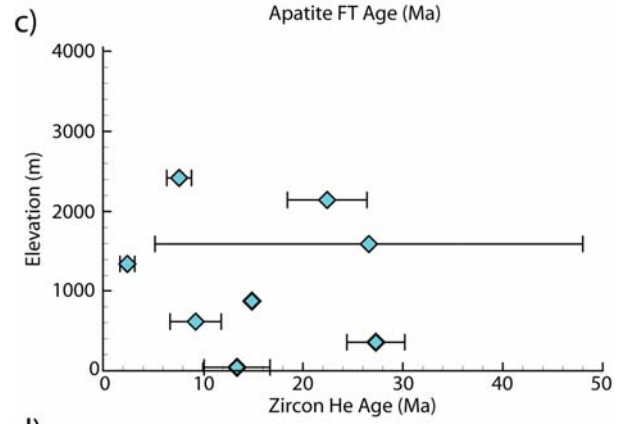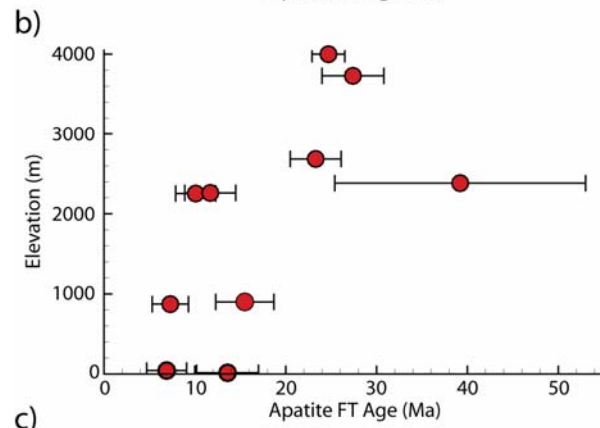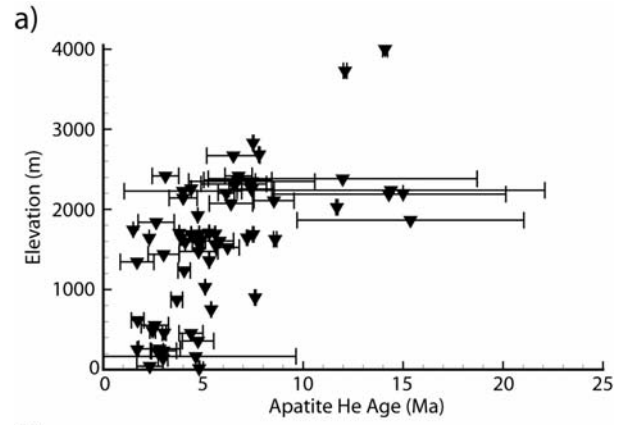
Figure 4-5. Cooling age data related to sample location. A: Min-mean-max elevation profile (from Figure 4-3) with samples projected to center line. KV= Klinaklini Valley, MJ= Mount Jubilee, MW= Mount Waddington. B: Associated cooling age data projected along same profile line. C: Similar elevation apatite fission track ages around 1000 m (filled circles) and 2500 m (open circles) to highlight differences in cooling age from comparable samples in each region.
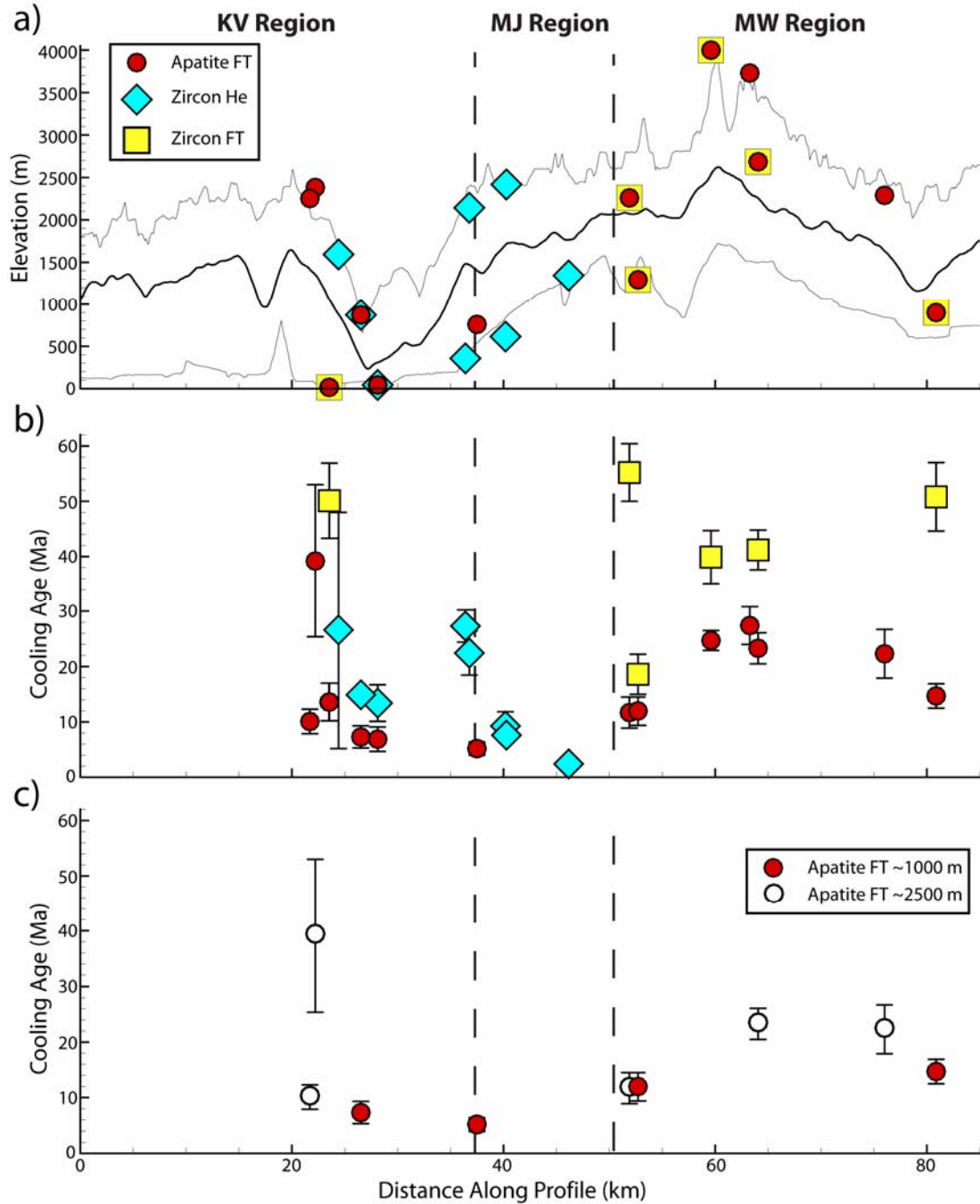
Figure 4-6. HeFTy model results for 3 vertical transects, locations in Figure 4-3. Insets are track-length distributions. N= number of spontaneous tracks, light grey regions denote acceptable fits and dark grey good fits, boxes are imposed thermal constraints, and center line indicates best-fit time-temperature path. A: Thermal history for the top and bottom (B) of Transect 1. Of note, modeling of TEKI038 using both apatite (U-Th)/He and apatite fission track produced no good or acceptable fits. Included is the envelope for acceptable fits using apatite fission track (light grey) and good fits using apatite (U-Th)/He (dashed line) data. C: Thermal history for top and bottom (D) of Transect 2. Note, there are no fission track samples used in C and D therefore no track-length distributions are present. E: Thermal history for top and bottom (F) of Transect 3. G: Min-mean-max profile defined in Figure 4-3 with projected samples.
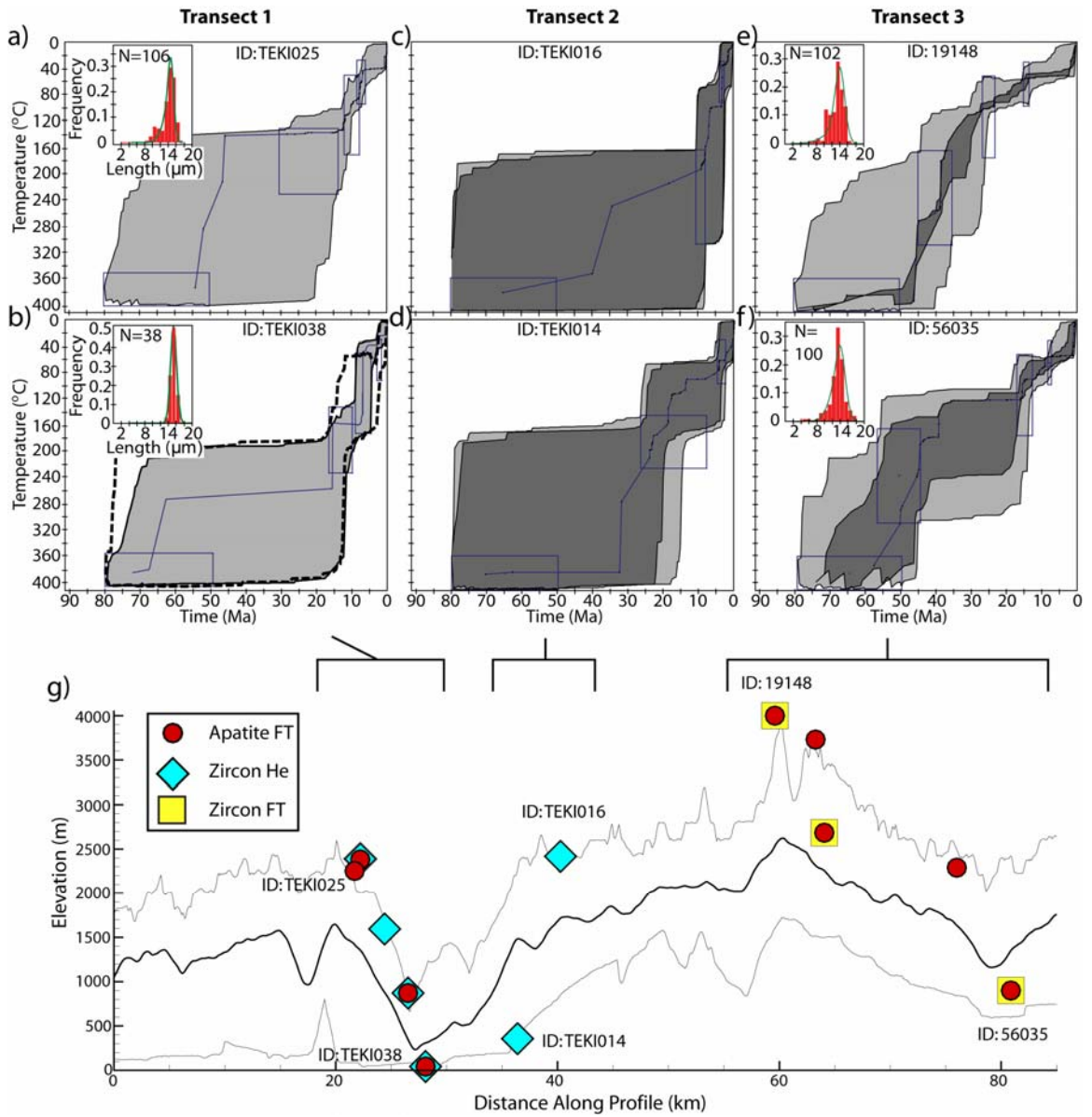
Figure 4-7. Calculated denudation rate related to sample location. A: Sample locations as Figure 4-5. KV= Klinaklini Valley, MJ= Mount Jubilee, MW= Mount Waddington. B: Denudation rates calculated using AGE2EDOT 1-D thermal model. Dot-dash line is average apatite fission track, zircon (U-Th)/He, and zircon fission track denudation rate (0.5 mm/yr). Error calculated by modeling 2σ extent of cooling ages and determining denudation rate. Rates derived from apatite (U-Th)/He ages (grey triangles) are included for comparison.
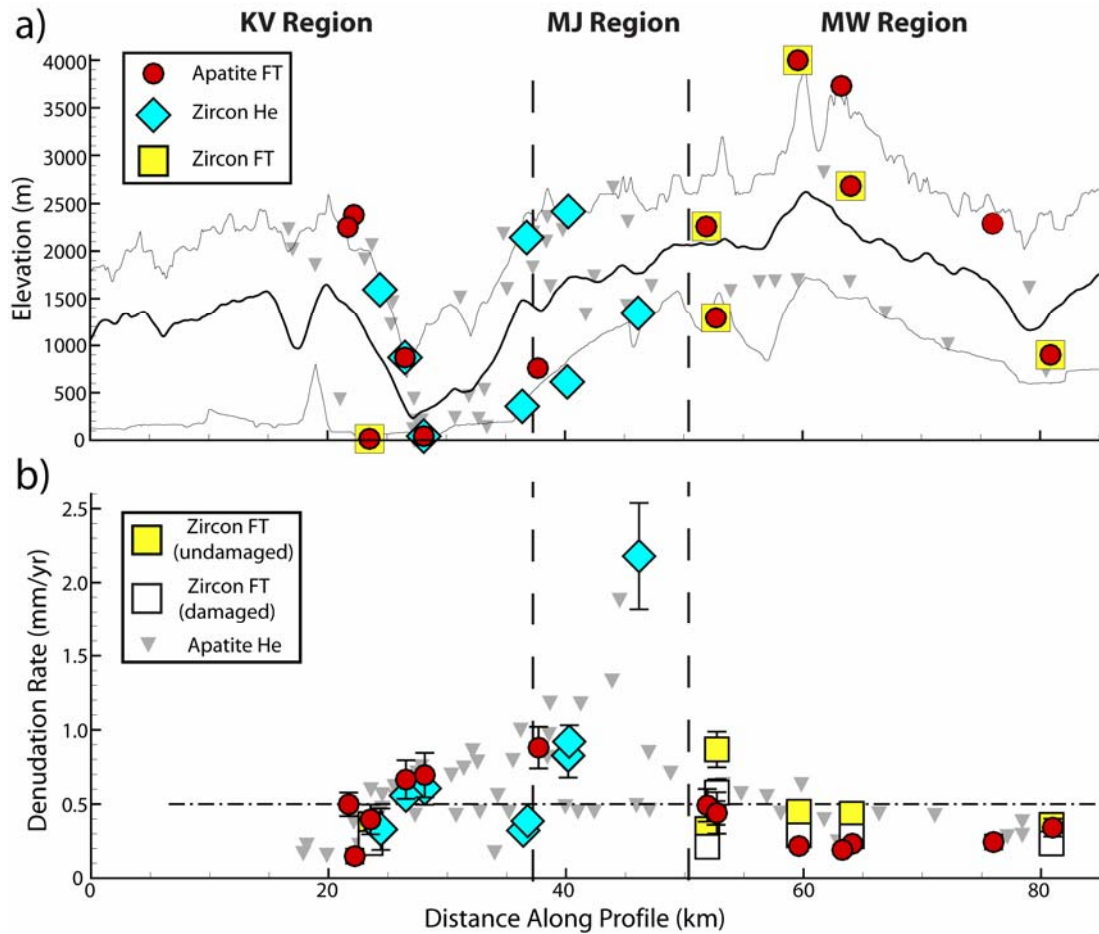
Figure 4-8. Regional denudation magnitudes across the study area. A: Min-mean-max elevation profile (from Figure 4-3). Dashed lines represent divisions used in (B) based on trends in calculated denudation rates. B: Denudation magnitude across profile. Black region determined from apatite (U-Th)/He data, dark grey from apatite fission track, light grey from zircon (U-Th)/He and light stipple region from zircon fission track. Each column represents total denudation over an amount of time equal to the average cooling age for the highest temperature thermochronometer available. The total magnitude is the product of this age with the corresponding average calculated denudation rate.
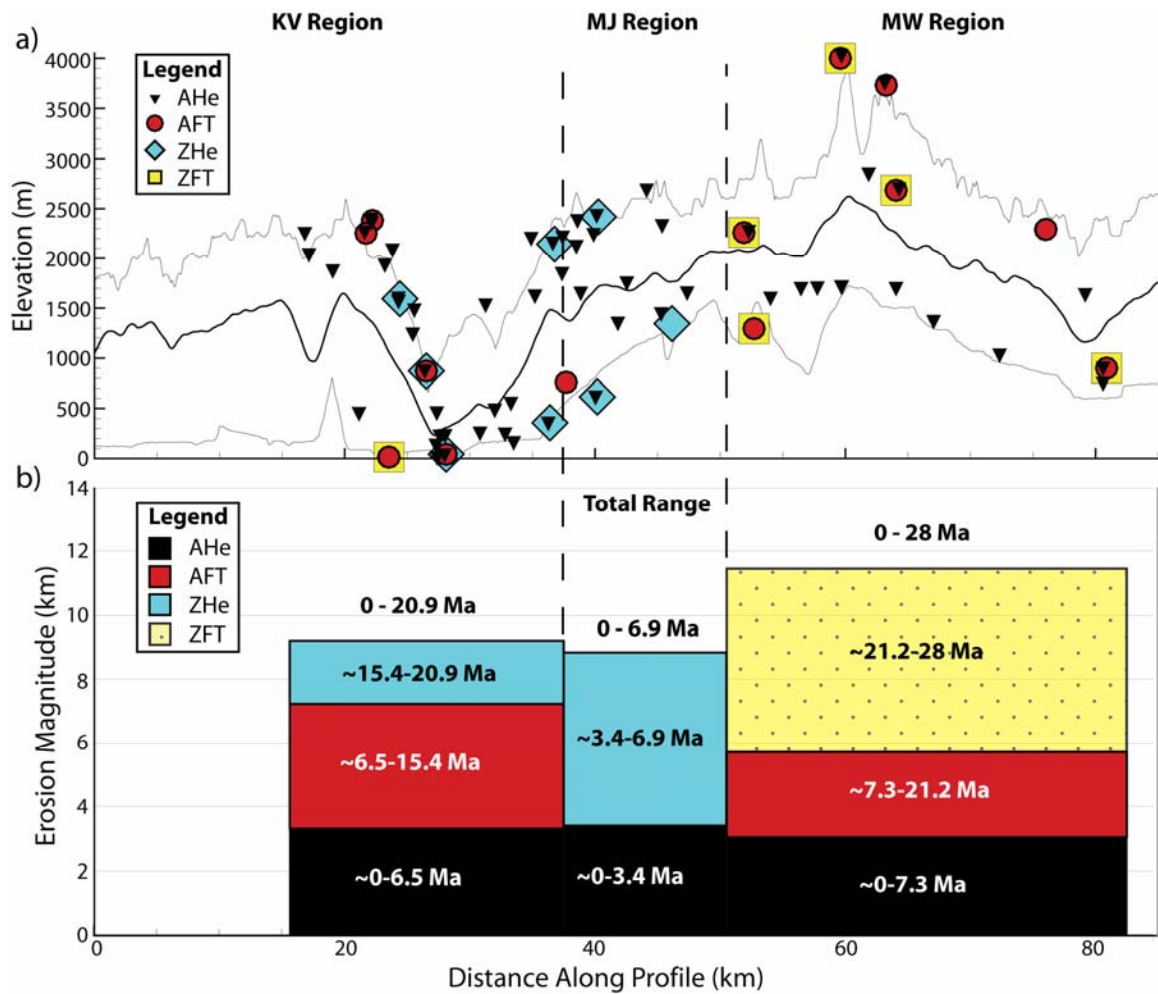
Figure 4-9. Long-term denudation rate estimates from the southern (this study), central and northern (Farley et al., 2001; Hickes, 2001; O'Sullivan and Parrish, 1995) Coast Mountains. Long-term average (0.5 mm/yr) derived from 1-D AGE2EDOT modeling of apatite fission track, zircon (U-Th)/He and zircon fission track ages. Wide range in rate estimates is due to resolving multiple quantitative techniques, namely 1-D thermal (AGE2EDOT) and time-temperature (HeFTy) modeling.
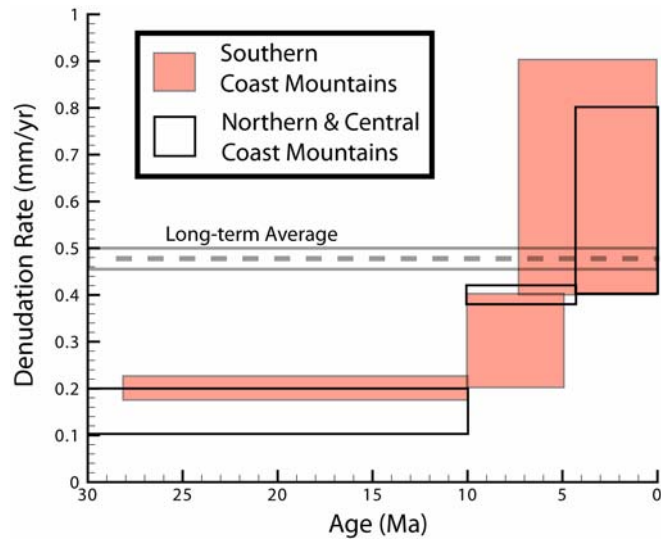
Table 4-1. Raw ZHe data from aggregates of 4 grains per analysis. UTM E. and N.= UTM Easting and Northing, respectively, using North American Datum 1983, FT Corr.= fraction of alpha particles retained, Corr. Age= FT corrected age.

Sample ID	Elev. (m)	UTM E. (m)	UTM N. (m)	Mass (µg)	U (ppm)	Th (ppm)	He (nmol/g)	FT Corr.	Raw Age (Ma)	Corr. Age (Ma)	Average Age (Ma)	Std. Dev. (Ma)
03TEKI024a	2382	306472	5677393	19.4	64.4	24.4	5.2	0.74	13.6	18.3	22.5	4.2
b				17.6	23.3	12.3	2.8	0.75	20.0	26.7		
03TEKI011a	357	324283	5675443	48.6	64.7	18.9	7.9	0.81	20.9	25.9	27.3	1.4
b				103.9	74.2	24.1	10.6	0.85	24.4	28.7		
03TEKI014a	2143	321944	5681045	19.7	193.9	99.2	21.4	0.74	18.1	24.4	22.4	2.0
b				14.3	196.8	60.4	16.9	0.72	14.7	20.4		
03TEKI010a	615	327002	5678185	175.5	45.7	2.6	1.7	0.87	6.9	8.0	9.3	1.3
b				141.0	55.3	7.1	2.8	0.86	9.1	10.5		
03TEKI009a	1345	330773	5682934	99.8	49.1	6.5	0.5	0.84	1.7	2.1	2.4	0.4
b				49.7	65.2	16.4	0.9	0.80	2.3	2.8		
03TEKI016a	2418	323861	5684352	81.0	87.4	34.9	3.7	0.83	7.2	8.7	9.1	0.7
b				109.8	75.4	35.3	3.7	0.84	8.1	9.6		

Table 4-2. Thermal model variables and justification. Diffusivity and heat production were measured on rock samples within field region, surface temperature from Ehlers et al. [2006], thermal gradient with no denudation from 3-D thermal model at steady state of Densmore et al. [2007] and depth to Moho (constant temperature boundary) from Hammer and Clowes (1997).

Constant	Value	Reference
Thermal Diffusivity	31.81 km^2/Myr	See Appendix 2
Internal Heat Production	6.76 °C/Myr	See Appendix 2
Surfact Temperature	4.0 °C	Ehlers et al., 2006
Surface Thermal Gradient (no erosion)	19 °C/km	Densmore et al., 2007
Depth to Constant Temperature	35 km	Hammer and Clowes, 1997

Chapter 5: Interpreting Thermochronometer Cooling ages in a Glaciated Orogen

5.1 ABSTRACT

Glaciers have long been acknowledged as important instruments in modifying landscapes, altering denudation rates from previously fluvial environments. A common tool for constraining denudation rates is low-temperature thermochronometer data interpreted with a 1- or 2-D numerical method. We utilize a 3-D thermo-kinematic finite element model to assess the validity of 5 such methods, including a 1-D thermal model, an assumed constant thermal gradient, an assumed constant elevation of critical isotherms, best-fit regression lines through an age-elevation profile and a 2-D correction of regression lines. The 3-D model incorporates variable denudation and differing relief change scenarios to test if relief change around present day topography is detectable in a thermochronometer dataset. Experiments were run to determine data sensitivity to basal temperature, denudation rate and relief change. Finally, an application of this model in a heavily glaciated terrain is presented.

All 1-D methods tested here reproduce average 3-D calculated denudation rate and cooling age to within ~20%. However, these methods significantly overemphasize local high amplitude, short wavelength features in the landscape leading to misfits of ~50%. Best-fit regression lines through age versus elevation profiles yield apparent denudation rates >70% different from the 3-D model input denudation rate, however a 2-

D correction for the effect of topography improves this estimate to ~10%. Of note, each of these methods is applied under ideal conditions with thermal and kinematic inputs derived from the 3-D model and error in estimated rates should be considered minimums.

The 3-D model is integrated with a large thermochronometer dataset to determine data sensitivity to input parameters, and constrain denudation rates and topographic evolution across a glaciated landscape. We find that the data are insensitive to variations in basal temperature and relief from 25 – 175% of the modern topography. Best-fit model parameters suggest long-term (>10^6 yrs) denudation rates of ~0.4 mm/yr with local variations of +/- 0.4 mm/yr. Results indicate simple changes in topography and relief can not reproduce the data. Additionally, relief change is difficult to detect in a thermochronometer dataset when incorporating sample error. Finally, the observed data include a wide distribution of cooling ages indicating some component of local variations in denudation or topography likely occurred as samples were cooling.

5.2 INTRODUCTION

Glaciers exert a fundamental control on alpine landscapes and are significant agents of erosion that modify topography and alter local relief. Glacial processes transform landscapes creating, among other features, sheer headwalls due to overdeepening and cirque retreat, steeply-sloped U-shaped valleys and large lateral and end moraines in previous fluvially dominated environments. These surficial variations cause perturbations in the subsurface thermal field as isotherms adjust to changes in the overlying topography. Therefore, quantifying the thermal field should lead to constraints on the denudation history. Previous work has documented the overprinting effect of glaciation on a fluvial landscape by analyzing hypsometry (Brocklehurst and Whipple, 2004), long- and cross-valley profiles (Brardinoni and Hassan, 2006; Brocklehurst and Whipple, 2006; Brook et al., 2008; Montgomery, 2002), cirque position through time (Oskin and Burbank, 2005) and hillslope angles (Naylor and Gabet, 2007). Moreover, recent numerical models have incorporated the effects of glacial denudation on landscape evolution from more simplistic 1-D (MacGregor et al., 2000) and 2-D (Herman and Braun, 2008; Kessler et al., 2006) predictions of glacial and topographic morphology, to fully integrated 3-D landform evolution models (Tomkin and Braun, 2002; Tomkin and

Roe, 2007) that predict how glaciated terrains evolve over $10^5 - 10^6$ yrs. However, observations of glacial denudation over timescales relevant to mountain building have lagged behind. Here, we augment and expand on previous works by exploring the thermal consequence of topographic changes in glaciated orogens using apatite (U-Th)/He (AHe) and fission track (AFT) thermochronology.

Thermochronometer data can constrain denudation and topographic evolution over long ($>10^5$ yr) timescales (Braun, 2002b; Ehlers and Farley, 2003; Ehlers, 2005; Hodges, 2003; Reiners, 2007; Reiners and Brandon, 2006). Each mineral system is sensitive to a particular temperature within the upper crust, commonly referred to as the closure temperature (Dodson, 1973). An accurate understanding of the subsurface thermal field enables interpretation of thermochronometer data in the context of exhumation and denudation by surface processes such as glaciation. Recent studies have applied various numerical methods to predict the thermal field as well as thermochronometer cooling ages in glaciated settings, including 1-D (Berger et al., 2008; Densmore, 2008b, c; Spotila et al., 2004) and 3-D with steady-state (Densmore et al., 2007; Ehlers et al., 2006) or temporally variable topography (Herman et al., 2007) modeling techniques. Here, a modified 3-D thermo-kinematic model, Pecube (Braun, 2003), is used to determine the thermal field with respect to background denudation and variable topography in order to assess the validity of 1- and 2-D methods in comparison to a sophisticated 3-D model. An application of this 3-D model within a heavily glaciated terrain is used to evaluate the effect of relief change due to glaciation on thermochronometer cooling ages.

Our 3-D model is used to predict cooling ages to compare with a compiled thermochronometer dataset within the Coast Mountains, British Columbia (Fig. 5-1a). Our field region has been heavily glaciated in the last ~7 Ma (Clague, 1991; Densmore, 2008b) and a dense dataset of thermochronometer cooling ages (Fig. 5-1b) has been collected (Densmore, 2008b; Ehlers et al., 2006; O'Sullivan and Parrish, 1995). The data and model are integrated to address the range of best-fit including basal temperature, background denudation rate and relief change scenarios. Specifically, we test whether relief change using modern topographic relief or larger scale changes to the topography such as changes in position of valleys and ridges are detectable in thermochronometer

data. The data used in this study are presented in two companion chapters that analyze (1) small-scale features in the landscape utilizing AHe data and 1-D modeling (Densmore, 2008b), and (2) broad, general trends in denudation and exhumation across the Coast Mountains from AFT, and zircon (U-Th)/He (ZHe) and fission track (ZFT) thermochronology with 1-D forward and inverse modeling (Densmore, 2008c).

5.3 BACKGROUND

Although the general aim here is an understanding of the effect of glaciation on the thermal field, pertinent geologic background of the field region within the Coast Mountains, British Columbia is presented. Additionally, we introduce various quantitative techniques available for data interpretation and summarize previous thermochronometer studies within this field region. These sections will provide context for comparison of modeling techniques and data presented in section 5.6.

5.3.1 Geologic Setting

The Coast Mountains of British Columbia are the product of long-term subduction of the Kula and Farralon plate (now Juan de Fuca and Explorer microplates) beneath the North American (Laurentian) west coast. This orogen stretches north-south along strike from southern Alaska to northern Washington, USA (Fig. 5-1) and encompasses over 4 km of relief from Mount Waddington, the highest peak in the range, to steeply-sloped fjords that terminate in the Pacific Ocean. The range consists primarily of granodiorite and diorite of generally Late Cretaceous age (Harrison et al., 1979; Woodsworth et al., 1991) with emplacement ceasing during the early Eocene (~50 Ma) (Harrison et al., 1979, and references therein) approximately coincident with termination of subduction of the Kula plate (Atwater and Stock, 1998; Engebretson et al., 1984). Reorganization from orthogonal to oblique subduction of the Juan de Fuca and Explorer microplates at ~2 Ma resulted in a decrease in tectonic activity throughout the range (Braunmiller and Nabelek, 2002; Dziak, 2006).

5.3.2 Thermochronometer Interpretation Techniques

A number of quantitative techniques are available to interpret thermochronometer data in the context of denudation. Widely available interpretation methods are introduced below with the details described in section 5.4.

AGE2EDOT: A simple 1-D thermal model that calculates a geothermal gradient with respect to various thermal properties and denudation (Brandon et al., 1998; Ehlers et al., 2005). Cooling ages are predicted as a function of the calculated thermal field. This program is advantageous in that denudation rates can be constrained with any number of samples (Reiners and Brandon, 2006; Schildgen et al., 2007). However, predicted ages are independent of elevation and assume a constant subsurface geotherm across the region. One way to circumvent this drawback is to compare samples from similar elevations across a landscape (e.g. Densmore, 2008c).

1-D draped isotherm: A spatially constant geothermal gradient across the landscape can be assumed causing isotherms to perfectly mimic the topography (Ehlers et al., 2001). Thermal data can be derived from empirical evidence such as boreholes, wells or previous thermochronometer data (e.g. O'Sullivan and Currie, 1996) that guide denudation estimates (e.g. Berger and Spotila, 2008; Spotila et al., 2004). An assumed isotherm geometry provides a simplistic means for interpreting data and estimating denudation rates. However, this method again neglects the effect of topography on subsurface temperatures. Additionally, the warming effect of denudation by drawing isotherms nearer to the surface is omitted.

1-D flat isotherm: Similar to the 1-D draped, this method assumes isotherms are not influenced by the surface topography and are therefore flat at depth (Ehlers et al., 2001). The closure temperature is assumed to be a plane at a constant elevation requiring a spatially variable geothermal gradient beneath topography. As with the draped isotherm, this simplistic method allows for rate constraints but does not account for the thermal effect of topography or denudation.

Best-fit regression line: Sample cooling ages are related to elevation and the slope of a line through these points yields an apparent denudation rate (Wagner et al., 1977). Implicit assumptions in this technique are constant denudation over the sampling region,

purely vertical exhumation, and that all samples pass through the closure temperature at the same depth.

2-D correction: Regression lines from a 1-D analysis can be improved by correcting for the effect of topography (Stuwe et al., 1994). With respect to topography, this effectively eliminates the assumption that samples passed through their closure temperature at the same time. This offers a significant improvement on the denudation rate derived from a regression line, yet requires intimate knowledge of the thermal field.

5.3.3 Local Thermochronology Studies

Recent thermochronology studies within the Mount Waddington region of the Coast Mountains (Fig. 5-1b) have used various thermochronometer systems to constrain denudation over the last ~30 Myr. Distinct periods of denudation have been identified for this region with relatively subdued (~0.2 mm/yr) through the Late Paleogene and Early Neogene (>30 to ~10 Ma) representing a stable, nonglacial regime. Denudation rates increased (~0.2 – 0.6 mm/yr) during the latest Miocene (~10 – 7 Ma) with an intensification to upwards of 1.5 mm/yr perhaps within the last 4 Myr (Densmore, 2008b; Ehlers et al., 2006; O'Sullivan and Parrish, 1995; Parrish, 1983; Shuster et al., 2005). The interpretation that this most recent event is coincident with the onset of glaciation has been recognized, however the timing remains unclear. Work by Densmore, et al (2008b; 2008c; 2007) suggests glaciation began around 6 Ma, Ehlers et al. (2006) indicates sometime within the last 1.5 – 7 Myr and Shuster, et al. (2005) finds a more recent, early Pleistocene (~1.8 Ma) pulse of denudation. Taken together these studies may suggest glaciation began in the late Miocene and intensified during the Pleistocene. Scattered evidence suggest glaciers were present ~9 Ma in the northernmost region near Yukon Territory from dated tillites (Denton and Armstrong, 1969), however only limited sedimentological and volcanic evidence exists in the central and southern regions of the range which suggest the existence of glaciers since ~2 Ma (Higgs, 1991; Mathews and Rouse, 1986; Souther et al., 1984).

5.4 METHODS

5.4.1 Thermochronology

Low temperature thermochronometers record the time since cooling through their specific cooling rate dependent closure temperature. We focus primarily on AHe and AFT with closure temperatures of ~68 °C (Farley, 2000) and ~105 °C (O'Sullivan and Parrish, 1995; Parrish, 1983) at a rate of 10 °C/Myr, respectively. Measured thermochronometer cooling ages are sensitive to processes that influence the upper crustal thermal field. These processes include the background thermal state of the crust, faulting, sedimentation and denudation, volcanism, topography and fluid flow. Of primary interest is the signal of cooling ages associated with topography and denudation (e.g. Braun, 2005; Ehlers, 2005; Mancktelow and Grasemann, 1997b; Stuwe et al., 1994).

Thermochronometers are ideal tools for studying how topography and denudation have changed spatially and temporally over long ($>10^6$ yrs) timescales. High denudation rates cause rapid exhumation of material and an increase in the geothermal gradient, compressing near-surface isotherms and decreasing cooling ages. Additionally, long-wavelength topography can alter isotherms to a sufficient depth to be recorded in thermochronometer data (Braun, 2002a), increasing thermal gradients below valleys and decreasing them beneath peaks. Transients in either denudation or topography during the time which samples cooled through their closure temperatures can be captured in cooling ages (Braun, 2002b; Ehlers and Farley, 2003; Reiners and Brandon, 2006). In the following sections various models used to interpret thermochronometer data are compared. Specifically we test whether simplistic 1- and 2-D methods can reproduce cooling ages and background denudation rates from a sophisticated 3-D thermo-kinematic model.

Thermochronometer data applied here consists of 83 published AHe samples (Fig. 5-2a) and 11 AFT samples (Densmore, 2008b; Ehlers et al., 2006; O'Sullivan and Parrish, 1995). AHe ages range from 1.7 – 15.4 Ma with an average error of 17.4% (2σ) based on a minimum of 3 replicate analyses per sample. Samples span nearly 4 km of relief from 15 m at the mouth of Knight Inlet to 4000 m at the peak of Mount Waddington (Fig. 5-1b). These samples were collected over the ~60 x 60 km field region at roughly 4 km

lateral distance from each other. This spacing was designed to capture the critical wavelength of topography that the AHe system is sensitive to (Braun, 2002a), allowing maximum interpretation with minimal overlap and redundancy. The data is divided into three vertical transects (Fig. 5-1b) for comparison: the west flank of the Klinaklini Valley (Fig. 5-2b), Mount Jubilee (Fig. 5-2c), and the northeast slope of Mount Waddington (Fig. 5-2d).

5.4.2 Coupled 3D Thermal and Erosion Models for Age Prediction

A 3-D numerical method is applied to predict cooling ages under a prescribed set of boundary conditions and denudation histories. A modified version of the Pecube program is used (Braun, 2003) which integrates a 3-D thermal, kinematic, topographic evolution and cooling age prediction model. This combined model solves for a transient thermal field including the heat transport effects of topography, denudation, conduction and advection as well as internal heat production (Fig. 5-3). The governing partial differential equation of Pecube is:

Equation 5.1:

$$\rho c\left(\frac{\partial T}{\partial t} + \dot{E}\frac{\partial T}{\partial z}\right) = \frac{\partial}{\partial x}k\frac{\partial T}{\partial x} + \frac{\partial}{\partial y}k\frac{\partial T}{\partial y} + \frac{\partial}{\partial z}k\frac{\partial T}{\partial z} + \rho H \ ,$$

where ρ is density, c is heat capacity, T is temperature, t is time, $\dot{E}$ is denudation rate, x, y and z are spatial coordinates, k is thermal conductivity and H is heat production per unit mass. Fixed input parameters include model duration, total and crustal thickness, thermal conductivity, specific heat capacity, crustal and mantle density as well as volumetric heat production, surface temperature at sea level and atmospheric lapse rate, Young's Modulus, Poisson's Ratio and the effective elastic thickness (Table 5-1). The total thickness of the model is set to 50 km depth, the approximate thickness of the lithosphere in the study region (Clowes et al., 1995; Currie and Hyndman, 2006 and references therein) and crustal thickness of 35 km depth corresponding to the local moho discontinuity (Hammer and Clowes, 1997). The top surface is defined by the present day topography using a 90 m digital elevation model (DEM). All models simulate a duration of 50 Myr corresponding to cessation of plutonic emplacement. Variable parameters in

the model include basal temperature, background denudation rate, initial relief and timing of relief change as well as various relief change scenarios (Table 5-2).

The thermal model uses separate crustal and upper mantle values of density (2765 and 3200 km/m^3; (Waples and Waples, 2004)), and heat production. Heat production is 0.8 µW/m^3 at the surface and decays exponentially with depth reaching a value of 1/e at 10 km and is constant below 35 km at 0.02 µW/m^3 (Currie and Hyndman, 2006). Thermal conductivity and specific heat capacity are assumed to be constant throughout the domain, and are set to 2.24 W/mK (Densmore, 2008b) and 956 J/kgK (Waples and Waples, 2004), respectively. Temperature at sea level is fixed at 9.8 °C (see National Climate Archive, http://climate.weatheroffice.ec.gc.ca) with an imposed atmospheric lapse rate of 6.7 °C/km. A uniform basal temperature is assumed, however this value can vary from 900 – 1300 °C between model runs corresponding to the range of possible values suggested for this region by Currie and Hyndman (2006). This model outputs a steady-state thermal field, which is then modified by the kinematic model.

The kinematic model is defined by strictly vertical denudation. This background denudation is constant across the landscape, ranging from 0.2 – 1.4 mm/yr, consistent with the range reported by (Densmore, 2008b). The effective denudation rate can be modified locally by variations in topography as well as isostasy. For example, if the initial DEM was 50% of modern (0.5x at all elevations), the region would linearly increase in relief towards the modern and therefore a negative component would be added to the background denudation rate. Initial topography ranges from 25 – 175% of modern, evolving to present day beginning at 10, 8 or 2 Ma, corresponding to varying interpretations of increased denudation in the region (Densmore, 2008b; Ehlers et al., 2006; Parrish, 1983; Shuster et al., 2005). For example, if the initial topography is input at 50% of modern, both the initial and modern are assumed to be isostatically compensated however transitioning between the two causes a negative velocity component. The isostatic calculation uses constant values for Young's Modulus of 1.0e11 Pa (Turcotte and Schubert, 2002), Poisson's ratio of 0.25 (Braun and Robert, 2005), and an effective elastic thickness of 15 km (Flueck et al., 2003). The temperature field is output incorporating the effect of evolving topography and denudation.

Thermochronometer cooling ages for a number of systems are predicted at each point along the surface using the temperature field and kinematic history. Here, both AHe and AFT ages are predicted. For AHe ages are calculated using pristine Durango kinetics (Farley, 2000) as well as low (effective uranium, or eU = 12.4 ppm) and medium (eU = 61.8 ppm) radiation damaged grains (Shuster et al., 2006) are calculated. Of note, samples presented here have an average eU value of 33.5. Using kinetics for medium damaged grains yields an AHe closure temperature of ~64 °C (Shuster et al., 2006) and predicted ages that differ by ~10% from Durango kinetics. AFT ages are calculated using kinetics from Crowley et al., (1991) and Laslett et al., (1987).

5.4.3 Thermal Modeling Approaches Considered

The 3-D model is compared to commonly used 1- and 2-D approaches to evaluate the rigor of these methods for quantifying the thermal field. Methods compared here are: (1) a 1-D thermal model incorporating rock thermal properties and denudation, (2) a 1-D assumed draped isotherm method, (3) a 1-D assumed flat isotherm method, (4) a 1-D and (5) 2-D best-fit regression line technique. The difference in predicted cooling ages as well as calculated denudation rate is compared to the 3-D method, with results shown along a single elevation profile (Fig. 5-1b).

A single 3-D model was run (see Table 5-1 for constant parameters) with a background denudation rate of 0.6 mm/yr and constant relief throughout the model to provide the basis for comparison (Fig. 5-4). The program CLOSURE (Brandon et al., 1998; Ehlers et al., 2005), is used to estimate the cooling-rate dependent closure temperature of the AHe system for all techniques reviewed here. This program outputs a closure temperature of 72 °C using the default settings for Durango apatite kinetics (Farley, 2000) and a cooling rate of 22 °C/Myr. Of note, this value is slightly higher than reported above due to the higher cooling rate.

AGE2EDOT: This program uses input thermal properties of diffusivity, heat production, surface temperature, and a near surface thermal gradient with no denudation (Brandon et al., 1998; Ehlers et al., 2005). A solution is determined for a thermal field in steady state including the effect of denudation by solving (Reiners and Brandon, 2006):

Equation 5.2:

$$T(z) = T_s + (T_L - T_S + \frac{H_T L}{\dot{\varepsilon}}) \frac{1 - e^{\dot{\varepsilon} z / \kappa}}{-e^{-\dot{\varepsilon} L / \kappa}} - \frac{H_T z}{\dot{\varepsilon}},$$

where z is the depth, T_S the surface temperature, T_L the temperature at the base of the layer, H_T the heat production, L the layer thickness, $\dot{\varepsilon}$ the denudation rate, and κ the thermal diffusivity (Table 5-3). From this, a cooling age is predicted for each thermochronometer system using a range of denudation rates. This method assumes a constant depth to closure and does not account for lateral variations in thermal gradients caused by topography.

The next few methods discussed require information on the near-surface (<1 km) thermal gradient, such as from borehole measurements. Comparisons made here assume an idealized case with perfect thermal measurements and knowledge of the background denudation rate. In this case, thermal gradients were derived from the 3-D thermal model every 500 m across the topography in the upper 1 km of the model, and the denudation rate is a constant (0.6 mm/yr). The extraction of these synthetic thermal gradients from the model represents the idealized case of having abundant observed heat flow measurements in the study area. In reality, such measurements are sparse and uncertainties in calculated exhumation rates would be greater than reported here.

1-D draped isotherm: For a draped scheme, the average near-surface thermal gradient is used (34.4 °C/km) to determine the depth to a closure isotherm at each location. This produces an isotherm which perfectly mimics the overlying topography. A consequence of this is cooling ages will be constant across the entire profile.

1-D flat isotherm: Similar to the draped isotherm, this method uses the average surface thermal gradient from the 3-D model (34.4 °C/km) applied at the average elevation (1135 m). Therefore, the calculated depth to the closure isotherm is constant across the entire profile. Cooling ages are determined using the calculated depth to the 72 °C isotherm and the background denudation rate.

Best-fit regression line: This method does not require modeling or knowledge of the thermal gradient. Here, the slope of the best-fit line through a plot of cooling age versus sample elevation yields an apparent denudation rate (e.g. Wagner et al., 1977).

Samples collected along a vertical profile and plotted in this fashion generally have a positive relationship with increasing elevation yielding older cooling ages (Fig. 5-6). This method is based on assumptions of constant vertical exhumation across the profile and depth to closure. A synthetic transect of cooling ages is extracted from the 3-D thermal model to apply this technique.

2-D correction: A potential improvement to the regression line technique applies a 2-D numerical model-based correction to account for the topographic effect on the temperature field. The apparent exhumation rate is corrected using the ratio of differences in sample elevation to closure isotherm amplitude derived here from the 3-D thermal model (Stuwe et al., 1994):

Equation 5.3

$$U_{(real)} = U_{(apparent)} * \frac{\Delta z}{H},$$

where U_{real} is the actual denudation rate, $U_{apparent}$ the apparent denudation rate, Δz the difference in depth to the closure isotherm between the ridge and valley of the profile, and H the amplitude of the topographic profile. This approach has the advantage of accounting for topography in 2-D, but neglects any influence of topography on isotherms in the 3rd dimension.

5.5 RESULTS

We illustrate how the thermal field and predicted cooling ages are affected by topography and each applied thermal model (Fig. 5-5) as well as the influence of input parameters of basal temperature, denudation rate and relief change on 3-D model outputs. Each thermal model is compared along a single topographic profile from figure 1b. Additionally, the sensitivity experiments of the 3-D model are analyzed along a single transect for simplicity (Mount Waddington transect, Fig. 5-1b).

5.5.1 Thermal Field Under Complex Topographies

Figure 5-4 is a topographic profile similar to that in Figure 5-5a using the same 3-D model as above. This profile reveals the effect of topography on isotherms critical to thermochronometer cooling ages. Approximate closure temperature isotherms for zircon (U-Th)/He (~190 °C, Reiners et al., 2002) and fission track (~220 °C, Brandon et al., 1998) are included for comparison. Here, The largest topographic features (peak to peak, λ = ~30 km) in the landscape, for example between 60 and 90 km along profile, perturb even the 300 °C isotherm at a depth greater than 10 km. Shorter wavelength (λ = ~15 km) features such as the large U-shaped valley ~45 km along profile affect the thermal field to a depth of ~6 km with a demonstrable expression in the 220 °C isotherm. Consequently, features of similar wavelength but lower amplitude, such as the valley at 10 km along profile perturb the AHe and AFT isotherms with little to no effect at depths greater than ~4 km. Finally, high amplitude (>1 km), short wavelength features (<5 km) such as the multiple peaks near 100 km along profile have very little effect on even the AHe isotherm.

In this 3-D model, AHe and AFT closure temperature isotherms are affected similarly by topographic features with a wavelength greater than ~10 km and amplitude ~ 2 km. This observation indicates these thermochronometers do capture a signal of large-scale topographic change, such as incision of U-shaped valleys or removal of large peaks.

5.5.2 Effect of Assumed Thermal Model on AHe Closure Isotherm and Cooling Ages

AGE2EDOT: Using AGE2EDOT, a single age for all elevations is calculated for a given denudation rate; with our thermal inputs, 0.6 mm/yr yields an AHe age of 3.1 Ma. The product of the input denudation rate from the 3-D model and this predicted cooling age yields the depth to closure. Here, this depth is ~1.9 km below the surface and therefore will perfectly mimic the topography (Fig. 5-5b). The general trend and depth to the closure temperature is similar between our 1-D and 3-D models. However, this 1-D model overemphasizes the thermal effect from short wavelength topographic features, such as the narrow peaks at ~100 km along profile. The predicted AHe age is comparable to the average 3-D model predicted age (3.3 Ma) along the selected profile

but is significantly different locally where features in the landscape are high amplitude and short wavelength. Consequently, 1-D predicted ages can misfit 3-D predicted ages by ~40% in these regions (Fig. 5-5c). In regions of broad, long-wavelength topography ages agree within ~10% between the two model schemes.

1-D draped isotherm: The 3-D model derived average thermal gradient along our profile is 34.4 °C/km, therefore the depth to AHe closure (72 °C) assuming a draped isotherm is ~2.1 km below the surface (Fig. 5-5a). The calculated draped isotherm matches well (<10%) with the AGE2EDOT calculated closure isotherm. AHe cooling ages are predicted using a-priori knowledge of the input denudation rate (Fig. 5-5b). The draped method yields a single AHe age of 3.5 Ma for all samples. Again, this constant age across the landscape overemphasizes short wavelength topographic features while reproducing the average age within ~10%. This method deviates from 3-D predicted ages by over 60% in certain regions (Fig. 5-5c), namely in relatively low regions with short wavelength, high amplitude topography (e.g. ~16 km across profile).

1-D flat isotherm: This method yields a flat closure isotherm of ~ -1 km elevation (Fig. 5-5a). In regions well above the average elevation the flat isotherm significantly misfits the 3-D predicted depth by nearly 1 km. AHe ages are predicted along the profile using the depth to the flat isotherm and input denudation rate from the 3-D model of 0.6 mm/yr (Fig. 5-5b). In this case, ages mimic the shape of topography and follow general trends in the 3-D predicted ages. Ages predicted using this method match well (<10%) in regions near the average elevation (Fig. 5-5c). However, misfits of ~50% occur in regions well above or below the average elevation.

Best-fit regression line: A regression line technique is applied on two hypothetical transect locations in Figure 5-5b. The slope of the best-fit regression lines yield apparent denudation rates of 1.1 mm/yr along transect A (Fig. 5-6a), and 1.0 mm/yr along transect B (Fig. 5-6b). These calculated rates are >70% different from the 3-D input value of 0.6 mm/yr. This discrepancy is primarily due to violating the assumption of a flat closure isotherm.

2-D correction: A 2-D correction as described above is applied to the hypothetical transects to correct for topographic effects on the thermal field. This method yields denudation rates of 0.7 and 0.5 mm/yr, respectively (Fig. 5-6), significantly improving

the initial estimate to within 10% for both transects. However, this represents an idealized case with perfect knowledge of the subsurface thermal field using the 3-D model.

5.5.3 Effect of Variable Basal Temperature and Denudation Rate on AHe Ages

Basal temperatures were varied between each 3-D model run at 900, 1100 and 1300 °C. Increased basal temperature results in enhanced thermal gradients and younger predicted cooling ages (Fig. 5-7a). However, the age difference produced by an increase of 400 °C in basal temperature is relatively minor (~25%). This signal is indistinguishable within ~17% sample error utilized here. This range in ages is reduced as background denudation rate increases and the signal becomes more difficult to recognize.

Background denudation rates were varied from 0.2 – 1.4 mm/yr. Higher denudation rates result in a more narrow age distribution as well as younger predicted ages (Fig. 5-7b). The full range of tested denudation rates produces a significant effect on cooling ages, nearly an order of magnitude difference from ~1 Ma to >10 Ma. However, denudation rates above 0.6 mm/yr produce very young ages (<3 Ma) and age distributions from these models become separated by a narrow margin.

5.5.4 AHe Signal of Changes in Topographic Relief

5.5.4.1 Relief Change Magnitude and Timing

Relief change in the 3-D model is accomplished by amplifying or damping the initial DEM and linearly morphing it into the modern topography over an imposed time interval. The effect of increasing from 25%, 50% or 75% modern topography (Fig. 5-8a) as well as decreasing from 125%, 150% or 175% (Fig. 5-8c) occurring over 2, 8 or 10 Myr is tested (Fig. 5-8b and d). Additionally, the initial topography is adjusted to maintain a mean elevation equal to that of the modern topography (1135 m). Therefore a scenario with increasing relief from 75% of modern maintaining a constant mean would have an initial topography modified by:

Equation 5.4:

$$z_{(init)} = (z_{(modern)} * 0.75) + (z_{(mean)} * (1 - 0.75)),$$

where z_{init} is the initial input elevation at a single point, z_{moden} the modern elevation at that point, and z_{mean} the modern mean elevation. This scheme centers relief change on the mean, affecting the largest magnitude of change at extreme elevations. For all relief change scenarios, basal temperature and denudation rate are constant at 1100 °C and 0.4 mm/yr, respectively.

Increasing relief (Fig. 5-8a) causes cooling ages from samples above the mean elevation (1135 m) to increase. For example, in Figure 8a predicted ages for an initial topography of 25% modern are ~10% older than those with an initial topography of 75% modern. However, all cases yield predicted ages that fall within ~17% sample error.

In contrast, decreasing relief models (Fig. 5-8b) effectively cause peaks to erode and valleys to fill until the modern topography is achieved. Here, cooling ages from samples above the mean elevation decrease with increasing magnitude of relief change. Similar to increasing relief scenarios, there is <10% change in ages between 125% and 175% initial topography indicating little sensitivity in cooling ages with respect to sample error.

Finally, the effect of timing of relief change on cooling ages is evaluated. Increasing relief (Fig. 5-8c) from 50% to modern in the last 10 to 2 Myr produces virtually no change in predicted cooling ages and is indistinguishable with respect to sample error. Decreasing relief (Fig. 5-8d) from 150% to modern in the last 10 to 2 Myr predicts slight variations in ages (~10%), irresolvable when sample errors are considered. These findings indicate that increasing or decreasing relief within the last 10 – 2 Myr is difficult to quantify using AHe thermochronology when sample uncertainties are considered.

5.5.4.2 Relief Change Scenario

Thus far only relief change around a constant mean elevation has been considered. Other possible scenarios include change around a fixed minimum or maximum elevation (Fig. 5-9). If we assume increasing relief around a fixed maximum elevation then effective denudation rates are zero at the highest peaks and increase in

magnitude with decreasing elevation. In this instance the highest magnitude of relief change will occur in valley bottoms (Fig. 5-9a). Here predicted cooling ages should be equivalent at the highest elevation and younger at low elevations compared to a constant topography scenario. Conversely, increasing relief with a fixed minimum elevation causes the largest magnitude of change at high elevations, as peaks grow from initial low-relief topography to the modern (Fig. 5-9c). In this case, predicted cooling ages are similar at low elevations and become progressively older at higher elevations compared to a constant topography scenario. A fixed minimum scenario is unreasonable in a region where tectonic input is less than the background denudation rate as there is no influx of material to build peaks. However, we include this scenario for completeness and to address predicted cooling ages in field regions where there is a positive tectonic flux.

Our conceptual model (Fig. 5-9) is evaluated with a 3-D calculation and the sensitivity of predicted cooling ages from various relief change scenarios is determined. Models were run with a basal temperature of 1100 °C, background denudation rate of 0.4 mm/yr and relief change of ±50% (increasing or decreasing) at 8 Ma. However, only the increasing relief case is presented for brevity as models with decreasing relief show similar results. Predicted ages from increasing relief models around a fixed maximum are distinguishable from a constant relief run, but are younger than expected and do not follow the trend of our conceptual model. Both isostasy and advective heat transport complicate our simple cartoon. Increasing relief from a fixed maximum elevation causes focused incision within the valleys. This removal of mass causes a two-fold decrease in cooling ages: (1) the isostatic component increases rock velocities towards the surface, and (2) increased effective denudation resulting in advective heat transfer and warmer temperatures, even near the high peaks. Samples near the high peak experience a maximum cooling rate of 11.1 °C/Ma for no change in topography and 18.2 °C/Ma with increasing relief around a fixed maximum. The end result is predicted ages ~50% younger at all elevations than in a constant relief model (Fig. 5-10a, diamonds). A higher background denudation rate would decrease this effect. However, a higher rate would also decrease cooling ages and make differences from relief change less apparent.

In fixed mean elevation scenarios the isostatic component is minimized and the advective heating is balanced by both incision in valleys and growth of peaks. However,

our predicted ages do not intersect at the mean elevation as shown in the conceptual cartoon. In this case, the profile encompasses the highest topography in the field area over a short horizontal distance and therefore has an average elevation higher than that of the entire region. This causes predicted ages to be slightly older (Fig. 5-10a, circles) than expected from our simple cartoon.

Lastly, with increasing relief around a fixed minimum, predicted ages are generally older as predicted in our conceptual cartoon (Fig. 5-10a, squares). However, the two trends do not intersect at sea level. In this case a negative isostatic component causes a decrease in effective denudation and a damped thermal field. These effects result in slightly older ages than our simple cartoon illustrates. The maximum cooling rate at the valley bottom is 15.5 and 12.6 °C/Ma for constant relief and increasing around the minimum, respectively.

Predicted ages from both increasing and decreasing relief scenarios can be distinguished from cases with no relief change when modifying topography around the maximum or minimum elevations. Increasing relief from 50% modern can be recognized with respect to sample error (Fig. 5-10a). Ages are ~50% younger in fixed maximum and ~50% older in fixed minimum elevation scenarios compared to no topographic change. However, change around the mean cannot be distinguished, resulting in ages comparable to predicted ages with no relief change. Conversely, decreasing relief scenarios follow an opposite trend. Change around a fixed minimum elevation causes predicted ages to be distinguished within ~17% sample error. Additionally, decreasing relief around a fixed maximum elevation results in significantly older ages (>150%) that are beyond the range sample error. Of note, both increasing and decreasing relief models can result in predicted ages younger and older than a model with no relief change implying any trend in cooling ages is not necessarily indicative of a specific scenario.

5.6 DISCUSSION

This section assesses general principles for thermal models and predicted cooling ages and presents an application of the 3-D model to the Coast Mountains, British Columbia. The validity of each modeling scheme is examined here. Additionally, our 3-

D model is compared to observed data to constrain combinations of parameters that produce statistically significant fits.

5.6.1 Modeling Comparisons

In general, 1- and 2-D methods for cooling age prediction constrain AHe ages calculated by our complex 3-D model within ~20%. However, in detail high amplitude, short wavelength features in the topography or regions significantly deviating (>1 km) from the average elevation can produce large age anomalies of 50% or more, even at modest (~0.6 mm/yr) denudation rates. For example, a small ridge within the major U-shaped valley at ~46 km along profile (Fig. 5-5a) is misfit by >25% by all methods reviewed here (Fig. 5-5c). In addition, each 1-D method requires an initial assumption to analytically solve for the thermal field. Significant a-priori knowledge of the denudation rate or thermal field is required to produce results that correlate well between 1- and 3-D methods. Below, each method is assessed in terms of validity and possible applications.

AGE2EDOT: Misfits between predicted cooling ages from this program and our 3-D model along an arbitrary topographic profile average 18%. AGE2EDOT is best suited for applications of actively eroding landscapes with low relief due to the fact that the calculated thermal field accounts for denudation but not elevation. Furthermore, to minimize errors introduced in mountainous topography, calculated cooling ages and denudation rates can be compared from samples collected at similar elevations (Densmore, 2008c). Finally, this program is useful in that first order interpretations can be made on individual samples or sparsely sampled regions.

1-D draped isotherm: This assumed thermal field results in cooling ages that misfit our 3-D model by 19% on average (Fig. 5-5c). Assuming a draped thermal field provides a simplistic means for constraining cooling ages and is best applied in regions of predominantly long wavelength (>10 km) topography where critical isotherms will mimic the topography. However, geothermal gradients must be consistent within a field region therefore care should be taken to avoid any known thermal anomalies.

1-D flat isotherm: This method reproduces 3-D predicted cooling ages within 25% on average. Due to the constant elevation of the closure isotherm, this method is

appropriate in regions of low denudation rates and either muted or high frequency but short wavelength (<10 km) topography where critical isotherms are not perturbed. Alternatively, this method could successfully be applied for predicting higher temperature thermochronometers such as zircon (U-Th)/He or fission track (Fig. 5-4).

Best-fit regression line: Along the synthetic vertical transects here apparent denudation rates misfit the 3-D model rate by more than 70%. A transect of samples must be collected over a very short horizontal distance (~5 km total) in order to maximize the utility of this method. A best-fit regression line technique is a simple and straightforward approach for interpreting cooling age data.

2-D correction: A corrected regression line technique can significantly improve calculated denudation rates, here to within 10%. However, due to the necessity of thermal measurements, it is best applied in regions where independent data is available, such as from boreholes. If the thermal field is well constrained, a 2-D correction of an age-elevation profile may be used to minimize error introduced from topography.

Consequently, none of the above methods provide a means for accurately predicting cooling ages and background denudation rates across a complex landscape. All 1- and 2-D methods here assume a steady-state condition whereas the 3-D model can incorporate changing topography and denudation rates to address the effect of transients on the thermal field. Application of a rigorous 3-D thermo-kinematic model is necessary when predicting cooling ages in an actively evolving landscape or when comparing cooling ages across a wide spatial and vertical range. In the following, an example application is presented in the heavily glaciated Coast Mountains.

5.6.2 Application to the Coast Mountains: Best Fit Simulations

Cooling ages derived using any modeling technique are generally non-unique as different model parameters can yield similar predicted cooling ages. For example, a higher basal boundary temperature or denudation rate results in younger cooling ages. Therefore, a statistical comparison of model results with multiple variable input parameters is needed. Here we quantify the goodness of fit of >800 model runs to our thermochronometer dataset by applying a χ^2 goodness of fit test. This value is the sum of

the squared difference between observed and model predicted ages divided by the squared sample error:

Equation 5.5:

$$\chi^2 = \sum_{i=1}^{n} \frac{(Obs_i - Pre_i)^2}{\sigma_i^2},$$

where n is the number of samples, Obs_i the ith observed cooling age, Pre_i the ith predicted cooling age, and σ_i the ith 1σ sample error. The χ^2 value is a one-sided distribution with a value of 0 equaling a perfect fit and higher values a progressively worse fits to the data. For samples with 1σ error below the mean (8.7%) we set the sample error equal to the mean to ensure no single sample dominates this statistic. This step is necessary as some data have <1% error causing high χ^2 values where potentially only one point is misfit. We compare our values to a compiled χ^2 distribution (e.g. Bevington and Robinson, 1992, appendix C-4) for the 5% significance level to determine a statistically significant fit, meaning there is a 5% probability of obtaining a higher χ^2 value. These compiled tables relate degrees of freedom (v) to significance level, with degrees of freedom defined as the number of samples minus model free parameters. Model free parameters are defined here as any variable in the model space that is allowed to change, namely basal temperature, denudation rate, and timing, magnitude and relief scenario. For AHe, this gives us a v value of 78 and a statistically significant χ^2 value of 101. Of note, O'Sullivan and Parrish (1995) identified a partial annealing zone for AFT ages along the Mount Waddington transect presented here at an elevation of ~2400 m. Due to this, we omit the three highest elevation (>2400 m) AFT samples from our χ^2 calculations. Consequently, this yields a v value of 3 and a corresponding significant χ^2 value of 8 for our AFT data. χ^2 misfits for all models range from 1450 to >50000 for AHe and 80 to 2200 for AFT. These values indicate no combination of model parameters provide a statistically significant fit to all of the data. However, we analyze all model results to determine which combinations of parameters yield better fits.

Here χ^2 misfits of AHe and AFT ages are evaluated from models with no relief change but variable background denudation rate and basal temperature (Fig. 5-11). Variable relief models are discussed below. For AHe models, all basal temperatures explored yield similar patterns in χ^2 values. At the lowest denudation rate of 0.2 mm/yr

χ^2 misfit values are >10000, more than 3 orders of magnitude higher than a statistically acceptable fit. However, increasing denudation rates significantly reduces the misfit, to a minimum of 0.6 mm/yr regardless of basal temperature. This denudation rate creates a pronounced minimum in χ^2 values ranging from 1475 to 1650. The total range in AFT misfits is significantly lower than that of AHe due to the lower number of samples. Subsequently, increasing denudation rates cause progressively worse fits to the data again regardless of basal temperature. Misfit patterns to AFT data follow a similar trend as AHe data. Each basal temperature scenario yields high χ^2 values (>700) at 0.2 mm/yr background denudation. Increasing the denudation rate leads to a χ^2 minimum at 0.4 mm/yr with basal temperatures of 1100 and 1300 °C, and 0.6 mm/yr for 900 °C. Following this, each modeling scenario produces progressively worse fits with increasing denudation rate.

These patterns suggest denudation rate and basal temperature produce similar effects in predicted ages, but ages are generally dominated by background denudation rate. The inversion of basal temperatures that produce best-fit χ^2 values at 0.6 mm/yr is unsurprising as a high basal temperature and high denudation rate create very young ages throughout the landscape. Conversely, a low denudation rate and lower basal temperature yields older predicted ages. Neither of these extremes is observed in the data and therefore an interplay between the two factors must be the case. However, changes in basal temperature are subsidiary to increases in denudation rate as AHe ages are more sensitive to denudation. There is some distinction between AFT models however only a slight shift in the best-fit denudation rate from 0.4 to 0.6 mm/yr occurs when decreasing the basal temperature by 400 °C. Consequently, the difference between denudation rate of best-fit AFT and AHe data indicates samples likely experienced an increasing rate through time. The region may have had a low background denudation rate (~0.4 mm/yr) through ~7 Ma and a higher rate (~0.6 Ma) for ~7 Ma to present because the AFT system is sensitive to higher temperatures

Next, we compare the goodness of fit relating background denudation rate and relief change (Fig. 5-12). For these comparisons basal temperature is fixed at 1100 °C and relief change occurring at 8 Ma, taking the median value for each parameter. The general pattern of χ^2 values is remarkably similar to that of denudation rate versus basal

temperature (Fig. 5-11). For both AHe and AFT sample ages, misfit is very high at 0.2 mm/yr denudation rate regardless of relief scenario, >30000 and >1100, respectively. There is a marked decrease in χ^2 values with increasing denudation rate for both systems, reaching a minimum at 0.6 and 0.4 mm/yr for AHe and AFT, respectively. Following this, χ^2 values increase with increasing denudation rates. However, χ^2 values are very similar between different relief scenarios converging to within ~5% at 1.4 mm/yr. This implies higher denudation rates over-print any relief change signal. Moreover, the similar χ^2 values for all modeling scenarios indicate that relief change (increasing, decreasing or constant) is difficult to discern from the data.

Braun (2002b) presented an example of age-elevation relationships with a signal characteristic of specific relief change using a similar version of the 3-D model used here. In his paper, Braun detailed varying slopes in age-elevation plots from recent relief change, specifically a negative slope for regions that experienced decreasing relief (Braun, 2002b, Fig. 3). While this age-elevation distribution is encouraging, real data with natural variability and uncertainties will infrequently distinguish between differing scenarios. Even a 10% error can sufficiently obscure any statement of relief change. Additionally, the circumstances involved in producing an inverted age-elevation relationship are especially fortuitous. The relief change must be accomplished around a fixed mean elevation as a fixed minimum or maximum will not allow ages in the valleys to get older as the peaks become younger. Furthermore, background denudation rates have a limited range over which a signal of relief change will be preserved. At rates >1.0 mm/yr predicted cooling ages will be ubiquitously young and show little variation regardless of relief change. If the background denudation rate is much less than the rate of relief change, samples recording paleorelief will not be exhumed to the surface and the signal of relief change will not be apparent. These aspects make capturing a signal in actual data by analyzing age-elevation plots challenging.

5.6.3 Potential Sources of Large AHe Age-Anomalies

Large χ^2 values indicate some process must be active that the 3-D model does not capture. In this section we evaluate misfits by examining potential sources that could

influence cooling ages. Specifically, the data do not have a simple linear relationship between age and elevation or relative position within a catchment (Fig. 5-1b and 2a). This range of AHe cooling ages may be the result of: (1) faulting, (2) thermal perturbations at the base of the crust, (3) localized magmatism, (4) fluid flow, or (5) spatially variable topographic modification, presumably by glacial erosion. Below, each of these possible scenarios is addressed and the validity evaluated.

Faulting within the Coast Mountains could exhume material and perturb the thermal field by both shear heating and locally enhancing exhumation rates. Unfortunately field mapping in the Mount Waddington area is sparse and the homogenous nature of the pluton obscures physical evidence of faulting. However, cooling ages should change sharply between the footwall and hanging wall (depending on fault displacement) and no such linear feature exists in the data. Continuous lateral and end moraines throughout the region indicate little to no displacement since at least the last glacial maximum. Furthermore, inspection of Landsat images of the area does not reveal any linear features displacing Quaternary sediments and suggesting active faulting within the area. Although faulting is difficult to rule out, it seems an unlikely explanation for our observed age distribution.

Another possible explanation for lateral variations in cooling ages is deep-seated perturbations in the thermal field. Thermal perturbations at the base of the crust would cause variation in near surface thermal gradients, over lateral distances similar to the crustal thickness. Here, the base of the crust is ~35 km, creating very diffuse age anomalies over the spatial scale considered here (~60 x 60 km). As shown below, the observed age anomalies occur over smaller spatial scales (~10 – 20 km) such that variations in the basal crustal temperatures are an unlikely explanation for the misfits to the data. As discussed earlier (Fig. 5-7) cooling ages are insensitive to variations in the basal temperature due to the advection dominated nature of the thermal field in this area.

Alternatively, magmatism could be a point source thermal anomaly that would effect cooling ages. A large, intrusive body may have sat atop some of the field area which has since been eroded away, effectively altering cooling ages while leaving little to no evidence of its existence. However, this type of feature is difficult to constrain. Additionally, a magma body at depth near that has not been exposed may have affected

122

immediately adjacent samples. A local hot spring within the Klinaklini Valley may be indicative of shallow magmatism. However this feature has not been measured or the location confirmed (Woodsworth, 1997, chapter 9). An intrusive body remains a distinct possibility within the field area but is again difficult to evaluate. If an intrusion is responsible for the observed age anomalies the distance over which a thermal perturbation could affect cooling ages scales with the size of the intrusion. The affected area would be ~500 m for intrusions of 1 km diameter (Ehlers, 2005). Given the lateral distance over which He age anomalies occur and the lack of evidence for Neogene intrusions of this size here we do not feel plutonism is responsible for the data misfits.

Fluid flow generally causes a redistribution of heat in the subsurface and can be either topographically or magmatically driven. In either case, the thermal field could be altered sufficiently to affect cooling ages (Whipp and Ehlers, 2007). However, the granitic rocks within the Coast Mountains have a low permeability and porosity, and are not highly fractured such as in the Himalaya where this process was documented. Therefore, it is unlikely fluid flow has significantly altered the thermal field in the Mount Waddington region. Future studies could test this by inventorying hot-springs in the area.

Finally, we consider some component of topographic modification to have caused differences in cooling ages and calculated denudation rates. Variable ages at similar elevations could have experienced differing rates of denudation. Since we have explored a wide range of relief scenarios that do not reproduce our observed cooling ages, a major reorganization of the topography could have occurred, i.e. lateral motion of the position of valley's and ridges. Previous studies have documented focused denudation on the southwest flank of Mount Waddington (Densmore, 2008b; Ehlers et al., 2006). These findings are indicative of spatially variable denudation.

5.6.4 Goodness of Fit Along Data Transects

A method for assessing spatial variability in cooling ages is to subset the data into individual transects in order to compare model misfits within each region. We evaluate goodness of fit by comparing predicted and observed ages from all data as well as across three data transects outlined in Figure 5-1b, Klinaklini Valley, a major glaciated valley,

Mount Jubilee, a local high peak, and Mount Waddington, the highest peak in the range (Fig. 5-13). For simplicity only outputs from two model runs are examined including no relief change, a basal temperature of 1100 °C and background denudation rates of 0.6 and 0.4 mm/yr, corresponding to best fit AHe and AFT rates, respectively. Increasing and decreasing relief scenarios yield very similar results and for brevity are not discussed here but are included in Appendix 3.

The best fit AHe model ($\chi^2 = 1475$) generally reproduces observed AHe cooling ages while not capturing the full range of the data (Fig. 5-13a). This is apparent when the data is divided into individual transects. Along the Klinaklini transect (Fig. 5-13b) ages are reproduced well, especially at lower elevations. The model fit decreases with increasing elevation and predicted ages do not show the observed break in slope at ~2000 m (Densmore et al., 2007). Predicted ages are too young at higher elevations perhaps suggesting the chosen denudation rate is too high. However, along the Mount Jubilee transect (Fig. 5-13c) the opposite is true, where predicted ages are too old compared to data. Consequently, along the Mount Waddington transect all ages predicted with a denudation rate of 0.6 mm/yr are younger than observed (Fig. 5-13d), suggesting the applied rate is too high at all elevations. Additionally, this rate causes predicted AFT ages that are too young at nearly every data point (Fig. 5-13e).

Predicted ages and data are compared using a lower denudation rate of 0.4 mm/yr along each transect. This lower denudation rate predicts ages too old for the majority of data (Fig. 5-13a) especially for the Klinaklini and Mount Jubilee transects (Figs. 5-13b and c) where only 3 points at high elevations are within sample error. However, the trend of AHe ages along Mount Waddington is fit well (Fig. 5-13d). AFT ages are fit well using a denudation rate of 0.4 mm/yr (Fig. 5-13e).

These spatial patterns elucidate the shortcomings of our 3-D model as well as where misfits occur across the landscape. Although the entire dataset appears to have a rough correlation between age and elevation, each transect has a clear correlation with minimal outliers. Similar to Densmore et al. (2008b), this suggests that each transect location has experienced different denudation histories. No model in our suite of >800 captures observed local variations. Simple scaling of the topography to accomplish relief change does not account for the dynamic nature of glaciation.

5.6.5 Topographic Change Required to Produce Observed Age Anomalies

Here the distribution of observed cooling ages is interpreted to be caused strictly by varying degrees of denudation therefore the variance in age between observed and predicted is due to differences in the modeled and real denudation rates. We use the same constant relief models as above (1100 °C basal temperature and denudation rates of 0.6 or 0.4 mm/yr) to determine the AHe age anomaly as well as the change in elevation required to reconcile this anomaly (Fig. 5-14). We define the age anomaly as the difference between predicted and observed AHe ages. Figure 5-14 b and c are contoured age anomaly maps for denudation rates of 0.6 and 0.4 mm/yr, respectively. A positive age anomaly equates to a model denudation rate that was too low to reproduce the observed cooling age while negative anomalies are from too high a denudation rate. Discussion here focuses on the higher denudation rate model (0.6 mm/yr) as the 0.4 mm/yr denudation rate model yields identical trends with a positive shift in age anomaly at all points.

Analysis of age anomalies across the landscape reveal four apparent signals: (1) near zero age anomalies within the Klinaklini Valley (Fig. 5-14, KV), (2) negative values on the upper slopes on the western flank of the valley, (3) a positive age anomaly of ~3 Myr centered near Mount Jubilee (Fig. 5-14, MJ) which radiates outward, and (4) a negative age anomaly of -5 Myr to the north and east of Mount Waddington (Fig. 5-14, MW). The trace of the Klinaklini Valley is evident as a low age anomaly indicating the background denudation rate is very near that experienced by each sample. However, on the ridge and western flank of the valley age anomalies progressively decrease suggesting that both higher elevations and regions west of the main valley trace experienced lower denudation rates. The east slope of the valley does not exhibit this relationship as the signal is dominated by the positive anomaly associated with Mount Jubilee. This positive anomaly covers ~300 km^2 from the eastern slope of the Klinaklini Valley, up Mount Jubilee and extending to the southwest slope of Mount Waddington. The large spatial extent suggests the paleotopographic high and increased denudation identified by Ehlers et al. (2006) is a large, local feature. Conversely, traversing over the peak of Mount

Waddington and onto the northern and eastern slopes sample cooling ages are older than predicted with age anomalies between -2 and -11 Myr. The apparent low denudation rate extends both northward and eastward including adjacent peaks and valley bottoms. This implies denudation has been focused in the Klinaklini Valley region relative to surrounding valley basins and most intense near Mount Jubilee.

These age anomalies can be viewed as either variable denudation, differences in paleo and modern topography, or some combination of the two. Relative paleotopography can be constrained assuming the age anomaly equates strictly to a difference in elevation. Here the change in elevation is equal to the product of the background denudation rate and age anomaly (Figs. 5-14d and e). This approach is based on the assumption that differences in elevation are generated by instantaneous denudation. Therefore this technique yields an approximation of the magnitude of topographic change required to improve misfits. Future work is using identified age anomalies to guide an estimate of paleotopography which is then input as the initial topography which evolves to the modern. This process can be iterated to produce a landscape that minimizes misfits with data and represents a preglacial topography.

Here we use dz, the product of age anomaly and the assumed denudation rates (again, 0.6 and 0.4 mm/yr), to constrain preglacial topography. Figures 5-14d and 14e are very similar to those of age anomaly but are expressed in terms of Δ km. The paleotopography on the western slope of the Klinaklini Valley is -1 to -2 km lower than modern. Additionally, Mount Jubilee may have been ~1 to 2 km higher than the present day peak (2263 m) perhaps forming a continuous ridgeline at ~3 – 4 km with Mount Waddington. Finally, both Mount Waddington and the southern portion of the Klinaklini Valley indicate large negative values of dz (-6 km). These negative values likely represent a lower denudation rate than applied and not a paleoelevation decrease of >5 km. A likely scenario is a long-term regional denudation rate near 0.4 mm/yr (Fig. 5-14e) with an increase throughout the Klinaklini Valley (~0.6 mm/yr) and near Mount Jubilee (~0.8 mm/yr) accompanied with reorganization of local topographic features.

A constant relief model with a background denudation rate of 0.6 mm/yr yields general age anomalies of +3/-6 Myr compared to the data. These anomalies equate to the removal of perhaps ~2km of material. The distribution of these anomalies indicates

denudation does not follow a simple pattern across the landscape with, for instance, focused denudation at low elevation. Instead, glaciation has caused complex interactions between denudation and morphology. Alternatively, we can not rule out completely that these age signals are generated by plutonism, large scale fluid flow, or perhaps faulting. As above, these explanations are possible, although unlikely.

5.7 CONCLUSIONS

The presented 3-D thermo-kinematic model is used here to test the validity of numerous 1- and 2-D interpretation techniques, analyze data sensitivity to model parameters, and determine best-fit model parameters within the Coast Mountains, British Columbia. Comparison of these techniques yields the following:

- Using AGE2EDOT a 1-D thermal field is predicted incorporating the effect of denudation. In the best case scenario with a known denudation rate, predicted cooling ages are within ~10% of the average predicted age from the 3-D model. However, this method assumes a constant thermal gradient and overemphasizes high amplitude, short wavelength topographic features with misfits of >40%. AGE2EDOT is best suited for actively eroding but relatively low relief field locations.

- The 1-D draped and flat isotherm methods assume a constant geothermal gradient and elevation of closure temperature, respectively. These methods reproduce 3-D model predicted ages within ~15% on average. However, similar to AGE2EDOT, these methods introduce large errors in regions of short wavelength topography or in regions significantly above or below the average elevation where errors can be >50%. Neither method accounts for the thermal effect of denudation therefore applications should focus on low-denudation, long topographic wavelength regions.

- Best-fit regression lines through age-elevation data is the most common method for interpreting thermochronometer data. Arbitrary data transects from our 3-D model yield apparent denudation rates >70% from the "true" background rate input in the model, mainly caused by violating a key assumption of a flat closure isotherm. To minimize this transects should be collected over a narrow (~5 km) horizontal distance.

- A 2-D correction to the best-fit regression line incorporates the thermal perturbations of topography. Here, again using the best case scenario with "measured"

127

thermal data from the 3-D model, this correction significantly reduces the error improving the estimated denudation rate to within 10%. The additional thermal information needed to accurately apply this correction necessitates a field region with appropriate data.

Of note, all of these methods require some a-prior knowledge of the thermal field or denudation rate. Usually this can be thermal gradient measurements from boreholes, or independent measurements on the denudation rate, etc. Approximating these input values can increase the associated errors for each calculation.

Sensitivity experiments conducted here indicate our 3-D model is insensitive to a number of key parameters. Incorporating a 2σ sample error of 17% into our analysis, this model is intrinsically insensitive to variations in basal temperature, and increasing or decreasing relief change around the mean elevation. However, a signal of both denudation rate and relief change around either the maximum or minimum topography can be resolved. A consequence of these experiments is that a wide range of model parameters predict similar cooling ages, and therefore produce similar fits to the data.

We apply Pecube to test whether simple relief change over the modern topographic wavelength can reproduce our observed AHe cooling age distribution. Changes in background denudation rate as well as relief change around a fixed maximum or minimum elevation are resolvable with a 2σ sample error of 17%. However, no models within our tested space statistically reproduce the observed data. Trends in age anomalies and changes in initial topography (dz) suggest misfits are locally correlated. Increases in denudation and changes in paleotopography are caused by variable denudation in glacial erosion. Finally, our results indicate that relief change is difficult to detect in actual thermochronometer data, and simple relief change over the modern landscape in the Coast Mountains cannot reproduce our observed cooling ages.

5.8 ACKNOWLEDGMENTS

sample collection, K. Farley and L. Hedges for analytical work at the C.I.T. laboratory, and D. Whipp and C. Spath for 3-D code development.

Citation:

5.9 FIGURES

Figure 5-1. Shaded relief digital elevation model (DEM) of the Coast Mountains, British Columbia with thermochronometer sample locations. A: Physiography of western British Columbia. The Coast Mountains stretch from northern Washington to southern Alaska, USA. Black box is study area in the Mount Waddington region. B: Apatite (U-Th)/He (AHe) and fission track (AFT) sample locations and data transects used in subsequent figures. Dashed line is swath profile used in Figure 5-4.
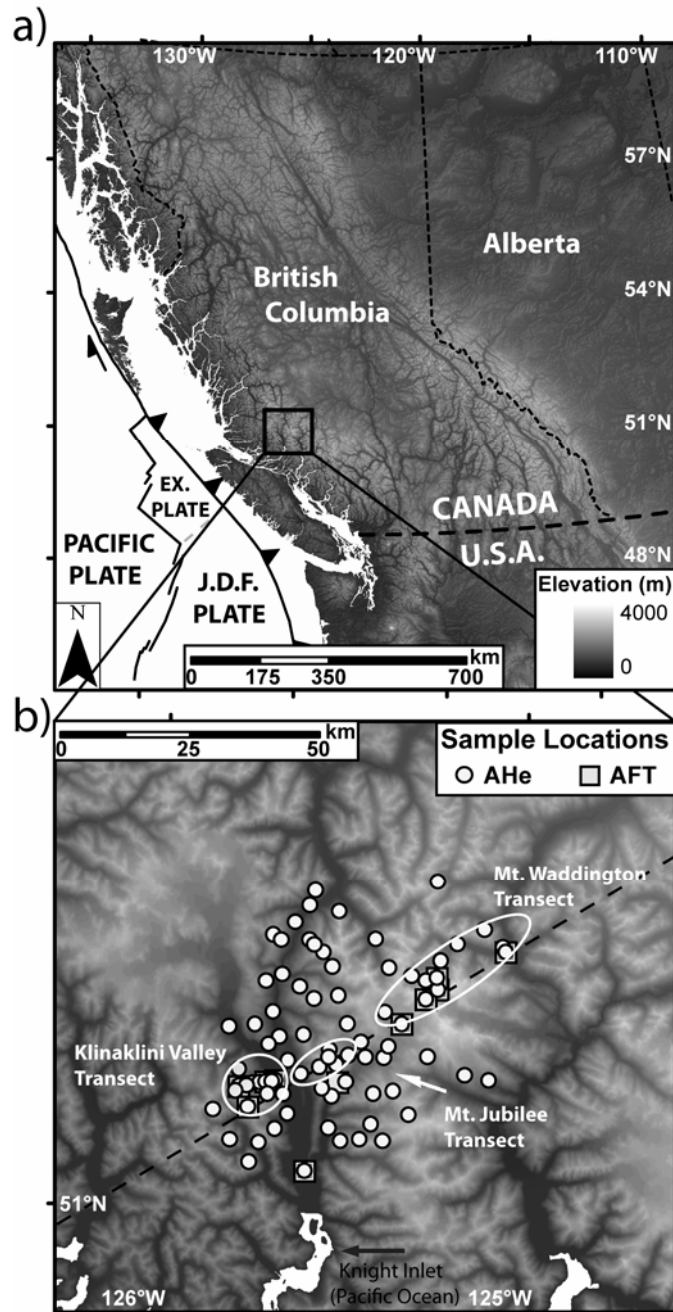
Figure 5-2. AHe thermochronometer ages in cooling age versus sample elevation and 2σ errors. Error bars contained within symbol if not visible. Note vertical axis shift. A: All 83 data points from Figure 5-1b. B: Klinaklini Valley transect, representing the major valley and trunk stream in the region. C: Mount Jubilee transect, a local high relief peak. D: Mount Waddington transect, the highest point within the Coast Mountains (4019 m).

a) All AHe Data

b) Klinaklini Valley Transect

c) Mt. Jubilee Transect

d) Mt. Waddington Transect

132
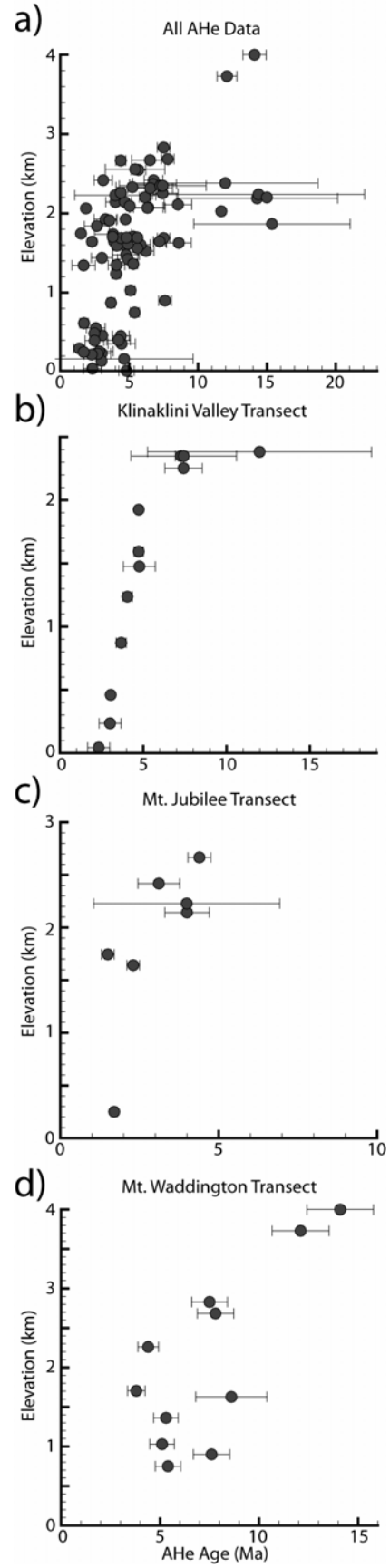
Figure 5-3. Box diagram of 3-D thermal model including constant model parameters and boundary conditions.
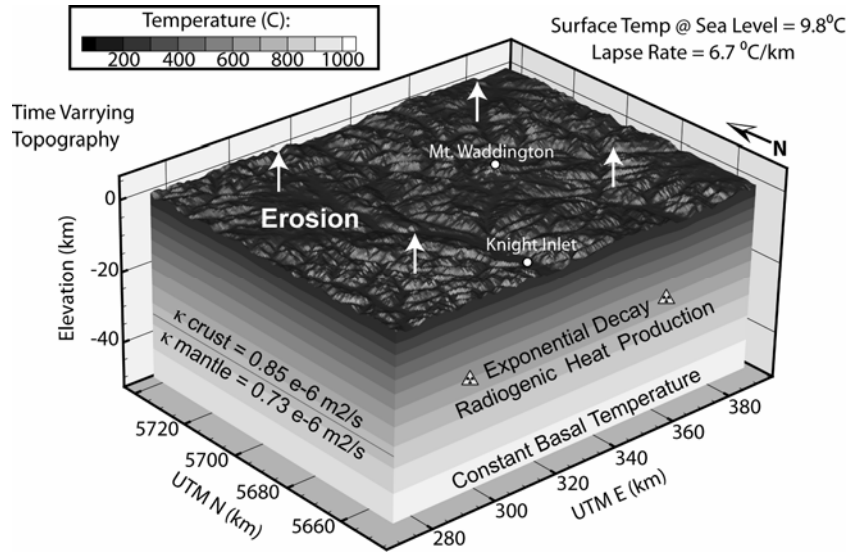
Figure 5-4. Topographic profile from Figure 5-1b with pertinent isotherms derived from 3-D Pecube model. Numbers are approximate closure temperature isotherms apatite (U-Th)/He (72 °C) and fission track (110 °C) and zircon (U-Th)/He (190 °C) and fission track (220 °C). Note how perturbations caused by topography decay with depth.
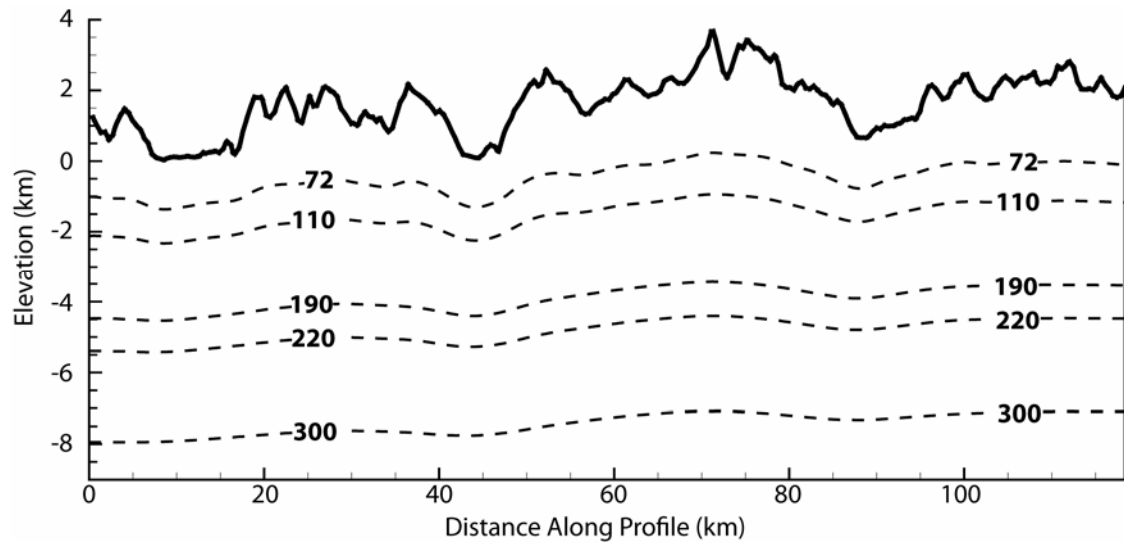
Figure 5-5. Comparison of 1- and 3-D thermochronometer cooling age and denudation rate prediction methods. A: Elevation swath profile from Figure 5-1b with modern topography and the AHe closure temperature isotherm calculated using our 3-D model (Pecube), a simple 1-D thermal model (AGE2EDOT) and a draped and flat isotherm method. B: Cooling ages derived from closure temperatures derived in (A). Boxes denote hypothetical transects used in Figure 5-5. C: Per cent difference in predicted cooling ages between 1- and 3-D methods across the landscape in (A).
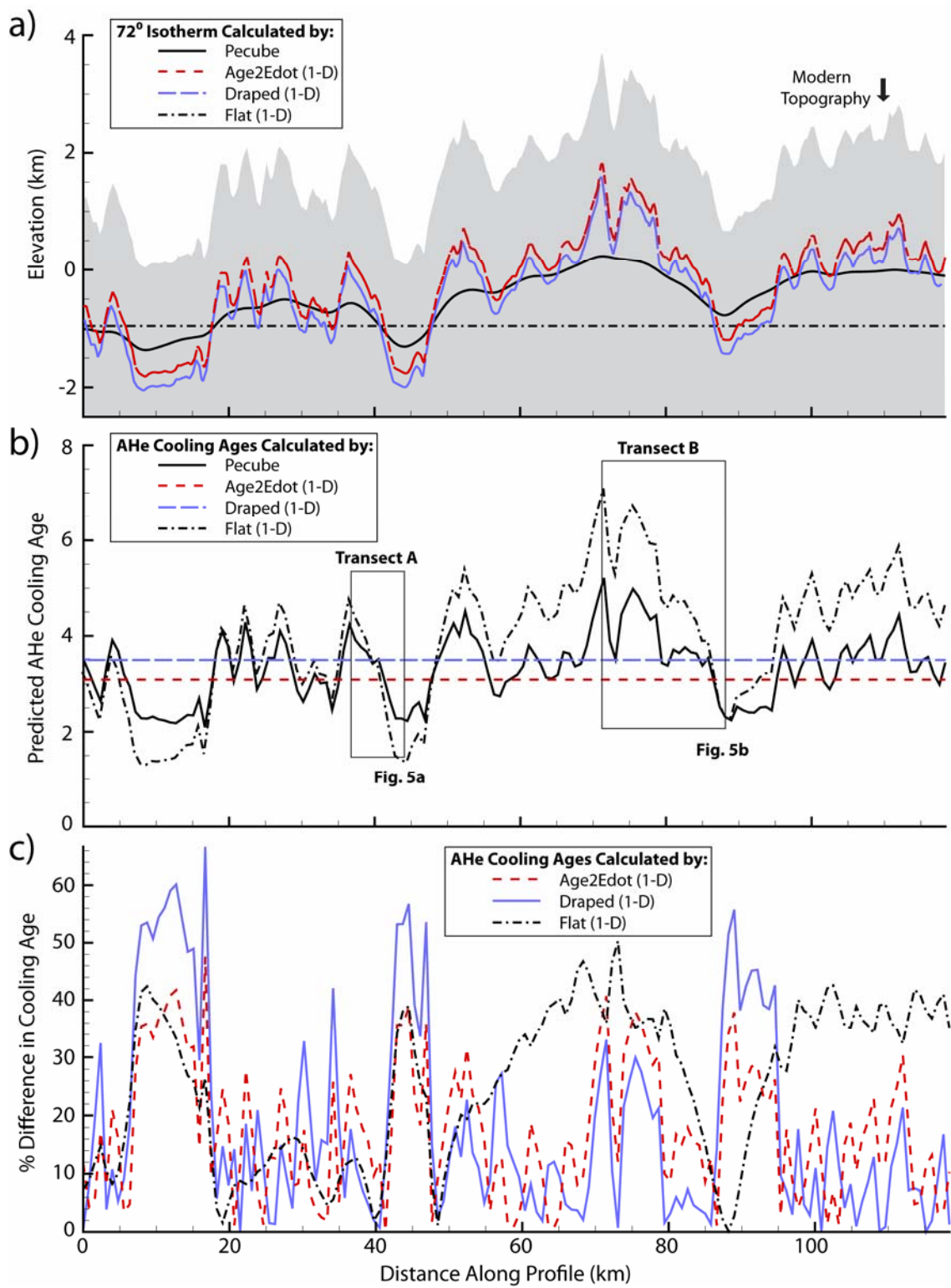
Figure 5-6. Best-fit regression line through age-elevation profile and 2-D correction for transects in Figure 5-4c. Model is run with a prescribed denudation rate of 0.6 mm/yr and samples shown with 17% error. A: Transect A, where 2-D correction improves apparent denudation rate estimate from 78% difference to 10%. B: Transect B – note vertical axis change. Here, apparent denudation rate improved from 72% different to <10%.
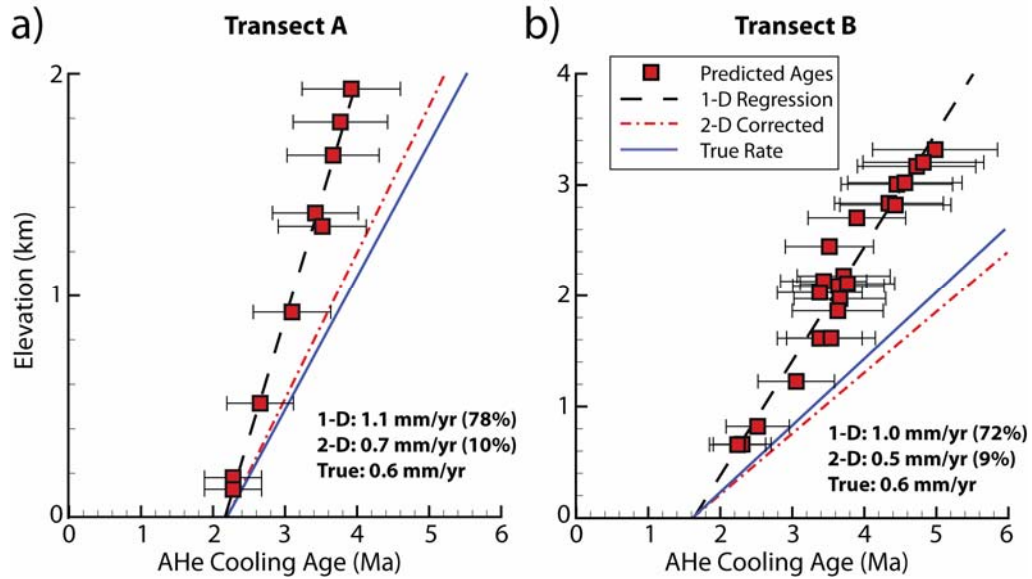
Figure 5-7. 3-D thermal model predicted AHe cooling ages showing sensitivity to various parameters. Samples shown are from Mount Waddington transect with 17% error. A: Cooling ages along Mount Waddington transect for 900, 1100 and 1300 °C basal temperatures. B: Cooling ages with effect of range of denudation rate. Light symbols are all predicted ages emphasizing the narrowing of age distribution with increasing denudation rate.
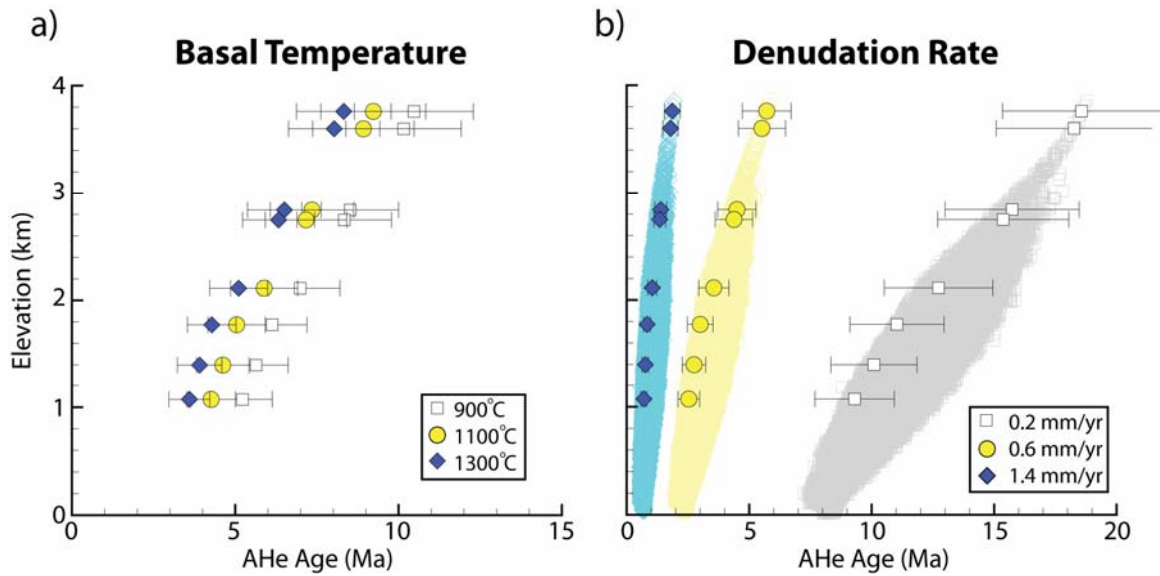
Figure 5-8. 3-D thermal model predicted AHe cooling ages showing sensitivity to relief change scenarios. Samples shown are from Mount Waddington transect with 17% error. A: Predicted cooling ages with increasing relief from an initial DEM 0.25x, 0.5x and 0.75x of modern that began morphing at 8 Ma. B: As (A) but with decreasing relief from an initial topography 1.25x, 1.5x and 1.75x of modern. C: Increasing relief change from 0.5x to modern beginning at different time periods (10, 8 and 2 Ma). D: As (C) with decreasing relief from 1.5x modern.
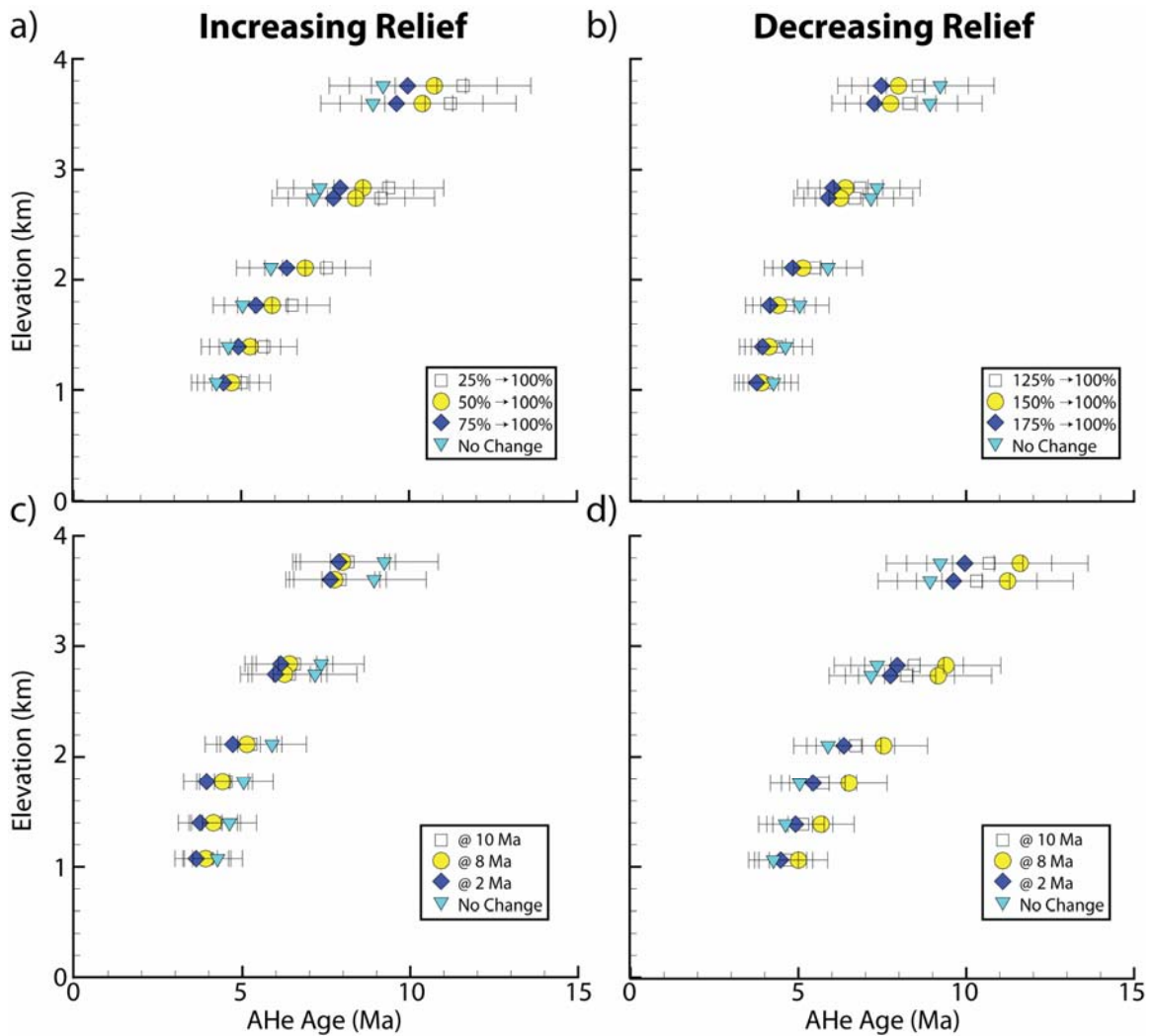
Figure 5-9. Conceptual cartoon with the effect of various increasing relief scenarios. A: Increasing relief from $time_0$ to $time_1$ while maintaining a fixed maximum. This should cause ages within the valley to become younger while those on the ridge line do not change (dashed line). However, due to advective heat transport, ages are younger everywhere (dotted line). B: As (A) maintaining a fixed mean elevation. Here, conceptual model and 3-D model outputs are very similar. C: Increasing relief maintaining a constant minimum elevation. Here predicted ages should stay similar at low elevations and get older at high elevation due to topography growing. Again, due to changes in heat transport, the conceptual (dashed) and predicted ages (dotted) maintain a similar trend but do not line up.
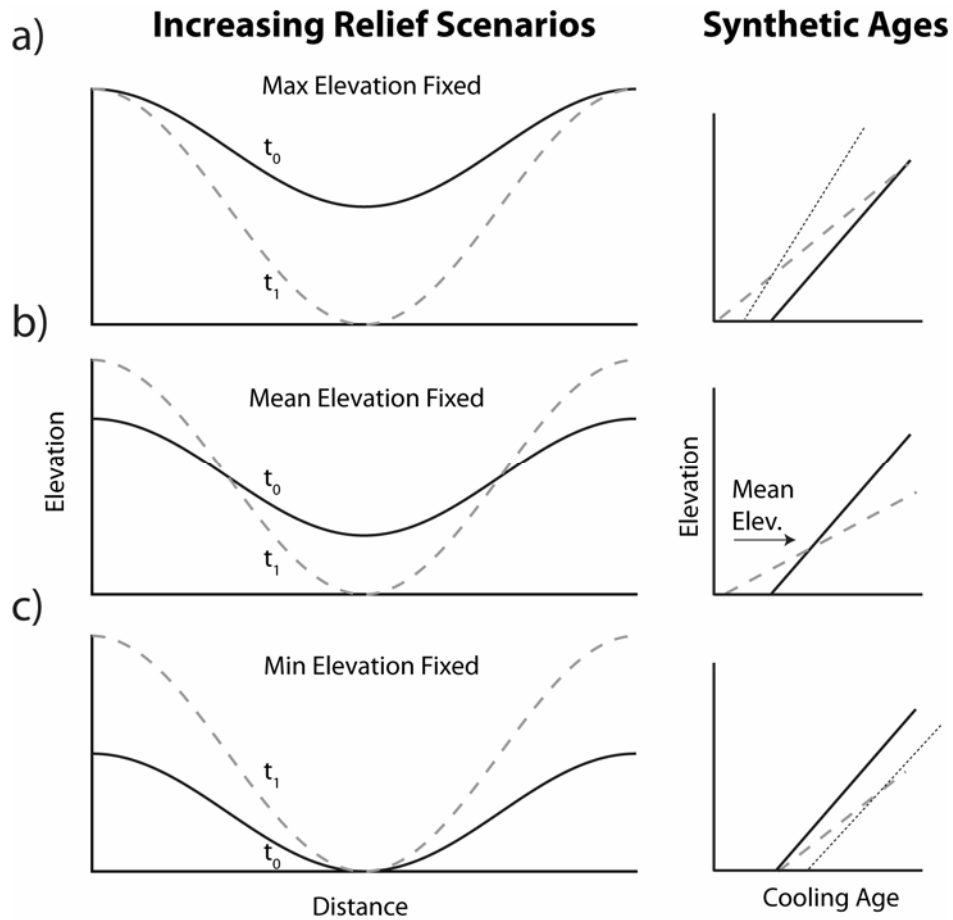
Figure 5-10. 3-D thermal model predicted AHe cooling ages showing sensitivity to relief change around minimum, mean and maximum elevations. Samples shown are from Mount Waddington transect with 17% error. A: Increasing relief model from 0.5x modern to present at 8 Ma. B: As (A) with decreasing relief from an initial DEM 1.5x modern.
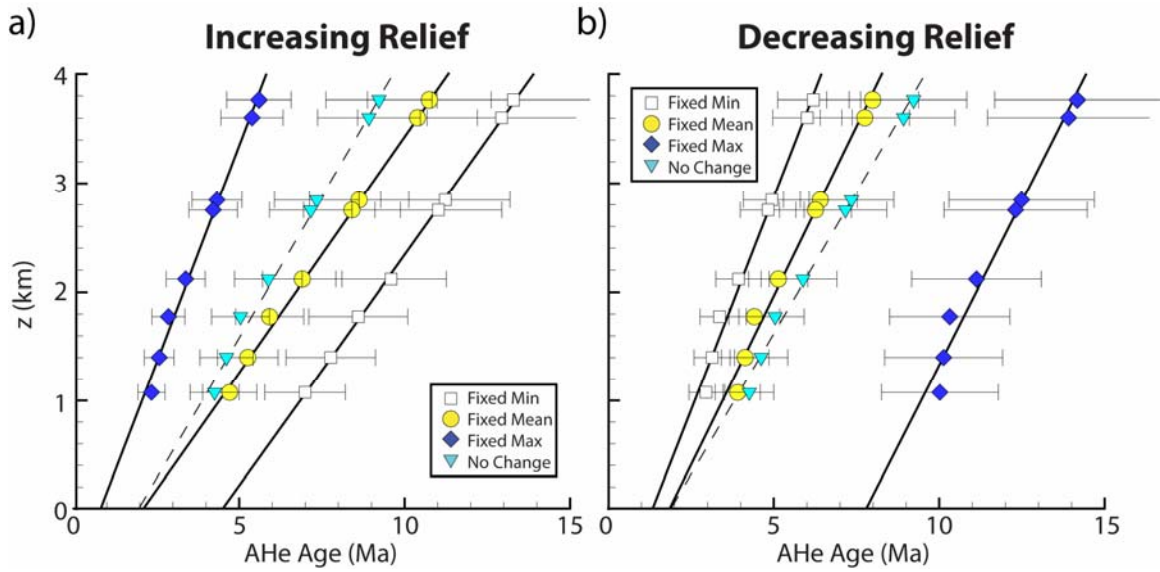
Figure 5-11. χ^2 values for constant relief models relating basal temperature and background denudation rates. Note semilog axes. Basal temperatures held constant at 900 (squares), 1100 (triangles) or 1300 °C (circles) with χ^2 values from all (A) AHe, and (B) AFT samples.
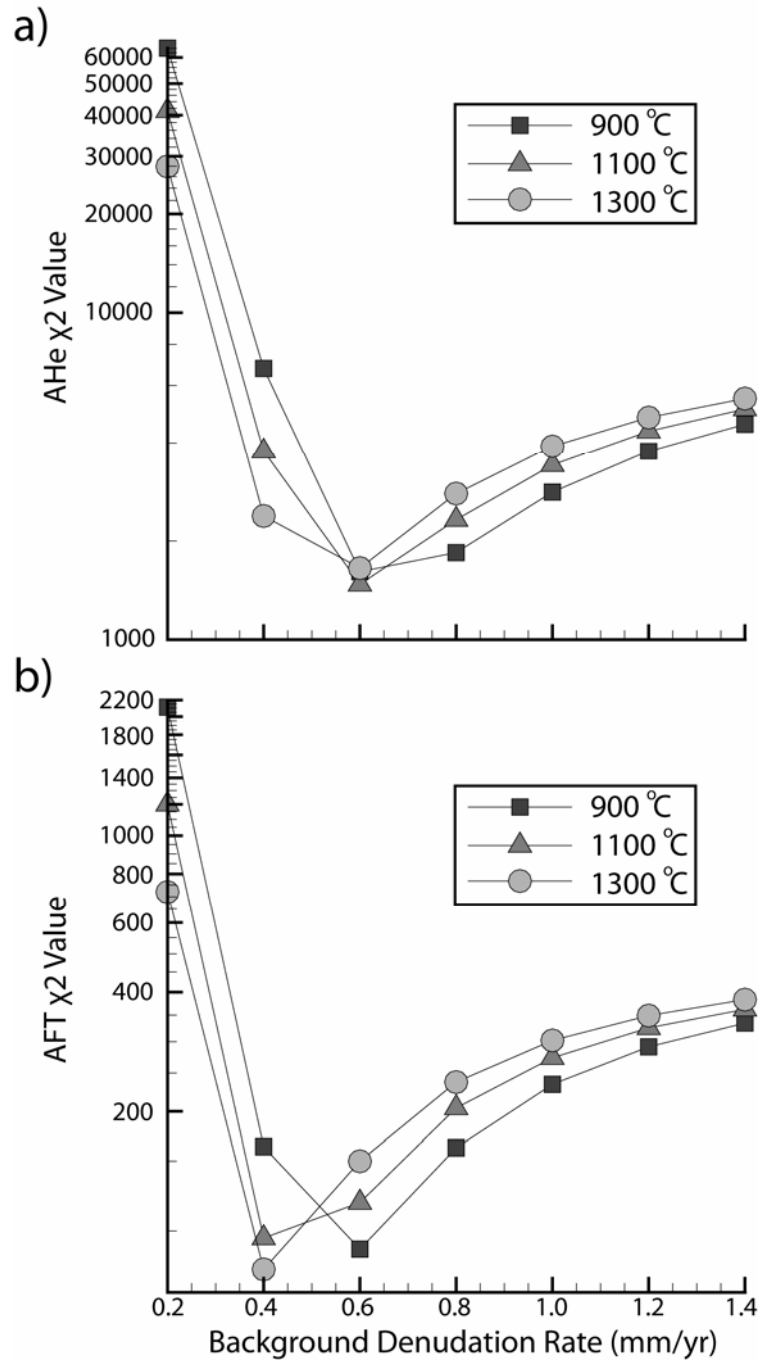
Figure 5-12. χ^2 values for variable relief models relating differing relief change scenarios and background denudation rates. Note semilog axes. Models were run with prescribed relief change occurring at 8 Ma, basal temperature of 1100 °C, and initial relief 50% (squares), constant (triangles) or 150% (circles) of modern with χ^2 values from all (A) AHe, and (B) AFT samples.
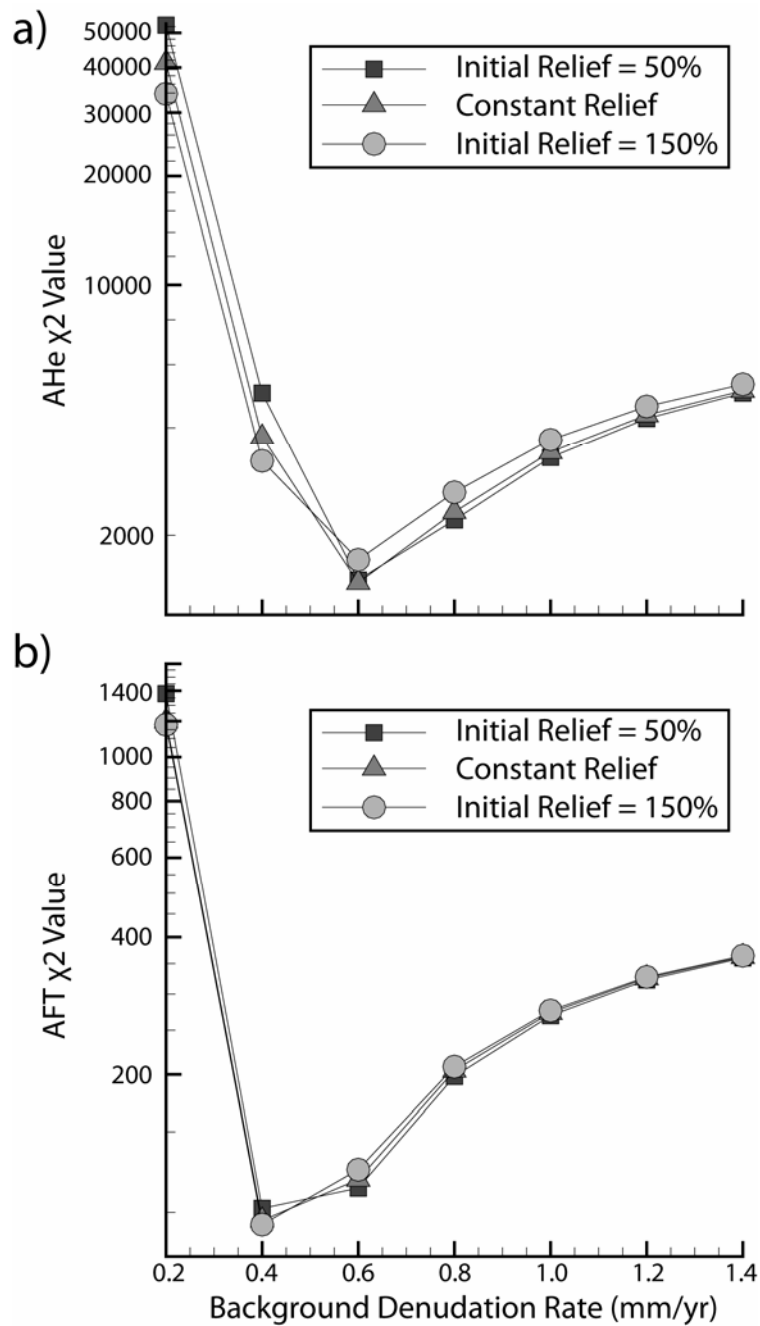
Figure 5-13. Constant relief models and data in age versus elevation. Models used here use background denudation rates of 0.4 (Cp009, diamonds) and 0.6 mm/yr (Cp010, squares). Data includes 2σ error. Note x-axis change throughout. Data divided into (A) all AHe data, (B) Klinaklini Valley transect, (C) Mount Jubilee transect, (D) Mount Waddington transect, and (E) all AFT data.
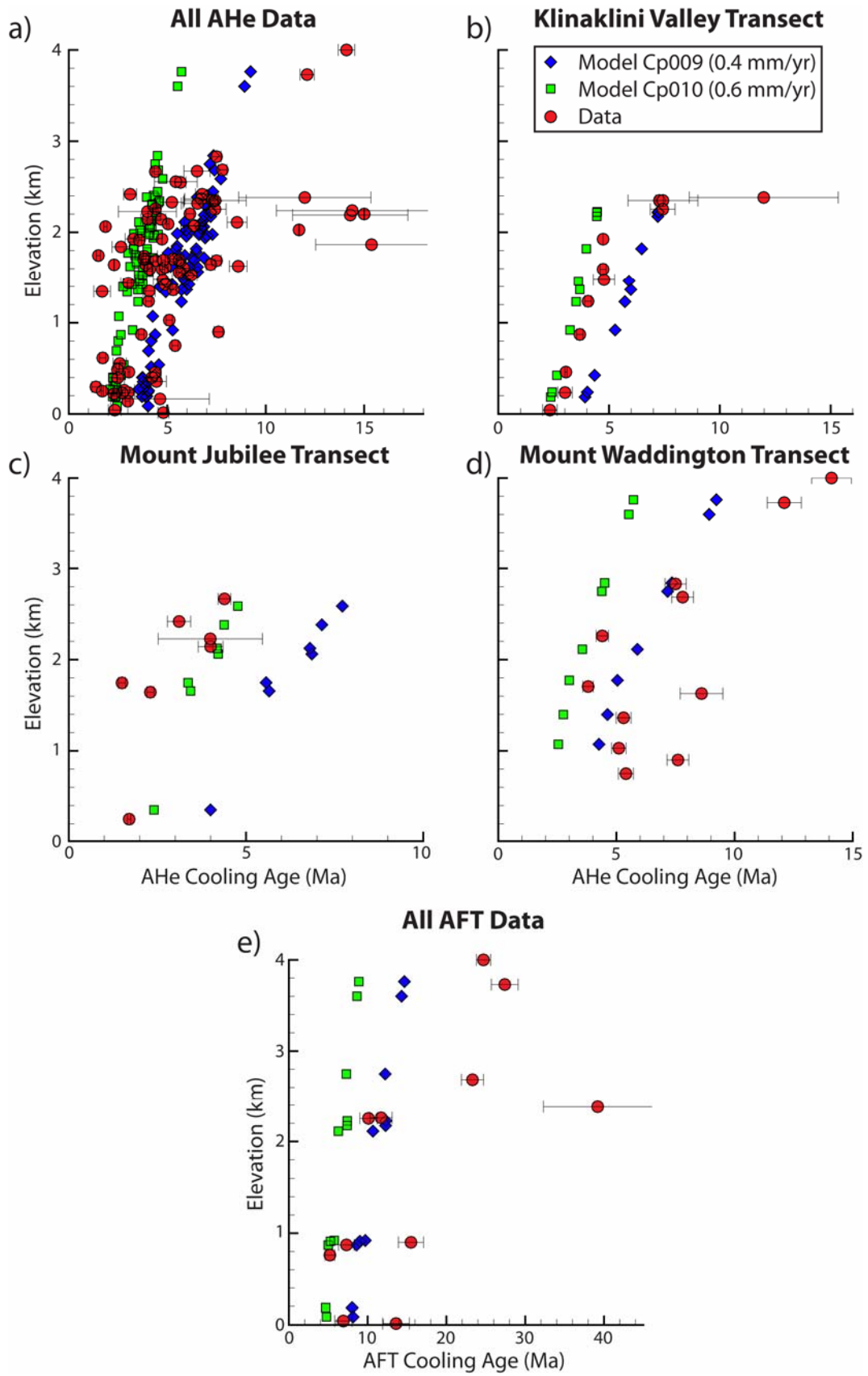
Figure 5-14. Topography and calculated differences between predicted and observed cooling ages in the Mount Waddington region. A: Shaded relief DEM with AHe sample locations as well as reference points for the Klinaklini Valley (KV), Mount Jubilee (MJ), and Mount Waddington (MW). Contoured age anomaly, defined as predicted – observed AHe cooling age, for constant relief with (B) 0.6 and (C) 0.4 mm/yr background denudation rate. Contoured change in elevation (dz), defined as the product between age anomaly and background denudation rate, for (D) 0.6 and (E) 0.4 mm/yr.
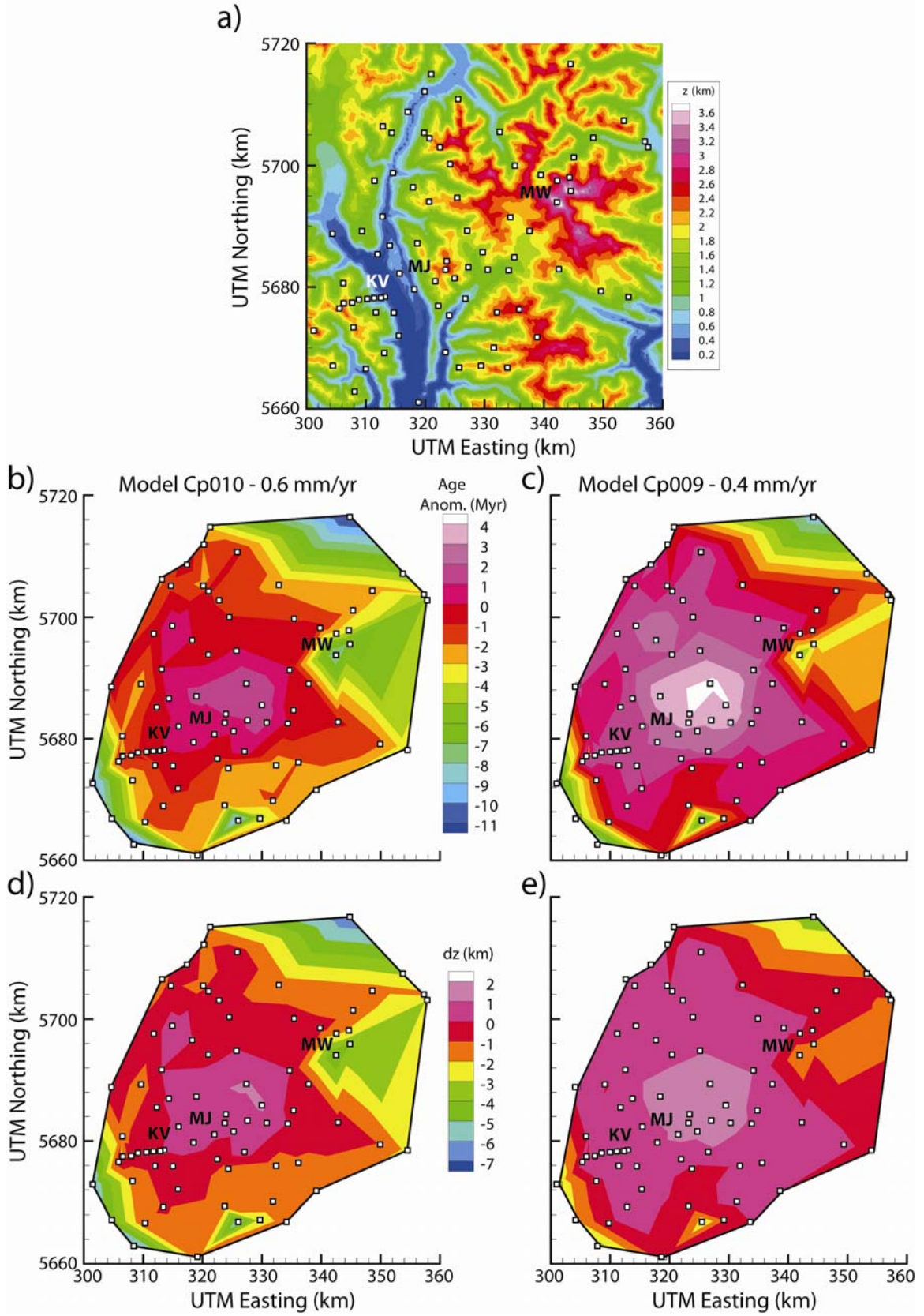
Table 5-1. Constant parameters used in Pecube 3-D thermo-kinematic finite element model.

Constant Parameters		
Model Duration	50 Myr	
Thermal Parameters		**References**
Model Thickness	50 km	Clowes et al., 1995; Currie and Hyndman, 2006
Crustal Thickness	35 km	Hammer and Clowes, 1997
Thermal Conductivity	2.24 W/mK	Densmore et al., IN PREP
Specific Heat Capacity	956 J/kgK	Waples and Waples, 2004
Crustal Density	3,200 kg/m3	Waples and Waples, 2004
Mantle Density	2765 kg/m3	Waples and Waples, 2004
Surface Temp at Sea Level	9.8°C	National Climate Archive,
Atmospheric Lapse Rate	6.69°C/km	http://climate.weatheroffice.ec.gc.ca
Crustal Volumetric Heat Production	0.8 uW/m3	Currie and Hyndman, 2006
E-folding Depth	10 km	Currie and Hyndman, 2006
Mantle Volumetric Heat Production	0.02 uW/m3	Currie and Hyndman, 2006
Isostacy Parameters		
Young's Modulus	1 e11 Pa	Turcotte and Schubert, 2002
Poisson's Ratio	0.25	Braun and Robert, 2005
Effective Elastic Thickness	15 km	Flueck et al., 2003

Table 5-2. Variable parameters and ranges used in 3-D thermo-kinematic finite element model.

Variable Parameters	
Basal Temperature	900-1,300°C
Background Denudation Rate	0.2-1.4 mm/yr
Initial Relief	25%-175%
Timing of Relief Change	10, 8, or 2 Ma
Relief Scenario	Fixed Min., Mean. or Max. Elevation

Table 5-3. After Densmore et al. (2008c), constant parameters used in 1-D AGE2EDOT thermal model.

1-D Model Parameters	Value
Thermal Diffusivity	26.71 km^2/Myr
Internal Heat Production	5.61 °C/Myr
Surfact Temperature	2.21 °C
Surface Thermal Gradient (no erosion)	24.5 °C/km
Depth to Constant Temperature	50 km

Chapter 6: Conclusions

Summary of Results and Conclusions

The primary objective of this dissertation is to constrain the exhumation history and chronology of denudation within the southern Coast Mountains, British Columbia, Canada. Below is a synopsis of each main dissertation chapter, including major findings and contributions as well as responses to hypotheses posed in the introduction (Ch. 1).

Chapter 2. This local study quantifies denudation rates for the last ~10 Myr within the major trunk stream in the study region. Findings indicate glaciation significantly alters low-temperature thermochronometer age-elevation relationships. Twelve samples along a vertical transect were used, a subset of the dataset presented in this dissertation. This transect yielded cooling information since ~15 to 20 Ma and displays a break in slope in age versus elevation at ~2000 m, corresponding to 5 – 7 Ma. This feature is interpreted as an increase in denudation coincident with the onset of glaciation. A best-fit regression line through the data yields an apparent denudation rate of 0.03 mm/yr. For a more quantitative constraint on denudation, this chapter utilizes 3-D thermo-kinematic modeling of spatially constant but temporally variable denudation. Data are best fit by rates of ~0.4 mm/yr prior to ~6 Ma and an increase to ~0.8 mm/yr for ~6 Ma to present. However, no combination of model inputs completely fit the data suggesting a spatially variable denudation rate with elevated rates below ~2000 m. This variable denudation is attributed to glacial processes with increased denudation due to valley widening and deepening.

Chapter 3. Fifty-eight new apatite (U-Th)/He samples are presented and interpreted by analyzing age-elevation profiles, comparison of similar elevation samples

151

across a topographic profile, and a 1-D thermal model. These techniques constrain denudation rates to 0.8 to 1.1 mm/yr (average of 1.0 mm/yr) using regression lines, and 0.2 to 1.5 mm/yr (averaging 0.6 mm/yr) using the thermal model. The increase in rate is interpreted to indicate the onset of glaciation, intensely altering the landscape below 2000 – 3000 m. Comparison of samples across the region indicates denudation rates are highest in large valleys (~3 – 5 km wide) with modern glaciers still present, averaging ~0.9 mm/yr at elevations <1000 m. Additionally, findings here indicate patterns of denudation with increased denudation north to south through the major valley, high rates near a local peak, Mount Jubilee, and perhaps locally high rates that migrated from Mount Waddington to the southwest in the last 5 to 8 Ma. Denudation rates determined here are lower by at least an order of magnitude than previous short-term (~10^2 – 10^3 yrs) estimates, and 3 to 5 times less than thermochronologic studies in southern Alaska.

Chapter 4. A number of published thermochronometer datasets and new samples were compiled, including apatite and zircon (U-Th)/He and fission track cooling ages. Cooling ages generally display a positive age-elevation relationship. These data were divided into 3 vertical transects and interpreted using forward and inverse thermal modeling in order to constrain cooling histories as well as denudation rates and magnitudes. Modeled cooling histories suggest monotonic cooling from ~160 ºC since 30 to 10 Ma and more rapid cooling within the last ~8 Myr. Specifically, three modeled transects indicate cooling histories of: (1) steady cooling from ~140 ºC in the last ~15 Ma (~0.4 mm/yr) along the western slope of the Klinaklini Valley, (2) rapid cooling from ~200 ºC since 10 – 15 Ma (>0.6 mm/yr) near Mount Jubilee, and (3) relatively slow cooling from ~100 ºC since ~20 Ma (~0.25 mm/yr) on the northeast flank of Mount Waddington. Calculated denudation rates from our 1-D model range from 0.2 to 2.2 mm/yr with an average of ~0.5 mm/yr. Using this model the transects presented exhibit (1) moderate (~0.6 mm/yr) rates slightly increasing to the east/northeast within the Klinaklini Valley, (2) high (>0.8 mm/yr) rates of denudation near Mount Jubilee, and (3) subdued (<0.5 mm/yr) denudation rates on the flank of Mount Waddington. A denudation magnitude for each transect is calculated incorporating the average denudation rate and cooling age. These estimates range from 8.8 to 11.5 km since 6.9 to

28.0 Ma. The chronology of exhumation indicates spatially and temporally variable denudation since at least 30 Ma. Moreover, three major phases of denudation are apparent throughout the Coast Mountains: (1) relatively rapid during the mid – late Paleogene (>30 – 20 Ma), perhaps associated with subduction off shore, (2) a period of subdued denudation during most of the Miocene (~20 – 7 Ma), and (3) an increase to fairly rapid rates from the latest Miocene (~7 Ma) to the present, presumably due to the onset of extensive glaciation.

Chapter 5. The final main chapter of this dissertation utilizes a sophisticated 3-D thermo-kinematic model to interpret the large dataset of cooling ages. This model is compared to a number of commonly used 1- and 2-D methods in order to evaluate the effectiveness of each. These more simplistic methods generally yield consistent (~20%) average cooling ages and denudation rates. However, high amplitude, short wavelength topographic features are overemphasized in 1-D simulations and can cause cooling age misfits of 40 – 60%. Best-fit regression lines yield apparent denudation rates >70% from the 3-D model input rate but a 2-D correction can improve these estimates to within ~10%. These simplistic methods require a-priori knowledge or an assumption of the subsurface thermal field or denudation rate. The 3-D thermal model is utilized to test the range of relief change, background denudation rate and basal temperature that can reproduce observed data. No models within the tested space yield statistically significant fits to the data. Some combination of locally increased denudation and topographic modification has influenced cooling ages such that there is a wide distribution of ages even. Spatially variable denudation and modification of local morphology is accomplished by glaciation over Myr timescales.

Contributions

The major contributions from this dissertation are: (1) a large, dense thermochronologic dataset, (2) a comparison and analysis of common quantitative techniques used to interpret this data and (3) identification of distinctive characteristics of long-term denudation by glacial processes.

Associated with this dissertation is a large thermochronometer dataset that was collected, processed and analyzed. This dataset consists of 58 samples with an additional 25 previously published samples. All samples were prepared using standard microscopy and analyzed for (U-Th)/He at the California Institute of Technology laboratory, and fission tracks analyzed at A to Z, Inc. This data yielded 58 apatite (U-Th)/He, 4 apatite fission track, and 9 zircon (U-Th)/He cooling ages of generally excellent quality. Additionally, 14 samples were made available for ^{4}He/^{3}He analysis, however only a small subset of these has been analyzed at the time of publication of this dissertation.

Various modeling techniques were evaluated through the course of this dissertation. Findings here indicate apparent denudation rates from age-elevation profiles can introduce large errors (~70%) associated with violating underlying assumptions. Additionally, 1-D methods reproduce average cooling ages and denudation rates while misfitting observed data significantly (>60%) on a local scale. Care must be taken when using these tools to interpret data over a wide spatial region. These simplistic methods represent means for constraining denudation rates over a limited spatial extent, when lacking thermophysical rock properties, or with limited computational power. In general, the novel approach used here was to combine multiple techniques in order to present a rigorous range of cooling age and denudation rate estimates.

Work here shows that more simplistic 1- and 2-D methods of interpreting thermochronometer data can be successfully implemented depending on the study goals. Assuming the sophisticated 3-D model presented here is a close approximation of the natural system, many of the simple approaches detailed yield mutually consistent results and reproduce the average cooling age and denudation rate predicted by our 3-D model to within ~15%. Therefore if the intent is to quantify a regionally averaged denudation rate, a simple 1-D thermal model may be appropriate. For more detailed studies of specific features within a landscape or dataset, a more sophisticated approach is required.

This dissertation demonstrates that glacial processes compared to non-glacial processes are more efficient at modifying alpine landscapes over long timescales. Long-term denudation rates appear to double with the onset of glaciation. Glacial rates here (~0.6 mm/yr average) are much lower than those quantified using stream gauge and sediment discharge data that quantify denudation over short (~$10^2 - 10^3$ yrs) timescales.

Moreover, denudation varies within a glaciated terrain reworking existing drainage networks and eroding local topographic features, or in some instances affecting very little change at all. Therefore, the modern landscape is not necessarily diagnostic of paleotopography.

Hypotheses Addressed

Below are the summarized responses to hypotheses stated in Chapter 1 of this dissertation.

(1) A pulse of denudation is observable coincident with the onset of glaciation.

There is a pronounced denudation rate increase characterized in thermochronometer data at 6 – 8 Ma correlating with a shift from presumably a stable fluvial environment to a predominantly glacial one. It appears that indeed a signal of glaciation overprints the observed data here. A more recent (<2 Ma) further increase is inferred, relating to the intensification of glacial erosion during the Pleistocene.

(2) Glaciers are more efficient agents of erosion than streams over long periods of time.

Similar to (1) above, the evidence for glaciation is a marked increase in long-term denudation coincident with the onset of glaciation in the range. Therefore glaciers are more efficient agents of erosion over long timescales. However, this dissertation does not distinguish between glacial advance, retreat or interglacial processes as thermochronometers incorporate different processes into a single cooling age. Regardless, the sum totals of these processes transport more material than a fluvial environment.

(3) Glacial denudation is highly variable across the landscape.

This dissertation identifies denudation rates of 0.2 to 1.6 mm/yr across the landscape. Moreover, three distinct regions are outlined, namely the Klinaklini Valley, Mount Jubilee and Mount Waddington regions, characterized by average, very high and low rates of denudation, respectively. Analysis of cooling ages from similar elevation samples between regions yields little correlation indicating patterns are locally derived

155

and not regionally correlative. Therefore, glacial denudation is a dynamic process that is both spatially and temporally variable.

(4) Glaciers modify topography by changing relief initially generated by a fluvial network.

Glaciers likely initially occupy the headwaters of alpine valleys. However, over time they rework the local drainage network and sculpt the landscape into a new form. Sophisticated 3-D thermal modeling of the Coast Mountains with variable relief over the modern topographic surface could not reproduce observed cooling ages. Therefore, glaciation does not simply alter the relief in a region by deepening existing valleys or smoothing ridgelines. Instead, glacial erosion creates an erratic distribution of denudation significantly altering the landscape to a degree that the local paleorelief may be indistinguishable from the modern.

Future Work

Further work to advance this dissertation should focus on field mapping within the Mount Waddington region and continued development of the presented 3-D thermal model. As discussed above, faulting, magmatism and fluid flow can complicate interpretations of thermochronometer cooling ages. A detailed mapping study in the field area could confirm or disconfirm locations of active structures and the presence of hot springs. Additionally, the extent of recent volcanism can be determined in order to assess the effect of localized intrusive bodies on presented cooling ages. Finally, further development of the 3-D code could use observed age anomalies and calculated changes in paleotopography to guide estimates of initial pre-glacial topography. This calculated surface could be iteratively input in to the model and evolved to the modern topography to constrain how glaciation has affected the landscape.

Appendices

Appendix 1 : Supplemental Material for: Densmore et al. (2007) Effect of Alpine Glaciation on Thermochronometer Age-Elevation Profiles.

ANALYTIC METHODS

To determine apatite (U-Th)/He ages (AHe), pristine grains were selected using standard microscopy under cross-polar filtered transmitted light. Each chosen grain was documented and measured along the a, b and c-axis to determine the α-emission correction (Farley et al., 1996). These grains were loaded into platinum packets and thermally outgassed by laser step-heating at the California Institute of Technology laboratory. Radiogenic helium released in this process was measured versus a spike of ^{3}He as a ^{4}He/^{3}He ratio on a quadrapole mass spectrometer. The remaining grain material was then digested, spiked with ^{235}U and ^{230}Th, then analyzed for ^{238}U and ^{232}Th using isotope ratios determined from an inductively coupled plasma mass spectrometer (ICP-MS). For each sample, a minimum of three grains were analyzed to determine reproducibility. For samples with low U and Th content, aggregates of four grains in a single packet were run using the same process outlined above. Zircon (U-Th)/He (ZHe) samples were prepared in a similar manner but two packets of four grains each were run for every sample.

Apatite fission track (AFT) analysis was done on four of the vertical transect samples. Apatite to Zircon, Inc., preformed the analysis using the laser ablation ICP-MS method (Donelick et al., 2005; Hasebe et al., 2004). Mounts were prepared with some number of apatite grains immersed in epoxy resin. These mounts were polished and then etched for 20.0 seconds in 5.5N HNO$_3$. Natural tracks from the spontaneous fission of ^{238}U are counted and the cooling age of the sample was determined relating this number to the amount of ^{238}U within the grain. Samples were then irradiated using ^{252}Cf and the resulting induced tracks are measured for length, width and crystallographic orientation. Raw data from these analyses are given in Table A-1-1 through A-3.

HIGEST ELEVATION AFT SAMPLE

The two highest elevation AFT samples differ in cooling ages by 29 Myr over 130 m elevation. This sizeable offset may be due to a change in erosion rate or variations in apatite composition. No simulations with large changes in erosion rates produced an acceptable fit to both samples, suggesting a rate change is not the cause. Therefore, we infer that the age difference likely reflects a compositional effect from variable Cl or low U content. A measured compositional proxy, Dpar (Burtner et al., 1994), suggests the highest elevation sample is more resistant to annealing compared to other samples (2.04 μm vs. ~1.46 μm, Table A-1-2; supplemental material). We investigated the effect of varying Dpar on sample cooling ages with forward modeling (Ehlers et al., 2005; Ketcham, 2005b), however a ~0.5 μm change in Dpar resulted in a ~2 Myr older age, considerably less than the observed difference. The most likely explanation for the large variation in sample cooling ages is the very low (~3.87 ppm) U content of the uppermost sample. The U content of this sample is nearly a factor of three lower than any other, perhaps due in part to a lithologic change from tonalite to dacitic dyke material, and may result in an unreliable age. Thus, we are unable to explicitly explain the unusually abrupt break in slope seen in the highest elevation AFT age and limit our interpretation of it.

MODELING

Figure S-1 is an example 3D thermal model block diagram. Model geometry is 48x32 km horizontally, with nodes every 250 m. This geometry is taken to a depth of 35, equivalent to the local Moho depth (Hammer and Clowes, 1997), km with 19 slices coarsening downward from every 100 m, to 500, 1000 and 5000 m totaling 473,043 nodes. The top surface is derived from a present-day digital elevation model of the field region. This surface is held in topographic steady-state and maintained at a constant temperature of 4°C at sea level with a nominal atmospheric lapse rate of 7°C cooler per kilometer elevation. Lateral heat flow is held at 0 to prevent heat flow out of the sides of the model. Heat transfer within the model is determined using FRACTure (Kohl and Hopkirk, 1995), which solves the 3D advection-diffusion equation with heat production.

The modeling approached used here is identical to that of Ehlers et al. (2006), and Ehlers and Farley (2003).

As is the case with most numerical modeling, our scheme does not define a single solution, rather a range of parameter combinations that sufficiently fit the observed data. In order to quantify how well each set of parameters match the data, a χ^2 value was determined for each model run using:

Equation A-1- 1:

$$\chi^2 = \sqrt{\frac{\sum_{i=1}^{N} \left(\frac{Age_{pi} - Age_{oi}}{U_i} \right)^2}{N - M}}$$

where Age_{pi} is the predicted AHe age, Age_{oi} the observed AHe age, U_i the one standard deviation uncertainty in the ith age, N the number of samples (12), and M the number of free parameters (6). Although this allows us to quickly evaluate each model run, many parameter combinations yield a similar χ^2 value, especially in modeling scenario (2) discussed in the main text. Table A-1-4 summarizes the combinations with a varying erosion rate with time that fall into this category. Each parameter has a specific effect on predicted cooling ages, and the reduction of one can be compensated by increasing another. This can be seen in similar model predicted ages from models with high basal heat flow and low erosion rate with those of lower basal heating and higher erosion.

FIGURES

160

Table A-1- 1. Raw data from AHe analysis, shown in Figure 2-1 of main text. UTM E. and UTM N. are UTM Easting and Northing, respectively, using North American Datum 1983, FT Corr. the fraction of alpha particles retained, and Corr. Age the FT corrected age. Replicate grains not reported (03TEKI024) if number of mols He was near machine blank level (<0.09). At least three single grain replicates were run for each sample, with additional grains used as needed due to low U and Th content.

Sample ID	Elev. (m)	UTM E. (m)	UTM N. (m)	Grains #	Mass (µg)	U (ppm)	Th (ppm)	He (nmol/g)	FT Corr.	Raw Age (Ma)	Corr. Age (Ma)	Average Age (Ma)	Std. Dev. (Ma)
03TEKI024 a	2382	306472	5677393	1	5.15	5.88	2.56	0.33	0.76	9.4	12.4	12.0	3.4
b				1	5.60	15.44	35.24	0.87	0.75	6.8	9.0		
c				1	5.86	3.81	5.91	0.27	0.77	9.5	12.4		
i				1	3.01	9.84	2.24	0.74	0.73	13.1	17.8		
k				4	18.61	4.21	4.68	0.18	0.77	6.4	8.3		
03TEKI025 a	2253	308159	5673448	1	6.23	9.20	7.26	0.31	0.80	5.3	6.6	7.4	0.6
b				1	4.75	7.30	7.39	0.30	0.77	6.0	7.8		
c				1	2.52	10.63	10.32	0.39	0.71	5.5	7.8		
03TEKI026 a	1476	311943	5675925	1	3.80	18.28	34.83	0.51	0.74	3.6	4.8	4.8	0.5
b				1	3.01	31.84	41.32	0.90	0.74	4.0	5.4		
c				1	4.91	15.26	28.50	0.38	0.77	3.2	4.2		
03TEKI027 a	235	314954	5675856	1	5.41	11.75	11.19	0.15	0.77	2.0	2.6	3.0	0.3
b				1	2.06	18.83	19.58	0.29	0.68	2.3	3.3		
c				1	2.02	9.01	11.24	0.14	0.70	2.2	3.1		
03TEKI030 a	1594	309064	5678027	1	4.14	18.86	15.46	0.43	0.75	3.6	4.8	4.7	0.1
b				1	5.09	14.91	14.35	0.35	0.78	3.5	4.5		
c				1	5.65	19.37	18.74	0.47	0.74	3.6	4.9		
03TEKI032 a	1237	310489	5678155	1	5.11	18.46	10.18	0.37	0.77	3.3	4.3	4.0	0.2
b				1	3.29	14.22	11.66	0.27	0.74	2.9	4.0		
c				1	4.51	15.48	7.97	0.28	0.76	3.0	3.9		
03TEKI034 a	872	311645	5678269	1	4.00	15.25	7.07	0.26	0.77	2.9	3.7	3.7	0.1
b				1	3.56	19.13	4.00	0.28	0.73	2.5	3.5		
c				1	6.31	11.37	6.36	0.21	0.77	3.0	3.8		
03TEKI036 a	460	312808	5678314	1	3.26	9.65	4.72	0.13	0.73	2.2	3.0	3.0	0.0
b				1	2.28	15.00	6.40	0.20	0.72	2.2	3.1		
c				1	2.82	18.04	7.46	0.24	0.73	2.2	3.0		
03TEKI038 a	43	313480	5678477	1	3.31	5.98	2.63	0.06	0.75	1.6	2.1	2.3	0.3

162

				1	3.91	10.10	10.33	0.14	0.76	2.1	2.8		
b				1	3.58	18.76	20.18	0.23	0.73	1.8	2.5		
c				1	4.36	5.27	4.52	0.05	0.77	1.5	2.0		
d				1	4.36	5.27	4.52	0.05	0.77	1.5	2.0		
05TEKI048 a	2349	306513	5677446	4	2.03	242.38	39.66	6.75	0.69	4.9	7.1	7.3	0.2
b				4	3.36	175.82	44.25	5.60	0.74	5.5	7.4		
05TEKI049 a	2349	306513	5677446	3	3.31	75.57	20.66	2.94	0.74	6.7	9.0	7.4	1.6
b				2	2.35	88.91	3.77	2.05	0.72	4.2	5.9		
05TEKI050 a	1925	307927	5677533	3	2.56	25.57	30.38	0.59	0.69	3.3	4.7	4.7	0.0
b				3	1.29	48.18	37.44	0.98	0.66	3.2	4.7		

Table A-1- 2. Track length and age data from AFT analysis, shown in Figure 2-1 of main text. Preparation and analysis by Apatite to Zircon, Inc., using the laser ablation method of Hasebe et al. (2004). Num is the number of grains, N_s is the number of significant tracks, Dpar and Dper are the diameter of etch pits parallel and perpendicular to crystallographic c-axis, respectively. Area is the grain area analyzed. ξ_{MS} is used in the radioactive decay equation used to determine fission-track ages. This term is determined by relating the ^{43}Ca background to signal (^{43}Ca bkg:sig) value to the ^{238}U background to signal (^{238}U bkg:sig). Q is the χ^2 test result, expressed as a per cent, with 5% passing the χ^2 test. Finally, T# is the number of tracks counted.

Sample ID	Track Lengths	Pooled AFT Age (Ma +/- 1σ)	Num	Dpar (μm)	Dper (μm)	N_s	Area (cm²)	Σ(PΩ) (cm²)	1σ Σ(PΩ) (cm²)	ξ_{MS}	1σ ξ_{MS}	Q %	T #	Mean +/- Error (μm)	Std. Dev. (μm)
03TEKI024	variable	39.2 +/- 6.9	25	2.04	0.66	35	1.25E-03	8.19E-06	3.89E-07	18.40	0.42	92.37	125	13.26 +/- 0.19	2.13
03TEKI025	long	10.1 +/- 1.1	26	1.58	0.42	106	1.23E-03	9.55E-05	3.42E-06	18.25	0.41	92.37	125	13.91 +/- 0.17	1.93
03TEKI034	long	7.28 +/- 1.02	26	1.41	0.36	56	1.26E-03	6.95E-05	2.27E-06	18.09	0.41	85.68	122	14.22 +/- 0.15	1.7
03TEKI038	long	6.93 +/- 1.15	26	1.39	0.34	39	1.25E-03	5.40E-05	1.70E-06	17.93	0.41	97.40	68	14.48 +/- 0.13	1.1

Table A-1- 3. Raw data from ZHe analysis, shown in Figure 2-1 of main text. See table
S-1 for column abbreviations.

Sample ID	Grains #	MWAR (μm)	Mass (μg)	U (ppm)	Th (ppm)	He (nmol/g)	FT Corr.	Raw Age (Ma)	Corr. Age (Ma)	Average Age (Ma)	Std. Dev. (Ma)
03TEKI030 a	4	52.140	47.415	45.867	14.067	8.054	0.805	30.06	37.31	26.60	10.71
b	4	61.425	77.578	46.541	13.279	3.582	0.834	13.26	15.88		
03TEKI034 a	4	49.283	41.743	113.905	25.099	7.715	0.797	11.84	14.84	14.91	0.07
b	4	44.998	28.508	59.974	14.263	4.002	0.775	11.62	14.99		
03TEKI038 a	4	47.855	41.435	97.642	33.102	5.350	0.794	9.33	11.76	13.41	1.65
b	4	44.998	30.243	95.200	35.627	6.597	0.777	11.71	15.06		

Table A-1- 4. Model parameter combinations producing an adequately fitting model. As numerical modeling generally does not yield an exact answer, various model combinations predict similar cooling ages. The combinations shown demonstrate the interplay between various parameters, as, for example, both higher erosion and higher basal heat flow yield younger predicted cooling ages.

Basal Heat Flow	Onset Time	Preglacial $\dot{E}$	Glacial $\dot{E}$
20 mW/m^2	4 - 8 Myr	0.4 - 0.6 mm/yr	0.6 - 1.0 mm/yr
35 mW/m^2	1.5 - 8 Myr	0.4 - 0.6 mm/yr	0.6 - 0.8 mm/yr
50 mW/m^2	1.5 - 6 Myr	0.2 - 0.4 mm/yr	0.6 mm/yr

Figure A-1- 1. 3D block diagram of an example thermal-kinematic model showing geometry and boundary conditions. Temperature is determined with basal heat flux (red arrows), radiogenic production (yellow), topographic effects and erosion considered. Highlighted results are shown in Figure 2-2 of the main text and summarized in Table A-1-4 above.
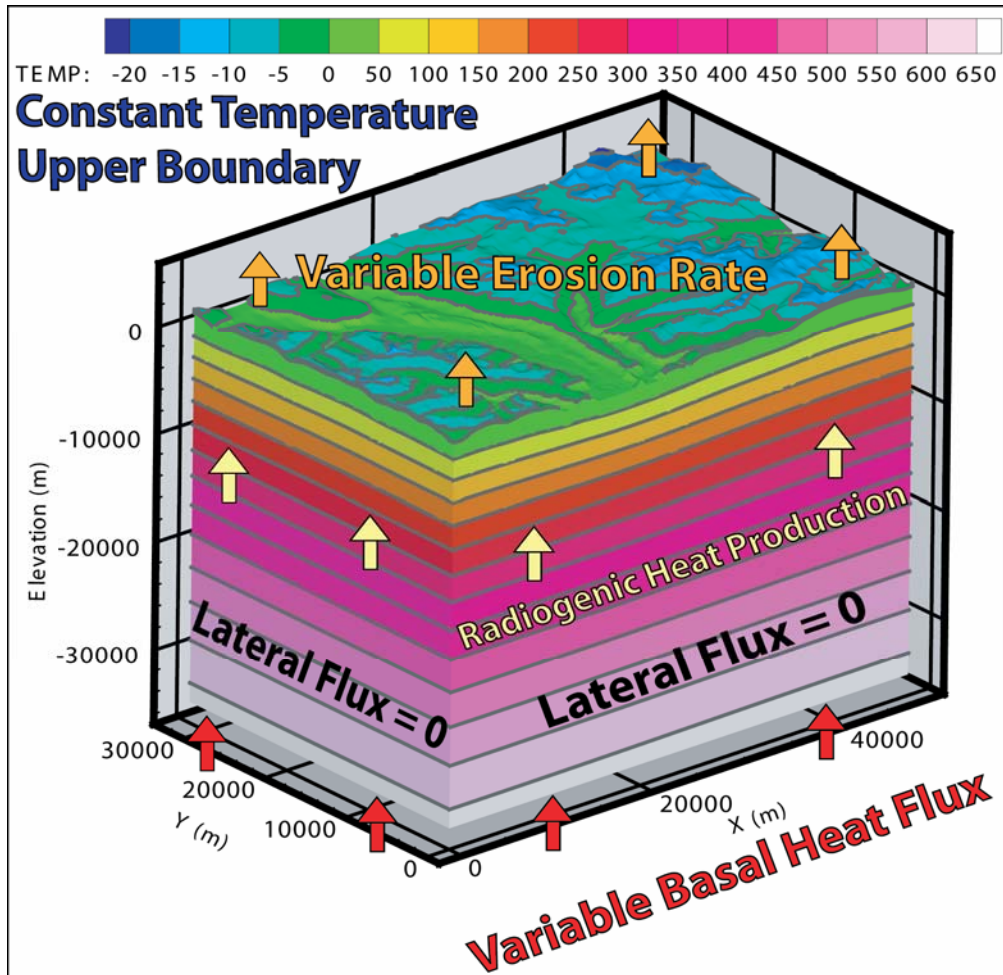
Appendix 2: Measurements of Thermal Conductivity and Heat Production

Table A-2- 1. Thermal conductivity measurements for samples presented here. Measurements were made by P. Galanis and C. Williams at the U.S. Geological Survey in Menlo Park, California using the technique of Sass et al. (1984). Samples were measured both parallel (A) and perpendicular (B) to apparent foliation, however there is no significant anisotropy.

Sample ID	Thermal Conductivity (A)	Thermal Conducivity (B)
03TEKI009	2.23	2.12
03TEKI015	2.55	2.74
03TEKI016	2.53	1.97
" run2	2.44	--
03TEKI018	1.95	2.11
03TEKI019	2.15	--
03TEKI030	2.12	2.18
03TEKI039	2.19	1.99

Table A-2- 2. Radiogenic heat production raw measurements for samples presented here. Concentrations measured using technique outlined in Whipp et al., (2007, Appendix A)

Sample ID	K, %	ppm 235U	ppm 238U	ppm 232Th	H [W/kg]	H [W/m3]	H [uW/m3]
03TEKI005	91.71%	0.0053	0.727	2.090	3.31E-09	8.95E-06	8.95
03TEKI009	0.73%	0.0021	0.288	0.481	6.66E-11	1.80E-07	0.18
03TEKI015	1.22%	0.0011	0.154	0.192	6.25E-11	1.69E-07	0.17
03TEKI016	0.75%	0.0059	0.819	0.563	1.22E-10	3.28E-07	0.33
03TEKI018	1.06%	0.0119	1.641	2.796	2.73E-10	7.36E-07	0.74
03TEKI030	0.44%	0.0027	0.368	0.783	7.24E-11	1.95E-07	0.20
03TEKI039	2.68%	0.0196	2.696	4.350	4.74E-10	1.28E-06	1.28

Table A-2- 3. Location for samples used in thermal conductivity measurements. UTM E. and UTM N. are UTM Easting and Northing, respectively, using North American Datum 1983.

SAMPLE	Elevation (m)	UTM E. (m)	UTM N. (m)
03TEKI009	1345	330773	5682934
03TEKI015	2228	325182	5681534
03TEKI016	2418	323861	5684352
03TEKI018	554	314268	5686900
03TEKI019	260	312221	5685482
03TEKI030	1594	309064	5678027
03TEKI039	454	310255	5666633

Appendix 3: Age Anomalies with Increasing and Decreasing Relief Scenarios

Figure A-3- 1. Topography and calculated differences between predicted and observed cooling ages in the Mount Waddington region for models with increasing relief over time from 50% modern over 8 Myr. A: Shaded relief DEM with AHe sample locations as well as reference points for the Klinaklini Valley (KV), Mount Jubilee (MJ), and Mount Waddington (MW). Contoured age anomaly, defined as predicted − observed AHe cooling age, for constant relief with (B) 0.6 and (C) 0.4 mm/yr background denudation rate. Contoured change in elevation (dz), defined as the product between age anomaly and background denudation rate, for (D) 0.6 and (E) 0.4 mm/yr.

Figure A-3- 2. Topography and calculated differences between predicted and observed cooling ages in the Mount Waddington region for models with increasing decreasing over time from 150% modern over 8 Myr. A: Shaded relief DEM with AHe sample locations as well as reference points for the Klinaklini Valley (KV), Mount Jubilee (MJ), and Mount Waddington (MW). Contoured age anomaly, defined as predicted – observed AHe cooling age, for constant relief with (B) 0.6 and (C) 0.4 mm/yr background denudation rate. Contoured change in elevation (dz), defined as the product between age anomaly and background denudation rate, for (D) 0.6 and (E) 0.4 mm/yr.
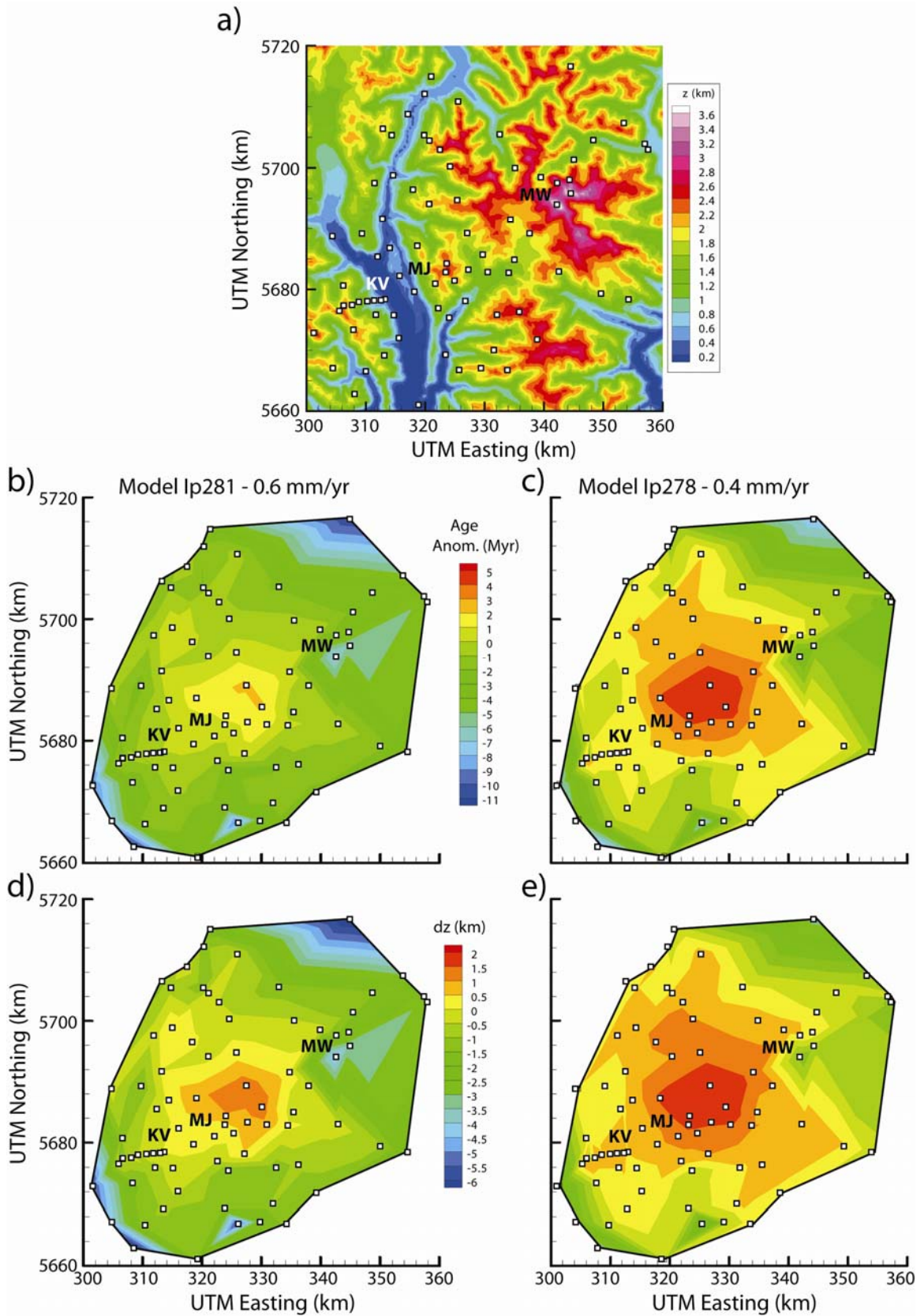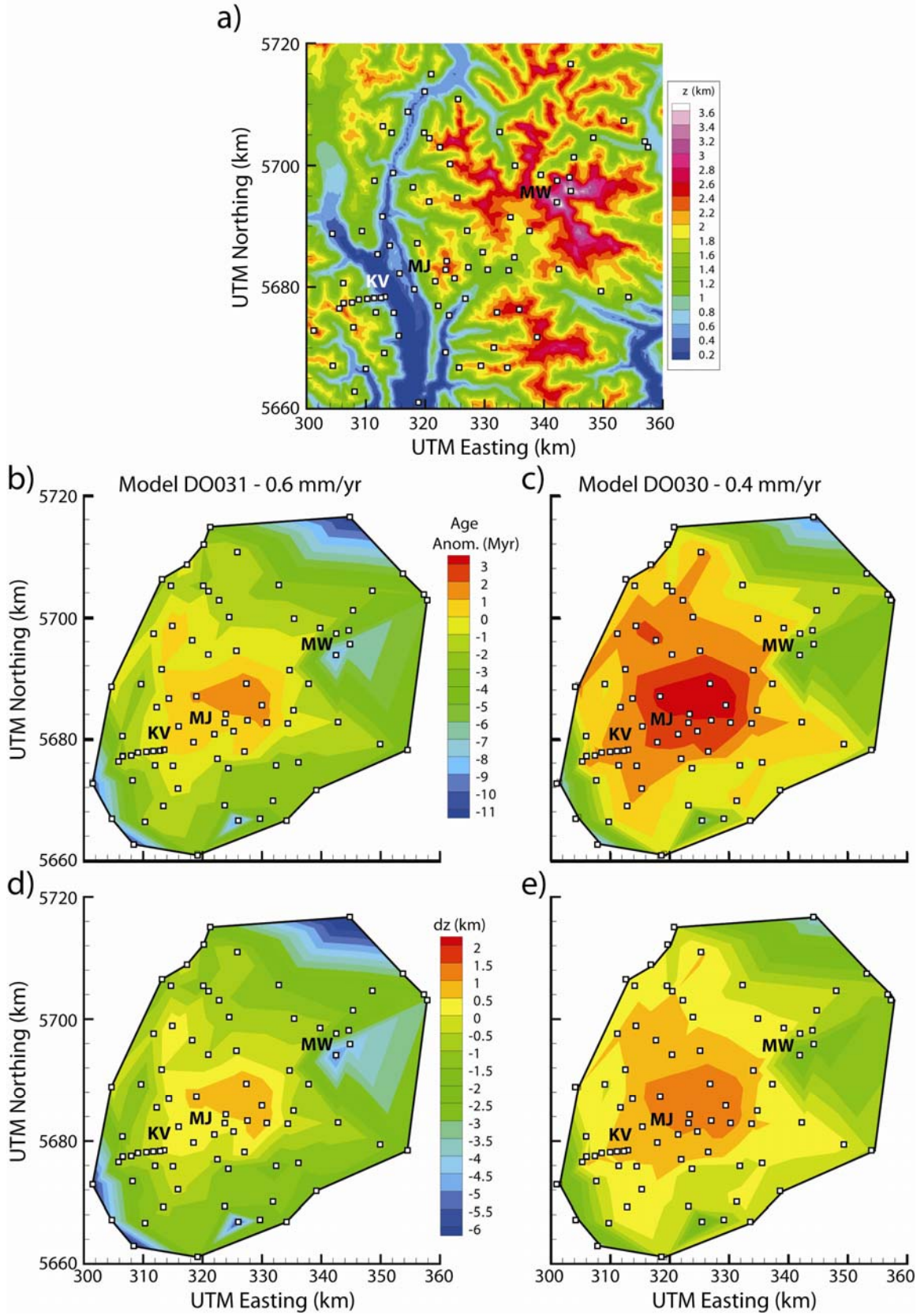
References

Agassiz, L., 1864, Glacial period: The Atlantic Monthly, p. 224-232.

Armstrong, J.E., 1981, Post-Vashon Wisconsin glaciation, Fraser Lowland, British Columbia: Geo. Surv. Canada. Bull., v. 322, p. 1-34.

Atwater, T., and Stock, J., 1998, Pacific-North America plate tectonics of the Neogene southwestern United States; an update: International Geology Review, v. 40, p. 375-402.

Balco, G., and Stone, J.O.H., 2005, Measuring middle Pleistocene erosion rates with cosmic-ray-produced nuclides in buried alluvial sediment, Fisher Valley, southeastern Utah: Earth Surf. Process. Landforms, v. 30, p. 1051-1067.

Barnes, J.A., Ehlers, T.A., McQuarrie, N., O'Sullivan, P.B., and Pelletier, J.D., 2006, Eocene to recent variations in erosion across the central Andean fold-thrust belt, northern Bolivia; implications for plateau evolution: Earth Planet. Sci. Lett., v. 248, p. 118-133.

Beaumont, C., Fullsack, P., and Hamilton, J., 1992, Erosional control of active compressional orogens, *in* McClay, K., ed., Thrust Tectonics: London, UK, Chapman & Hall, p. 1-18.

Berger, A.L., and Spotila, J.A., 2008, Denudation and deformation in a glaciated orogenic wedge: the St. Elias orogen, Alaska: Geology, v. 36, p. 523-526.

Berger, A.L., Spotila, J.A., Chapman, J.B., Pavlis, T.L., Enklemann, E., Ruppert, N.A., and Buscher, J.T., 2008, Architecture, kinematics, and exhumation of a convergent orogenic wedge: A thermochronological investigation of tectonic-climate interactions within the central St. Elias orogen, Alaska: Earth Planet. Sci. Lett., v. 270, p. 13-24.

Bevington, P.R., and Robinson, K.D., 1992, Data reduction and error analysis for the physical sciences, WCB McGraw-Hill.

Bierman, P.R., and Nichols, K.K., 2004, Rock to sediment, slope to sea with (super 10) Be; rates of landscape change: Annual Review of Earth and Planetary Sciences, v. 32, p. 215-255.

Blais-Stevens, A., Bornhold, B.D., Kemp, A.E.S., Dean, J.M., and Vaan, A.A., 2001, Overview of Late Quaternary stratigraphy in Saanich Inlet, British Columbia: results of Ocean Drilling Program Leg 169S: Marine Geology, v. 174, p. 3-26.

Blondes, M.S., Reiners, P.W., Edwards, B.R., and Biscontini, A., 2007, Dating young basalt eruptions by (U-Th)/He on xenolithic zircons: Geology, v. 35, p. 17-20.

Booth, D.B., 1986, Mass balance and sliding velocity of the Puget Lobe of the Cordilleran Ice Sheet during the Last Glaciation: Quat. Res., p. 269-280.

Booth, D.B., Troost, K.G., Clague, J.J., and Waitt, R.B., 2004, The Cordilleran ice sheet, *in* Gillespie, A.R., Porter, S.C., and Atwater, B.F., eds., Developments in Quaternary Science, Volume 1, p. 17-43.

Brandon, M.T., Roden-Tice, M.K., and Garver, J.I., 1998, Late Cenozoic exhumation of the Cascadia accretionary wedge in the Olympic Mountains, Northwest Washington State: Geological Society of America Bulletin, v. 110, p. 985-1009.

Brardinoni, F., and Hassan, M.A., 2006, Glacial erosion, evolution of river long profiles, and the organization of process domains in mountain drainage basins of coastal British Columbia: J. Geophys. Res., v. 111.

Braun, J., 2002a, Estimating exhumation rate and relief evolution by spectral analysis of age-elevation datasets: Terra Nova, v. 14, p. 210-214.

—, 2002b, Quantifying the effect of recent relief changes on age-elevation relationships: Earth Planet. Sci. Lett., v. 200, p. 331-343.

—, 2003, Pecube: a new finite-element code to solve the 3D heat transport equation including the effects of a time-varying, finite amplitude surface topography: Comp. & Geosci., v. 29, p. 787-794.

—, 2005, Quantitative Constraints on the Rate of Landform Evolution Derived from Low-Temperature Thermochronology, *in* Reiners, P.W., and Ehlers, T.A., eds., Low-Temperature Thermochronology: Techniques, Interpretations, and Applications, Volume 58: Reviews in Mineralogy and Geochemistry, MSA, p. 351-374.

Braun, J., and Robert, X., 2005, Constraints on the rate of post-orogenic erosional decay from low-temperature thermochronologic data; application to the Dabie Shan, China: Earth Surf. Process. Landforms, v. 30, p. 1203-1225.

Braunmiller, J., and Nabelek, J., 2002, Seismotectonics of the Explorer region: J. Geophys. Res., v. 107.

Brocklehurst, S., and Whipple, K., 2002, Glacial erosion and relief production in the eastern Sierra Nevada, California: Geomorphology, v. 42, p. 1-24.

Brocklehurst, S.H., and Whipple, K.X., 2004, Hypsometry of glaciated landscapes: Earth Surf. Process. Landforms, v. 29, p. 907-926.

—, 2006, Assessing the relative efficiency of fluvial and glacial erosion through simulation of fluvial landscapes: Geomorphology, v. 75, p. 283-299.

Brook, M.S., Kirkbride, M.P., and Brock, B.W., 2008, Temporal constraints on glacial valley cross-profile evolution: Two Thumbs Range, central Southern Alps, New Zealand: Geomorphology, v. 97, p. 24-34.

Brozovic, N., Burbank, D., and Meigs, A., 1997, Climatic limits on landscape development in the northwestern Himalaya: Science, v. 276, p. 571-574.

Burbank, D., Blythe, A., Putkonen, J., Pratt-Sitaula, B., Gabet, E., Oskin, M., Barros, A., and Ojha, T.P., 2003, Decoupling of erosion and precipitation in the Himalayas: Nature, v. 426, p. 652-655.

Burtner, R.L., Nigrini, A., and Donelick, R.A., 1994, Thermochronology of Lower Cretaceous source rocks in the Idaho-Wyoming thrust belt: AAPG Bulletin, v. 78, p. 1613-1636.

Champagnac, J.D., Molnar, P., Anderson, R.S., Sue, C., and Delacou, B., 2007, Quaternary erosion-induced isostatic rebound in the western Alps: Geology, v. 35, p. 195-198.

Church, M., and Ryder, J.M., 1972, Paraglacial sedimentation: A consideration of fluvial processes conditioned by glaciation: Geol. Soc. Amer., Bull., v. 83, p. 3059-3072.

Clague, J.J., 1986, The Quaternary stratigraphic record of British Columbia - evidence for episodic sedimentation and erosion controlled by glaciation: Can. J. Earth Sci., v. 23, p. 885-894.

—, 1991, Quaternary glaciation and sedimentation, *in* Gabrielse, H., and Yorath, C.J., eds., Geology of the Cordilleran Orogen in Canada, Volume 4, Geol. Surv. Canada, p. 421-434.

Clague, J.J., Armstrong, J.E., and Mathews, W.H., 1980, Advance of the Late Wisconsin Cordillera ice sheet in southern British Columbia since 22,000 B.P.: Quat. Res., v. 13, p. 322-326.

Clowes, R.M., Zelt, C.A., Amor, J.R., and Ellis, R.M., 1995, Lithospheric structure in the southern Canadian Cordillera from a network of seismic refraction lines: Can. J. Earth Sci., v. 32, p. 1485-1513.

Colpron, M., Nelson, J.L., and Murphy, D.C., 2007, Northern Cordillera terranes and their interactions through time: Geo. Soc. Am. Today, v. 17.

Crowley, K.D., Cameron, M., and Schaefer, R.L., 1991, Experimental studies of annealing of etched fission tracks in flourapatite: Geochim. Cosmochim. Acta, v. 55, p. 1449-1465.

Currie, C.A., and Hyndman, R.D., 2006, The thermal structure of subduction zone back arcs: J. Geophys. Res., v. 111, p. doi:10.1029/2005JB004024.

Densmore, M.S., 2008a, Interpreting thermochronometer cooling ages in a glaciated orogen, University of Michigan.

—, 2008b, Quantifying glacial denudation with thermochronology 1: Insights from apatite (U-Th)/He ages and 1-D thermal models, University of Michigan.

—, 2008c, Quantifying glacial denudation with thermochronology 2: Cenozoic exhumation history from thermochronometer data, University of Michigan.

Densmore, M.S., Ehlers, T.A., and Woodsworth, G.J., 2007, Effect of alpine glaciation on thermochronometer age-elevation profiles: Geophys. Res. Letters, v. 34, p. doi:10.1029/2006GL028371.

Denton, G.H., and Armstrong, R.L., 1969, Miocene-Pliocene glaciations in southern Alaska: Am. J. of Sci., v. 267, p. 1121-1142.

Dodson, M., 1973, Closure temperature in cooling geochronological and petrological systems: Contrib. Mineral. Petrol., v. 40, p. 259-274.

Donelick, R.A., O'Sullivan, P.B., and Ketcham, R.A., 2005, Apatite Fission-Track Analysis, Low-Temperature Thermochronology: Techniques, Interpretations, and Applications, Volume 58, Mineralogical Society of America, p. 49-94.

Dziak, R.P., 2006, Explorer deformation zone: Evidence of a large shear zone and reorganization of the Pacific-Juan de Fuca-North American triple junction: Geology, v. 34, p. 213-216.

Ehlers, T., and Farley, K., 2003, Apatite (U-Th)/He thermochronometry; methods and applications to problems in tectonic and surface processes: Earth Planet. Sci. Lett., v. 206, p. 1-14.

Ehlers, T.A., 2005, Crustal thermal processes and the interpretation of thermochronometer data, Low-Temperature Thermochronology: Techniques, Interpretations, and Applications, Volume 58: Reviews in Mineralogy and Geochemistry, p. 315-350.

Ehlers, T.A., Armstrong, P.A., and Chapman, D.S., 2001, Normal fault thermal regimes and the interpretation of low-temperature thermochronometers: Phys. of the Earth and Planet. Int., v. 216, p. 179-194.

Ehlers, T.A., Chaudhri, T., Kumar, S., Fuller, C.W., Willet, S.D., Ketcham, R., Brandon, M.T., Belton, D.X., Kohn, B.P., Gleadow, A.J.W., Dunai, T.J., and Fu, F.Q., 2005, Computational tools for low-temperature thermochronometer interpretation, *in* Reiners, P.W., and Ehlers, T.A., eds., Low-Temperature Thermochronology: Techniques, Interpretations, and Applications, Volume 58: Reviews in Mineralogy and Geochemistry, MSA, p. 589-622.

Ehlers, T.A., Farley, K.A., Rusmore, M.E., and Woodsworth, G.J., 2006, Apatite (U-Th)/He signal of large-magnitude accelerated glacial erosion, southwest British Columbia: Geology, v. 34, p. 765-768.

Ehlers, T.A., Willet, S.D., Armstrong, P.A., and Chapman, D.S., 2003, Exhumation of the central Wasatch Mountains, Utah: 2. Thermokinematic model of exhumation, erosion, and thermochronometer interpretation: J. Geophys. Res., v. 108, p. 12-1 - 12-18.

Engebretson, D.C., Cox, A., and Gordon, R.G., 1984, Relative motions between oceanic plates of the Pacific Basic: J. Geophys. Res., v. 89, p. 10291-10310.

Farley, K., 2000, Helium diffusion from apatite; general behavior as illustrated by Durango fluorapatite: J. Geophys. Res., v. 105, p. 2903-2914.

Farley, K., Wolf, R., and Silver, L., 1996, The effects of long alpha-stopping distances on (U-Th)/He ages: Geochimica et Cosmochimica Acta, v. 60, p. 4223-4229.

Farley, K.A., 2002, (U-Th)/He dating; techniques, calibrations, and applications, *in* Rosso, J.J., and Ribbe, P.H., eds., Noble Gases in Geochemistry and Cosmochemistry, Volume 47, MSA, p. 819-843.

Farley, K.A., Rusmore, M.E., and Bogue, S.W., 2001, Post-10 Ma uplift and exhumation of the northern Coast Mountains, British Columbia: Geology, v. 29, p. 99-102.

Fitzgerald, P.G., Sorkhabi, R.B., Redfield, T.F., and Stump, E., 1995, Uplift and denudation of the central Alaska Range; a case study in the use of apatite fission track thermochronology to determine absolute uplift parameters: J. Geophys. Res., B, Solid Earth and Planets, v. 100.

Flueck, P., Hyndman, R.D., and Lowe, C., 2003, Effective elastic thickness Te of the lithosphere in western Canada: J. Geophys. Res., v. 108(B9), p. doi:10.1029/2002JB002201.

Friedman, R.M., and Armstrong, R.L., 1995, Jurassic and Cretaceous geochronology of the southern Coast Belt, British Columbia, 49° to 51°N: Geo. Soc. Am., v. Special Paper 299.

Friele, P.A., and Clague, J.J., 2002, Younger Dryas readvance in Squamish river valley, southern Coast Mountains, British Columbia: Quat. Sci. Rev., v. 21, p. 1925-1933.

Fulton, R.J., 1984, Quaternary glaciation, Canadian Cordillera, *in* Fulton, R.J., ed., Quaternary Stratigraphy of Canada - a Canadian Contribution to IGCP Project 24, Volume Paper 84-10, Geological Survey of Canada, p. 39-48.

Gabrielse, H., Monger, J.W.H., Wheeler, J.O., and Yorath, C.J., 1991, Part A. Morphogeological belts, tectonic assemblages and terranes, *in* Gabrielse, H., and Yorath, C.J., eds., Geology of the Cordilleran Orogen in Canada, Volume 4, Geol. Surv. Canada, p. 15-28.

Gabrielse, H., and Yorath, C.J., 1991, Tectonic synthesis, *in* Gabrielse, H., and Yorath, C.J., eds., Geology of the Cordilleran Orogen in Canada, Volume 4, Geol. Surv. Canada, p. 677-705.

Gallagher, K., Brown, R.W., and Johnson, C., 1998, Fission track analysis and its applications to geological problems: Ann. Rev. of Earth and Planet. Sci., v. 26, p. 519-572.

Garver, J.I., Reiners, P.W., Walker, L.J., Ramage, J.M., and Perry, S.E., 2005, Implications for timing of Andean uplift from thermal resetting of radiation-damaged zircon in the Cordillera Huayhuash, northern Peru: J. Geol., v. 113, p. 117-138.

Gehrels, G.E., McClelland, W.C., Samson, S.D., Jackson, J.L., and Patchett, P.J., 1991a, U-Pb geochronology of two pre-Tertiary plutons in the Coast Mountains batholith near Ketchikan, southeastern Alaska: Can. J. Earth Sci., v. 28, p. 894-898.

Gehrels, G.E., McClelland, W.C., Samson, S.D., and Patchett, P.J., 1991b, U-Pb geochronology of Late Cretaceous and early Tertiary plutons in the northern Coast Mountains batholith: Can. J. Earth Sci., v. 28, p. 899-911.

Gilbert, G.K., 1906, Crescentic Gouges on Glaciated Surfaces: Geol. Soc. Amer., Bull., v. 17.

Goodfellow, B.W., 2007, Relict non-glacial surfaces in formerly glaciated landscapes: Earth Sci. Rev., v. 80, p. 47-73.

Hallet, B., 1979, A theoretical model of glacial abrasion: J. Glac., v. 23, p. 39-50.

Hallet, B., Hunter, L., and Bogen, J., 1996a, Rates of erosion and sediment evacuation by glaciers; a review of field data and their implications, *in* Solheim, A., Riis, F., Elverhoi, A., Faleide, J.I., Jensen, L.N., and Cloetingh, S., eds., Global and Planetary Change, Volume 12: Amsterdam, Elsevier, p. 213-235.

—, 1996b, Rates of erosion and sediment evacuation by glaciers; a review of field data and their implications: Global and Planetary Change, v. 12, p. 213-235.

Hallet, B., and Putkonen, J., 1994, Surface dating of dynamic landforms: young boulders on aging moraines: Science, v. 265, p. 937-940.

Hammer, P.T.C., and Clowes, R.M., 1997, Moho reflectivity patterns; a comparison of Canadian Lithoprobe transects: Tectonophysics, v. 269, p. 179-198.

Harbor, J., and Warburton, J., 1993, Relative rates of glacial and nonglacial erosion in alpine environments: Arct. Alp. Res., v. 25, p. 1-7.

Harbor, J.M., 1992, Numerical modeling of the development of U-shaped valleys by glacial erosion: Geol. Soc. Amer., Bull., v. 104, p. 1364-1375.

Harrison, T., Armstrong, R., Naeser, C., and Harakal, J., 1979, Geochronology and thermal history of the Coast Plutonic Complex, near Prince Rupert, British Columbia: Can. J. Earth Sci., v. 16, p. 400-410.

Hasebe, N., Barbarand, J., Jarvis, K., Carter, A., and Hurford, A.J., 2004, Apatite fission-track chronometry using laser ablation ICP-MS: Chemical Geology, v. 207, p. 135-145.

Hebbeln, D., Lamy, F., Mohtadi, M., and Echtler, H., 2007, Tracing impact of glacial-interglacial climate variability on erosion of the southern Andes: Geology, v. 35, p. 131-134.

Herman, F., and Braun, J., 2006, Fluvial response to horizontal shortening and glaciations: A study in the Southern Alps of New Zealand: Journal of Geophysical Research, F, Earth Surface, v. 111, p. F01008.

—, 2008, Evolution of the glacial landscape of the Southern Alps of New Zealand: Insights from a glacial erosion model: J. Geophys. Res., v. 113, p. doi:10.1029/2007JF000807.

Herman, F., Braun, J., and Dunlap, W.J., 2007, Tectonomorphic scenarios in the Southern Alps of New Zealand: J. Geophys. Res., v. 2007.

Hickes, H.J., 2001, Apatite and zircon (U-Th)/He thermochronology of the northern Coast Mountains, southeast Alaska, Washington State University.

Higgs, R., 1991, Sedimentology, basin-fill architecture and petroleum geology of the Tertiary Queen Charlotte Basin, British Columbia, Evolution and hydrocarbon potential of the Queen Charlotte Basin, British Columbia, Volume 90-10, Geol. Surv. Canada, p. 337-371.

Hodges, K.V., 2003, Geochronology and Thermochronology in Orogenic Systems, *in* Rudnick, R., ed., Treatise on Geochemistry, Volume 3, Elsevier, p. 263-292.

House, M., Wernicke, B., and Farley, K., 1998, Dating topography of the Sierra Nevada, California, using apatite (U-Th)/He ages: Nature, v. 396, p. 66-69.

House, M.A., Farley, K.A., and Stockli, D., 2000, Helium chronometry of apatite and titanite using Nd-YAG laser heating: Earth Planet. Sci. Lett., v. 183, p. 365-368.

Hyndman, R.D., and Hamilton, T.S., 1993, Queen Charlotte area Cenozoic tectonics and volcanism and their association with relative plate motions along the northeastern Pacific margin: J. Geophys. Res., v. 98, p. 14257-14277.

Irving, E., Baker, J., Wynne, P.J., Hamilton, T.S., and Wingate, M.T.D., 2000, Evolution of the Queen Charlotte Basin; further paleomagnetic evidence of Tertiary extension and tilting: Tectonophysics, v. 326, p. 1-22.

Johnston, S.T., and Borel, G.D., 2007, The odyssey of the Cache Creek terrane, Canadian Cordillera: Implications for accretionary orogens, tectonic setting of Panthalassa, the Pacific superwell, and break-up of Pangea: Earth Planet. Sci. Lett., v. 253, p. 415-428.

Kessler, M.A., Anderson, R.S., and Stock, G.M., 2006, Modeling topographic and climatic control of east-west asymmetry in Sierra Nevada glacier length during the Last Glacial Maximum: J. Geophys. Res., v. 111, p. doi:10.1029/2005JF000365.

Ketcham, R., 2005a, Forward and inverse modeling of low-temperature thermochronometry data, *in* Reiners, P.W., and Ehlers, T.A., eds., Low-Temperature Thermochronology: Techniques, Interpretations, and Applications, Volume 58: Reviews in Mineralogy and Geochemistry, MSA, p. 275-314.

Ketcham, R.A., 2005b, Forward and inverse modeling of low-temperature thermochronometry data, *in* Reiners, P.W., and Ehlers, T.A., eds., Low-Temperature Thermochronology: Techniques, Interpretations and Applications, Volume 58: Reviews in Mineralogy and Geochemistry, MSA, p. 275-314.

Ketcham, R.A., Donelick, R.A., and Donelick, M.B., 2000, AFTSolve: a program for multi-kinetic modeling of apatite fission-track data: Geo. Mat. Res., v. 2, p. 1-32.

Kohl, T., and Hopkirk, J., 1995, "FRACTure" a simulation code for forced fluid flow and transport in fractured, porous rock: Geothermics, v. 24, p. 333-343.

Koons, P., 1989, The topographic evolution of collisional mountain belts; a numerical look at the Southern Alps, New Zealand: Am. J. Sci., v. 289, p. 1041-1069.

Koppes, M., and Hallet, B., 2002, Influence of rapid glacial retreat on the rate of erosion by tidewater glaciers: Geology, v. 30, p. 47-50.

—, 2006, Erosion rates during rapid deglaciation in Icy Bay, Alaska: J. Geophys. Res., v. 111.

Kovanen, D.J., and Easterbrook, D.J., 2001, Late Pleistocene, post-Vashon, alpine glaciation of the Nooksack drainage, North Cascades, Washington: Geol. Soc. Amer., Bull., v. 113, p. 274-288.

Laslett, G.M., Green, P.F., Duddy, I.R., and Gleadow, A.J.W., 1987, Thermal annealing of fission tracks in apatite 2. A quantitative analysis.

Lees, C.H., 1910, On the isogeotherms under mountain ranges in radioactive districts: Pro. Roy. Soc., p. 339-346.

Lewis, T., Jessop, A., and Judge, A., 1985, Heat flux measurements in southwestern British Columbia; the thermal consequences of plate tectonics: Canadian J. Earth Sci., v. 22, p. 1262-1273.

MacGregor, K., Anderson, R., Anderson, S., and Waddington, E., 2000, Numerical simulations of glacial-valley longitudinal profile evolution: Geology, v. 28, p. 1031-1034.

Mancktelow, N., and Grasemann, B., 1997a, Time-dependent effects of heat advection and topography on cooling histories during erosion: Tectonophysics, v. 270, p. 167-195.

Mancktelow, N.S., and Grasemann, B., 1997b, Time-dependent effects of heat advection and topography on cooling histories during erosion: Tectonophysics, v. 270, p. 167-195.

Mathewes, R.W., Heusser, L.E., and Patterson, R.T., 1993, Evidence for a Younger Dryas-like cooling event on the British Columbia coast: Geology, v. 21, p. 101-104.

Mathews, W.H., and Rouse, G.E., 1986, An Early Pleistocene proglacial succession in south-central British Columbia: Can. J. Earth Sci., v. 23, p. 1796-1803.

Matthes, F.E., 1930, Geologic History of the Yosemite Valley: U.S. Geol. Surv., Prof. Paper

Meigs, A., and Sauber, J., 2000, Southern Alaska as an example of the long-term consequences of mountain building under the influence of glaciers: Quat. Sci. Rev., v. 19, p. 1543-1563.

Milliman, J.D., and Syvitski, J.P.M., 1992, Geomorphic/tectonic control of sediment discharge to the ocean; the importance of small mountainous rivers: J. Geol., v. 100, p. 525-544.

Molnar, P., and England, P.C., 1990, Late Cenozoic uplift of mountain ranges and global climate change; chicken or egg?: Nature, v. 346, p. 29-34.

Monger, J.W.H., 1993, Canadian Cordilleran tectonics: from geosynclines to crustal collage: Can. J. Earth Sci., v. 30, p. 209-231.

Montgomery, D.R., 2002, Valley formation by fluvial and glacial erosion: Geology, v. 30, p. 1047-1050.

Mosher, D.C., and Moran, K., 2001, Post-glacial evolution of Saanich Inlet, British Columbia: results of physical property and seismic reflection stratigraphic analysis: Marine Geology, v. 174, p. 59-77.

Naeser, N.D., Westgate, J.A., Hughes, O.L., and Péwé, T.L., 1982, Fission-track ages of late Cenozoic distal tephra beds in the Yukon Territory and Alaska: Can. J. Earth Sci., v. 19, p. 2167-2178.

Naylor, S., and Gabet, E.J., 2007, Valley asymmetry and glacial versus nonglacial erosion in the Bitterroot Range, Montana, USA: Geology, v. 35, p. 375-378.

Nokleberg, W.J., Parfenov, L.M., Monger, J.W.H., Norton, I.O., Khanchuk, A.I., Stone, D.B., Scotese, C.R., Scholl, D.W., and Fujita, K., 2000, Phanerozoic tectonic evolution of the Circum-North Pacific: U.S. Geol. Surv., Prof. Paper p. 122 p.

O'Leary, D.M., Clowes, R.M., and Ellis, R.M., 1993, Crustal velocity structure in the southern Coast Belt, British Columbia: Can. J. Earth Sci., v. 30, p. 2389-2403.

O'Sullivan, P., and Parrish, R., 1995, The importance of apatite composition and single-grain ages when interpreting fission track data from plutonic rocks: a case study from the Coast Ranges, British Columbia: Earth Planet. Sci. Lett., v. 132, p. 213-224.

O'Sullivan, P.B., and Currie, L.D., 1996, Thermoctectonic history of Mt. Logan, Yukon Territory, Canada: implications of multiple episodes of middle to late Cenozoic deformation: Earth Planet. Sci. Lett., v. 144, p. 251-261.

Oskin, M., and Burbank, D.W., 2005, Alpine landscape evolution dominated by cirque retreat: Geology, v. 33, p. 933-936.

Parrish, R.R., 1983, Cenozoic thermal evolution and tectonics of the Coast Mountains of British Columbia 1. Fission track dating, apparent uplift rates, and patterns of uplift: Tectonics, v. 2, p. 601-631.

Reiners, P.W., 2007, Thermochronologic approaches to paleotopography: Rev. Min. & Geochem., v. 66, p. 243-267.

Reiners, P.W., and Brandon, M.T., 2006, Using thermochronology to understand orogenic erosion: Ann. Rev. Earth Planet. Sci., v. 34, p. 419-466.

Reiners, P.W., Ehlers, T.A., and Zeitler, P.K., 2005, Past, Present, and Future of Thermochronology, in Reiners, P.W., and Ehlers, T.A., eds., Low-Temperature Thermochronology: Techniques, Interpretations, and Applications, Volume 58: Reviews in Mineralogy and Geochemistry, MSA, p. 1-18.

Reiners, P.W., Farley, K.A., and Hickes, H.J., 2002, He diffusion and (U-Th)/He thermochronometry of zircon: initial results from Fish Canyon Tuff and Gold Butte: Tectonophysics, v. 349, p. 297-308.

Reiners, P.W., Zhou, Z., Ehlers, T.A., Xu, C., Brandon, M.T., Donelick, R.A., and Nicolescu, S., 2003, Post-orogenic evolution of the Dabie Shan, Eastern China, from (U-Th)/He and fission track thermochronology: Am. J. of Sci., v. 303, p. 489-518.

Richards, T.A., and McTaggart, K.C., 1976, Granitic rocks of the southern Coast Plutonic Complex and northern Cascades of British Columbia: Geol. Soc. Amer., Bull., v. 87, p. 935-953.

Riddihough, R.P., and Hyndman, R.D., 1991, Modern plate tectonic regime of the continental margin of western Canada, *in* Gabrielse, H., and Yorath, C.J., eds., Geology of the Cordilleran Orogen in Canada, Volume 4, p. 435-455.

Ring, U., Brandon, M.T., Willet, S.D., and Lister, G.S., 1999, Exhumation processes, *in* Ring, U., Brandon, M.T., Lister, G.S., and Willet, S.D., eds., Exhumation processes: normal faulting, ductile flow and erosion, Volume 154, Geol. Soc. London, p. 1-27.

Roddick, J.A., and Hutchison, W.W., 1974, Setting of the Coast Plutonic Complex, British Columbia: Pacific Geology, v. 8, p. 91-108.

Rohr, K., and Currie, L., 1997, Queen Charlotte Basin and Coast Mountains; paired belts of subsidence and uplift caused by a low-angle normal fault: Geology, v. 25, p. 819-822.

Rouse, G.E., and Mathews, W.H., 1979, Tertiary geology and palynology of the Quesnel area, British Columbia: Bull. Canadian Pet. Geo., v. 27, p. 418-445.

Sass, J.H., Kennelly Jr., J.P., Smith, E.P., and Wendt, W.E., 1984, Laboratory line-source methods for the measurement of thermal conductivity of rocks near room temperature: U.S. Geol. Surv. Open File Rep., v. 84-91, p. 21.

Schildgen, T.F., Hodges, K.X., Reiners, P.W., and Pringle, M.S., 2007, Uplift of the western margin of the Andean plateau revealed from canyon incision history, southern Peru: Geology, v. 35, p. 523-526.

Schildgen, T.F., Phillips, W.M., and Purvers, R.S., 2005, Simulation of snow shielding corrections for cosmogenic nuclide surface exposure: Geomorphology, v. 64, p. 67-85.

Shackleton, N.J., and Opdyke, N.D., 1973, Oxygen-isotope and palaeomagnetic stratigraphy of equatorial Pacific core V28-238: oxygen isotope temperatures and ice volumes on a 10^5 and 10^6 year scale: Quat. Res., v. 3, p. 39-55.

Shuster, D.L., Ehlers, T.A., Rusmore, M.E., and Farley, K.A., 2005, Rapid Glacial Erosion at 1.8 Ma Revealed by ^{4}He/^{3}He Thermochronometry: Science, v. 310, p. 1668-1670.

Shuster, D.L., Flowers, R.M., and Farley, K.A., 2006, The influence of natural radiation damage on helium diffusion kinetics in apatite: Earth Planet. Sci. Lett., v. 249, p. 148-161.

Souther, J.G., Armstrong, R.L., and Harakal, J., 1984, Chronology of the peralkaline, late Cenozoic Mount Edziza Volcanic Complex, northern British Columbia, Canada: Geol. Soc. Amer., Bull., v. 95, p. 337-349.

Spotila, J.A., Buscher, J.T., Meigs, A.J., and Reiners, P.W., 2004, Long-term glacial erosion of active mountain belts; example of the Chugach-St. Elias Range, Alaska: Geology, v. 32, p. 501-504.

Staiger, J.K.W., Gosse, J.C., Johnson, J.V., Fastook, J., Gray, J.T., Stockli, D.F., Stockli, L., and Finkel, R., 2005, Quaternary relief generation by polythermal glacier ice: Earth Surf. Process. Landforms, v. 30, p. 1145-1159.

Stock, G.M., Ehlers, T.A., and Farley, K.A., 2006, Where does sediment come from? Quantifying catchment erosion with detrital apatite (U-Th)/He thermochronometry: Geology, v. 34, p. 725-728.

Stockli, D., Farley, K., and Dumitru, T., 2000, Calibration of the apatite (U-Th)/He thermochronometer on an exhumed fault block, White Mountains, California: Geology, v. 28, p. 983-986.

Stuwe, K., White, L., and Brown, R., 1994, The influence of eroding topography on steady-state isotherms; application to fission track analysis: Earth Planet. Sci. Lett., v. 124, p. 63-74.

Sweeney, J.F., Stephenson, R.A., Currie, R.G., and Delaurier, J.M., 1992, Tectonic framework; Part C, Crustal geophysics, *in* Gabrielse, H., and Yorath, C.J., eds., Geology of the Cordilleran Orogen in Canada, Geol. Surv. Canada, p. 39-53.

Thomson, S.N., 2002, Late Cenozoic geomorphic and tectonic evolution of the Patagonian Andes between latitudes 42°S and 46°S: An appraisal based on fission-track results from the transpressional intra-arc Liquine-Ofqui fault zone: Geol. Soc. Am. Bull., v. 114, p. 1159-1173.

Thorkelson, D.J., Mortensen, J.K., Creaser, R.A., Davidson, G.J., and Abbott, J.G., 2001, Early Proterozoic magmatism in Yukon, Canada: constraints on the evolution of northwestern Laurentia: Can. J. Earth Sci., v. 38, p. 1479-1494.

Tomkin, J., and Braun, J., 2002, The influence of alpine glaciation on the relief of tectonically active mountain belts: American Journal of Science, v. 302, p. 169-190.

Tomkin, J.H., and Roe, G.H., 2007, Climate and tectonic controls on glaciated critical-taper orogens: Earth Planet. Sci. Lett., v. 262, p. 385-397.

Turcotte, D.L., and Schubert, G., 2002, Geodynamics, Cambridge.

van der Heyden, P., 1989, U-Pb and K-Ar geochronometry of the Coast Plutonic Complex, 53°N-54°N, and implications for the Insular-Intermontane superterrane boundary, British Columbia, University of British Columbia.

Wagner, G.W., Reimer, G.M., and Jäger, E., 1977, Cooling ages derived by apatite fission-track, mica Rb-Sr and K-Ar dating: The uplift and cooling history of the Central Alps: Mem. degli Ist. di Geo. e Mineral. dell'Univ. di Padova, v. 30, p. 1-27.

Waples, D.W., and Waples, J.S., 2004, A review and evaluation of specific heat capacities of rocks, minerals, and subsurface fluids. Part 1: minerals and nonporous rocks: Nat. Resources Res., v. 13, p. 97-122.

Whipp, D.M., and Ehlers, T.A., 2007, Influence of groundwater flow on thermochronometer-derived exhumation rates in the central Nepalese Himalaya: Geology, v. 35, p. 851-854.

Whipp, D.M., Ehlers, T.A., Blythe, A.B., Huntington, K.W., Hodges, K.V., and Burbank, D.W., 2007, Plio-Quaternary exhumation history of the central Nepalese

Himalaya: 2. Thermokinematic and thermochronometer age prediction model: Tectonics, v. 26.

Whipple, K., Kirby, E., and Brocklehurst, S., 1999, Geomorphic limits to climate-induced increases in topographic relief: Nature, v. 401, p. 39-43.

Willett, S., 1999, Orogeny and orography; the effects of erosion on the structure of mountain belts: J. Geophys. Res., v. 104, p. 28957-28982.

Woodsworth, G., 1997, Hot springs of Western Canada: Vancouver, Canada, Gordon Soules Book Publishers Ltd.

Woodsworth, G.J., Anderson, R.G., Armstrong, R.L., Struik, L.C., and van der Heyden, P., 1991, Plutonic regimes, *in* Gabrielse, H., and Yorath, C.J., eds., Geology of the Cordilleran Orogen in Canada, Volume 4, Geol. Surv. Canada, p. 493-530.

Yingkui, L., Harbor, J., Stroeven, A.P., Fabel, D., Kleman, J., Fink, D., Caffee, M., and Elmore, D., 2005, Ice sheet erosion patterns in valley systems in northern Sweden investigated using cosmogenic nuclides: Earth Surf. Process. Landforms, v. 30, p. 1039-1049.